Reliable and Efficient Multicast Communication in WiFi Direct (P2P) 802.11Wireless Networks

Author

Khan, Gul Zameen

Published

2017-08

Thesis Type

Thesis (PhD Doctorate)

School

School of Info & Comm Tech

DOI

10.25904/1912/452

Reliable and Efficient Multicast Communication in WiFi Direct (P2P) 802.11 Wireless Networks

Gul Zameen Khan
MS (CSE), BS (CSE)

School of Information and Communication Technology
Griffith Sciences
Griffith University

A Thesis submitted in fulfillment
of the requirements of the degree of
Doctor of Philosophy

August 2017

ABSTRACT

This thesis focuses on exploring a multicast communication protocol for WiFi Direct (WD) 802.11 networks. The aim is to improve reliability and efficiency of multicast communication in WD networks. Multicast in WD has numerous potential applications such as local content sharing, sharing network services, playing multi-player games, and a number of other proximity based services in various fields, viz. health, sports, agriculture, transportation, and gaming. The two major issues with multicast, reliability and efficiency, have been extensively studied in literature for standard WiFi 802.11 networks. However, multicast protocols used in standard WiFi 802.11 networks cannot be straightforwardly used in WD networks because the two technologies are different. Some of these differences include multicast group formation, group architecture, network topology, role and capacity of multicast transmitter. As a result, a multicast protocol cannot achieve reliability and efficiency without taking into account the specifications of the MAC and PHY layers of WD 802.11 networks.

Motivated from the leader based approaches of standard WiFi, an Enhanced Leader Based Multicast (ELBM) protocol is proposed to achieve reliability in multicast communication in WD networks. It reduces collision and interference in multicast data transmission by improving the channel access mechanism and selecting an optimal representative multicast receiver. In order to assess the performance improvement which results from early detection of packet collision, Early Packet Loss Detection (EPLD) analytical model is proposed, which surpasses the standard protocol in terms of system throughput. Similarly, a theoretical model is formulated to investigate the new features of the MAC and PHY layers of 802.11ac, such as different Multiple In Multiple Out (MIMO) configurations, Modulation and Coding Schemes (MCS), and wider channel bandwidths under TGn channel models. Because hidden nodes can largely affect the throughput of WD networks, therefore an improved analytical model known as Vidden is developed to analyse the Very High Throughput (VHT) of 802.11ac in the presence of hidden stations. Vidden carefully calculates the collision probability by taking into account both the contending, as well as, the hidden stations

A novel adaptive algorithm is proposed to maximize the efficiency of WD 802.11 networks under a TGn channel model by choosing optimal PHY parameters in accordance with targeted Quality of Experience (QoE) for a particular application. The simulation results show that the proposed method outperforms the standard method, thereby achieving an optimal performance in

an adaptive manner. Thereafter, an efficient methodology is proposed to reduce the overall Packet Error Rate (PER) based on the simulation results.

Finally, the problem of selecting the most favourable transmission channel and rate is investigated for a multicast communication system in the context of WD 802.11 networks. To this end, a novel *M*ulti-rate *M*ulti-channel *M*ulticast (M^3-Cast) protocol is proposed, which not only chooses the most favourable communication channel and transmission rate but also takes into account the implementation details of the underlying WD technology, thereby optimizing the overall system performance. M^3-Cast is formulated analytically and evaluated by a complete system level simulation. The detailed results and analysis consider a number of performance metrics, such as bit error rate (BER), multicast capacity, and system throughput under different MIMO configurations, channel bandwidths, and various network radii. Consequently, the simulation and analytical results show that M^3-Cast protocol outperforms the standard multicast protocol of WD by almost two-fold in terms of system throughput.

STATEMENT OF ORIGINALITY

This work has not previously been submitted for a degree or diploma in any university. To the best of my knowledge and belief, the thesis contains no material previously published or written by another person except where due reference is made in the thesis itself.

Signed:

_____

Gul Zameen Khan
August 23, 2017

ACKNOWLEDGEMENTS

I am sincerely grateful to my principal supervisor Dr. Ruben Gonzalez for his excellent guidance and support throughout my PhD candidature. His encouragement, interactive and long scientific discussions, regular meetings and all his contributions have made the experience of my PhD studies a very productive and fruitful one. I am specially thankful to Dr. Ruben for his help and motivation which he provided when I needed them the most during the time of stress and uncertainty during my PhD studies. I would also express my gratitude to my associate supervisor Dr. Xin-Wen Wu and external supervisor Prof. Eun-Chan Park for their support and guidance. I cannot thank Prof. Park enough for his kindness, continuous guidance, and his detailed and effective feedback on my papers over email from South Korea.

I am also thankful to Griffith University for giving me the opportunity to pursue my PhD studies by granting me scholarships to cover my tuition fee and living expenses. I cannot forget to mention the state-of-the-art student services of Griffith University, which has always assisted me in my studies and made my stay at Griffith a pleasant and memorable experience. I am lucky enough to make great friends during my PhD studies. I am grateful to Muhammad Saqib, Owais Iqbal, Muhammad Fahim, Zahid Khalid, Afzal Qamar, Adel, Sultan, Hamid, AJ, Reza, KB, Usman, Khalid, Abdul Rehman, Gazele, Ranju, Nabeen, Rupam, and Adnan Khattak for their love and great company. They have always encouraged me in the time of despair and have also helped me in listening to my presentations and giving me feedback. I am particularly thankful to Adel for his fruitful discussions with me on probabilistic models. I am grateful to my Library rover friends especially, Lynda, Kirst, Laura, and Claire for their love and great company. I am also thankful to my dear friends back home especially Sajid, Aorangzeb, Sumair, Qazi Mudussir, Suleman, Aadil, Imran, Noman, Amir, Yousuf, and Basit, whose company has always cheered me up. I am thankful to great teachers at English Help Griffith, Owais Iqbal and Claire for proof reading some of writings in the thesis.

I would not have been able to focus on my PhD studies without the constant support, sincere prayers and unconditional love of dear Baba, Amma, and my family.

LIST OF PUBLICATIONS

List of Conferences

1. G.Z. Khan, E. C. Park, R. Gonzalez, "Performance Analysis of Early Packet Loss Detection in WiFi Direct 802.11 Networks," accepted in *The 13th IEEE International Conference on Wireless and Mobile Computing, Networking and Communications*, Rome, Oct 2017.
2. G. Z. Khan, R. Gonzalez, X. W. Wu and E. C. Park, "On the Field Level Loss of a VHT PPDU in a MIMO-OFDM System for a WiFi Direct 802.11ac WLAN," in *2016 International Conference on Frontiers of Information Technology (FIT)*, Islamabad, Dec 2016, pp. 164-169.
3. G. Z. Khan, R. Gonzalez and E. C. Park, "A performance analysis of MAC and PHY layers in IEEE 802.11ac wireless network," in *2016 18th International Conference on Advanced Communication Technology (ICACT)*, Pyeongchang, Jan 2016, pp. 20-25.
4. G. Z. Khan, R. Gonzalez, E. C. Park and X. W. Wu, "A reliable multicast MAC protocol for Wi-Fi Direct 802.11 networks," in *2015 European Conference on Networks and Communications (EuCNC)*, Paris, June 2015, pp. 224-228.

List of Journal

1. Gul Zameen Khan, Ruben Gonzalez, Eun-Chan Park , "M^3-Cast: A Novel Multicast Scheme in Multi-Channel and Multi-Rate WiFi Direct Networks for Public Safety," *IEEE Access*, vol. 5, pp. 17852-17868, 2017. DOI: 10.1109/ACCESS.2017.2749482
2. Gul Zameen Khan, Ruben Gonzalez and Eun-Chan Park, "On the Design of a WiFi Direct 802.11ac WLAN under a TGn MIMO Multipath Fading Channel," *KSII Transactions on Internet and Information Systems*, vol. 11, no. 3, pp. 1373-1392, 2017. DOI: 10.3837/tiis.2017.03.007
3. Gul Zameen Khan, Ruben Gonzalez, Eun-Chan Park, Xin-Wen Wu, "Analysis of Very High Throughput (VHT) at MAC and PHY Layers under MIMO Channel in IEEE 802.11ac

WLAN," *ICACT Transactions on Advanced Communications Technology (TACT)*, vol. 5, issue 4, July 2016, pp. 877888. [ISSN: 2288-0003 (Online)]

4. Gul Zameen Khan, Eun-Chan Park, Ruben Gonzalez, "Vidden: An Analytical Model for Very High Throughput WLAN in the Presence of Hidden Stations," submitted in *IEEE Communications Letters*, 2017.

CONTENTS

List of Figures

List of Tables

List of Acronyms

AARF	Adaptive Auto Rate Fallback
ACK	Acknowledgement
AHEC	Adaptive Hybrid Error Correction
AMSDU	Aggregated MAC Service Data Unit
AP	Access Point
ARF	Auto Rate Fallback
ARQ	Automatic Repeat Request
ARSM	Auto Rate Selection Mechanism
BA	Block Acknowledgment
BER	Bit Error Rate
BLBP	Beacon Driven Leader Based Protocol
BMMM	Batch Mode Multicast MAC
BO	Back Off
BPSK	Binary Phase Shift Keying
BSS	Basic Service Set
CRS	Cooperative Relaying Schemes
CSMA/CA	Carrier Sense Multiple Access with Collison Avoidance
CTS	Clear to Send
CTS-R	CTS Representative
CW	Contention Window
D2D	Device to Device
DBP	Delayed feedback Based Protocol
DCF	Distributed Coordination Function
DHCP	Dynamic Host Configuration Protocol
DIFS	DCF Inter Frame Spacing
DMS	Directed Multicast Service
DTIM	Delivery Traffic Indication Message
ELBM	Enhanced Leader Based Multicast
ERS	Error Recover Schemes
FEC	Forward Error Correction

GCR	Group Cast Retries
GE	Gilbert Elliott
GO	Group Owner
GPS	Global positioning system
HARQ	Hybrid Automatic Repeat Request
HLBP	Hybrid Leader Based Protocol
IBSS	Independent Basic Service Set
IE	Information Element
IoT	Internet of Things
IPTV	Internet Protocol Television
LAMM	Location Aware Multicast MAC
LAN	Local Area Networks
LB-ARF	Leader Based Auto Rate Fallback
LBM	Leader Based Multicast
LBMS	Leader Based Multicast Service
LBP	Leader Based Protocol
LBPW	Leader Based Protocol with a sliding Window
LDM	Leader-Driven Multicast
LOS	Line of Sight
MAC	Medium Access Control
MCS	Modulation and Coding Scheme
MIMO	Multiple In Multiple Out
MT	Mobile Terminal
MU-MIMO	Multi User Multiple In Multiple Out
NACK	Negative Acknowledgement
NAK	Negative Acknowledgement
NAV	Network Allocation Vector
NC	Network Coding
NCTS	Negative Clear to Send
NLOS	Non Line of Sight
NoA	Notice of Absence
OFDM	Orthogonal Frequency Division Multiplexing
P2P	Peer-to-Peer
P2P-PS	Peer-to-Peer Power Save
P2P-WMM	Peer-to-Peer Wi-Fi Multimedia
PBP	Probabilistic feedback Based Protocol
PCLP	Physical Layer Conformance Procedure
PDR	Packet Delivery Ratio
PER	Packet Error Rate
PHY	Physical
PID	Pseudo-broadcast Identity

PLR	Packet Loss Ratio
PM	Power Management
PPDU	PCLP Protocol Data Unit
QAM	Quadrature Amplitude Modulation
QoE	Quality of Experience
QoS	Quality of Service
QPSK	Quadrature Phase Shift Keying
RAK	Request for Acknowledgement
RAS	Rate Adaptive Schemes
RBAR	Receiver Based Auto Rate
RPMP	Reliable PLCP-based Multicast Protocol
RRAM	Robust Rate Adaptive Mechanism
R-S	Reed Solomon
RSSI	Received Signal Strength Indicator
RTP	Real-time Transport Protocol
RTS	Ready to Send
SIFS	Short Inter Frame Spacing
SISO	Single In Single Out
SM	Standard Multicast
SNR	Signal to Noise Ratio
SRM	Semi Reliable Multicasting
SS	Spatial Streams
STA	Station
TDLS	Tunneled Direct Link Setup
TDoA	Time Difference of Arrival
TGn	Task Group 802.11n (IEEE)
TIM	Traffic Indication Message
ToA	Time of Arrival
TXOP	Transmission Opportunities
UPnP	Universal Plug and Play
UR	Unsolicited Retries
USTA	Unicast Station
VHT	Very High Throughput
WD	WiFi Direct
WLAN	Wireless Local Area Networks
WPS	Wi-Fi Protected Setup

"If you want to find the secrets of the universe,
think in terms of energy, frequency and vibration."

Nikola Tesla (1856 – 1953)

1 Introduction

In recent years, Device to Device (D2D) communication has emerged as one of the most promising technologies in almost all popular wireless networks, including Cellular Networks, WiFi, Bluetooth, and Zigbee. It has several advantages such as increased spectral efficiency, high throughput and reduced communication delay [1]. IEEE 802.11 standard [2] is one of the mostly useful and common network access technologies that has evolved tremendously in the last decade. Just like other standards, WiFi has introduced a number of amendments in order to cope with the challenges of the new technological era where Internet of Things (IoT) is in the early stage of evolution. WiFi Direct (WD) is one such technology by WiFi Alliance which provides D2D connectivity. It enables direct communication between two or more nearby devices in an easy and quick way in the absence of an Access Point (AP) [3].

WD has a wide range of potential applications in the near future due to the following reasons.

- The number of devices that are equipped with WiFi interface is increasing exponentially [4]. At the end of 2016, the shipment of WiFi devices surpassed 15 billion units. As a result, a number of proximity-based services has evolved in the wake of IoT. With WD technology, a device can easily and quickly discover and connect to nearby devices and services [5].
- WD is a relatively cost effective and practical solution to offloading to cellular networks i.e., WiFi in conjunction with 3G/4G/5G [6], [7],[8] .
- WD can be easily implemented in the legacy WiFi devices without modifying the hardware.

Consequently, the WD is becoming an interesting and suitable candidate for communication in several application domains, including content distribution, resource sharing, emergency commu-

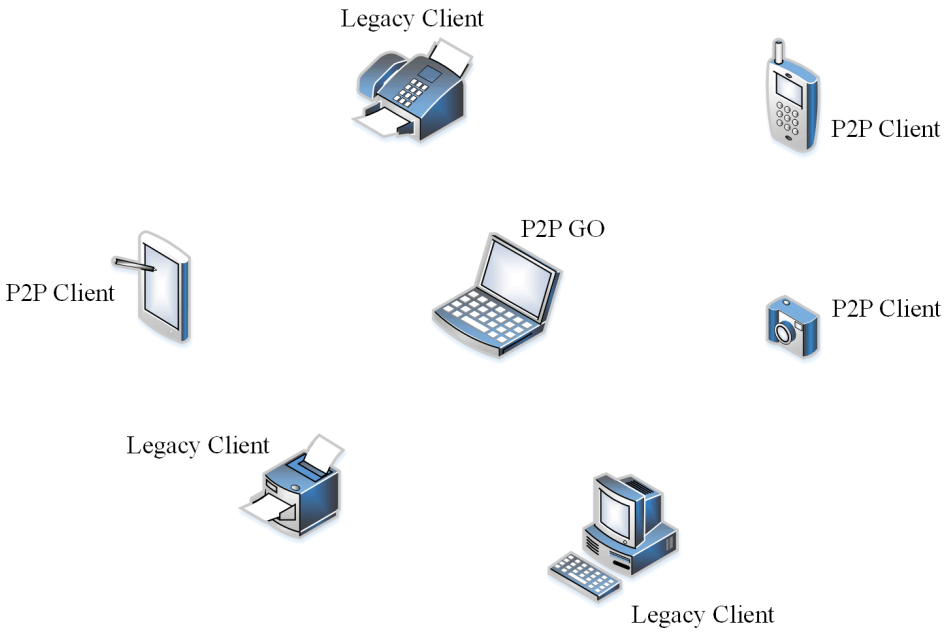

Figure 1.1: Leader Based Multicast Protocol

nication, alert dissemination, on-line gaming, proximity based advertising and social networking. The WD is also known as WiFi Peer-to-Peer (WiFi P2P). It is built upon the IEEE 802.11 infrastructure mode and offers direct, secure and rapid device to device communication. The recent WiFi P2P Technical Specification WiFi Alliance was released in 2016 [9]. WD enables devices to discover each other and form a P2P Group. In each P2P Group, one station is elected as a P2P Group Owner (GO) and the other stations join the group as clients [10]. The GO should be a WD enabled or P2P device. On the contrary, a client can either be a legacy WiFi device or P2P device.

Multicasting allows transmission of the same content to a group of receivers at the same time, thereby improving bandwidth consumption, reducing resource consumption, and increasing throughput when compared with unicasting techniques. With the proliferation of WD technology capability in current wireless devices, such as laptop, tablet, mobile phone, printer, digital camera/camcorder, IPTV, and speaker, there are number of applications where these devices participate in multicast communications as shown in Fig. 1.1.

1.1 Potential Applications

A few user cases in relation to multicast in WD networks are discussed in the following subsections.

1.1.1 Local Contents Sharing

A user wants to send some data (text file, image, audio, and/or video) from his/her mobile phone, tablet, or digital camera/camcorder with WD capability to many other nearby users, who have

wireless devices, each with a capability of WiFi and/or WD interface(s). In this case, the user does not necessarily need to connect to the internet via AP or 3G/4G to perform the task; rather, an easy and quick local solution can be provided by multicast in WD network.

1.1.2 Sharing Network Services

One of the most exciting features of WD is network services discovery which facilitates the location or proximity based services. Instant messaging among people gathered in closed proximity, for instance a campus, event spot, and community is one such example. Likewise, other similar applications are accessing application software by many participants in a training session, a video conferencing event, and sharing control information without the trouble of connecting to AP.

1.1.3 Playing Multiplayer Games

Multiplayer gaming is on the rise in the world. More and more people from all age groups are turning to games as a source of leisure and pass time. With multicast in WD networks, advanced multi-player gaming will not be just limited to cafes or gaming houses. People will be able to enjoy it on the go, from the waiting lounge of an airport to the lunch room of a corporation.

1.1.4 Social Activities

People often gather for common social activities in the real world or connect on-line on social networks for the same purpose. Multicast in WD can help people find other people with common interests in their closed proximity. A user case is an international conference in a city in which different people from various countries have participated. For the sake of example, consider a few participants are interested in visiting the popular attractions in the city, others want to taste the local cuisines in a restaurant, and similarly a few people wish to shop in the local popular market. In such a scenario, a participant can find people of similar interest in the conference with a simple application program which is based on local multicast communication in WD networks.

1.1.5 Public Safety and Health

Information about road incidents and traffic blockage can be multicasted to vehicles so that they can change their route. It can also be used if a shopping mall or any other such building is in trouble and people inside the building are needed to be alarmed and guided towards safe exits. Similarly, another use case is an emergency situation where a person needs medical treatment or first aid immediately. There may be a doctor in the closed proximity who can help right away if we manage to inform him/her instantly. In this, and many other cases, multicast capability of WD can be used to develop the required applications.

1.1.6 Commercial Services

This is an interesting application from a business point of view. A coffee shop, restaurant, or a store can send an instant message/announcement/advertisement about new deals to the subscribed customers when they come into the close proximity of the store. The marketing companies can

customize their advertisements for consumers and guide them if the customers are interested in their products.

1.2 Objectives

In spite of its useful applications, multicast in WD faces many problems and issues. There are three major problems, namely: reliability, efficiency and compatibility. The first two problems i.e., reliability and efficiency have already been explored in the literature for standard WiFi 802.11 networks. However, these protocols cannot be straightforwardly used for WD networks because the two technologies are different in many aspects such as: multicast group formation,; architecture and topology of the network; role and capacity of the multicast transmitter; and interference and collision effects on the multicast transmitter and receiver. Thus, it is necessary to explore these problems in the context of WD. The third problem i.e., compatibility arises due to different manufacturers and vendors, and can be solved by allowing interoperability among different manufacturers and vendors in the industry. Thus, the problem of compatibility is left to the industry and the two fundamental problems of reliability and efficiency in multicast communication in the WD network are investigated in detail in this thesis.

1.3 Scope of Research

In this thesis, the primary focus is on developing and testing algorithms which can improve the reliability and efficiency of multicast communication in the context of WD 802.11 networks. The techniques and methodologies presented are based on the literature related to the MAC and PHY layers of standard WiFi and WD 802.11 networks. First we define the research questions that can guide us to identify the research goals and then the proposed hypotheses on how to achieve the objectives are presented.

1.3.1 Research Questions

1. How to improve the reliability of a multicast protocol in WD 802.11 Networks?
2. How to reduce the packet loss in WD 802.11 Networks?
3. How to design an efficient multicast protocol in WD 802.11 Networks?

1.3.2 Hypotheses

In order to address the above research questions, the following hypotheses are proposed.

1. The reliability of a multicast MAC protocol can be enhanced if the level of collision and interference of multicast data with unicast data is reduced.
   (a) The channel access method can be improved as a function of changing contention window and inter frame timings.

   (b) A Leader Based Multicast (LBM) protocol can be used with an improved Ready to Send (RTS)/Clear to Send (CTS) mechanism. In addition, an effective feedback from the leader of the multicast group can be developed to provide a higher degree of reliability to multicast communication in the presence of unicast stations.

2. A detailed analytical and simulation analysis of new features of the MAC and PHY layers of 802.11ac [11] can provide an insight into developing a reliable and efficient multicast protocol for WD networks.

   (a) The system level design of a WD network under Multiple In Multiple Out (MIMO) TGn channel models can help propose the right parameter combination of the MAC and PHY layers under different environments.

   (b) Based on the Packet Error Rate (PER) analysis, a modified algorithm can be developed to improve the system level throughput.

   (c) The system performance can be improved by finding an optimal set of the MAC and PHY layers' parameters in accordance with Quality of Experience (QoE).

3. An improved analytical model of throughput in the presence of hidden nodes can be formulated to better understand the performance of WD networks.

4. New algorithms can be designed for choosing the best transmission rate and transmission channel for multicast communication in WD networks by taking into account the MAC and PHY layers of the new standards such as 802.11ac in the context of WD networks.

1.4 Contributions

The proposed techniques described and introduced in this thesis intend to achieve the research objectives. The main research contributions made in this thesis are listed below.

1. Proposal of a new protocol called Enhanced Leader Based Multicast (ELBM) to reduce the collision and maximize reliability in the presence of AP and other unicast stations.

2. Formulation of a theoretical model of the MAC and PHY layers of WD 802.11 networks under MIMO TGn channel models to achieve improved performance under given configurations.

3. Proposal of a modified analytical model known as Vidden to evaluate the performance of Very High Throughput (VHT) under hidden stations.

4. Development of novel adaptive algorithm to choose an optimal set of parameters according to targeted QoE for a particular application.

5. Development of a new method to reduce the PER of VHT PHY layer frame of WD 802.11ac networks by investigating the loss of individual fields in a packet.

6. Formulation of Early Packet Loss Detection (EPLD), which is an analytical model to evaluate the throughput with an early collision detection for WD networks by careful consideration of the MAC layer in terms of backoff counter, successful transmission time, and the time spent in collision
7. Proposal of a novel protocol known as M^3-Cast which chooses the most favourable channel and rate for a multicast communication system in the context of WD 802.11ac networks.
8. Proposal of an analytical model of early packet loss detection in WD networks

1.5 Thesis Organization

The rest of the thesis is organized as follows.

- Chapter 2 presents a review of the state of the art research related to multicast communication in WD networks. The chapter also summarizes and identifies the research gaps in the current literature.
- Chapter 3 presents the proposed algorithms which can reduce collision.
- Chapter 4 describes the proposed models to improve the performance of the multicast in WD 802.11 networks based on the analysis of the VHT.
- Chapter 5 presents the proposed adaptive QoE-based algorithm for improving the system performance.
- Chapter 6 contains the proposed M^3-Cast protocol to choose the most favourable transmission rate and channel for multicast communication in WD 802.11ac networks.
- Chapter 7 summarizes the research contributions and outlines the future research.

"If we knew what we were doing, it would not be called research."

Albert Einstein (1879 – 1955)

2

Literature Review

In this chapter, we present and discuss the relevant literature and state-of-the-art approaches related to multicast in standard WiFi and WiFi Direct (WD) networks. We investigate the limitations of the current approaches in order to identify the research scope of this thesis.

The review of the related work presented in this chapter is organised into different sections. As multicast in standard WiFi networks works as a foundation for multicast in WD networks, therefore multicast protocols described in the 802.11 baseline standard [12] are reviewed in Section 2.1. The new extensions added to 802.11 family to improve multicast protocol are presented in Section 2.2. Similarly, Section 2.3 and Section 2.4 present the recent published work on Pseudo Broadcast Multicast (PBM) and Leader Based Multicast (LBM) protocols, respectively. Then, a comprehensive literature review of Rate Adaptive Schemes (RAS) is presented in Section 2.5. In Section 2.6, few state of the art papers on Error Recovery Schemes (ERS) are discussed in Sub-section 2.6.1, which is followed by Cooperative Relaying Schemes (CRS) in Sub-section 2.6.2. A conclusion and major research gaps are discussed in Section 2.7. Finally, summary of all the techniques, which are discussed in this chapter, is presented in Section 2.8.

2.1 Multicast in the Standard 802.11 Networks

When the first IEEE 802.11 standard was released back in 1997, multicast communication in WiFi networks was not much popular among the research community [12]. At that time, multicast in IP network was the most popular area of interest both for researchers and developers interested in one-to-many communication due to its compelling applications such as audio/video streaming, sharing

control information among routers, and sharing resources [13]. However, soon after the release of 802.11 standard, multicast communication in WiFi drew the attention of many researchers due to its wide range of promising applications. Some of these applications are listed below:

- Sharing multimedia contents i.e. image, audio, video
- Real time streaming like IP TV and video conferencing
- Transmitting data and control packets in natural disasters
- Playing of video games among a group of people
- Sharing board and screen in a class room
- Providing data and application files in training sessions
- Sending text messages and alerts to a group of people in an organization or public hot spots
- Sending messages in a an environment where many people are interested in the same information like stock exchange, and airports

The first and foremost problem of the multicast 802.11 protocol which takes place at Medium Access Control (MAC) layer is reliability both in standard as well WD networks. The reason for the unreliable nature of the multicast protocol at MAC layer is collision which occurs due to the transmission of multiple packets at the same time by more than one stations. The 802.11 uses Distributed Coordination Function (DCF) at the MAC layer which is based on CSMA/CA (Carrier Sense Multiple Access with Collision Avoidance). Thus, only one station can successfully transmit at a time, otherwise collision may take place between the data and/or control frames if more than one stations try to transmit at the same time. The packet may also be lost due to weak signal in addition to collision. However, the standard WiFi and WD do not differentiate between the loss due to collision and weak signals on the first failure. There are many papers in the literature that focus on distinguishing the loss due to collision and weak signal [14], [15], [16], [17]. In order to detect the loss, the DCF protocol uses control packets such as Acknowledgement (ACK) in unicast transmission. As a result every successful unicast transmission is followed by an ACK frame. If the transmitter does not receive an ACK frame from the receiver within a specified amount of time, it is considered as a loss. When collision occurs, the transmitter doubles its backoff contention window and retransmits the packet. However, unlike unicast communication in which there is only one transmitter and one receiver, there are multiple receivers in the case of multicast communication. If the protocol allows all receivers to send an ACK packet to acknowledge the successful reception of the transmitted packet then the ACK packets from multiple receivers will always collide together and as a result the transmitter will keep re-sending the same packet over and over. In order to solve the problem of collision of ACK packets from multiple receivers, the first standard of 802.11 [12] discarded the ACK packets for multicast transmission. It solves the problem of ACKs' collision but it makes the multicast 802.11 protocol an unreliable protocol. As a result the transmitter of a multicast frame always assumes that the transmission is

successful and thus the contention window is always set to the minimum contention value after every multicast frame. Since there is no retransmission of multicast packets, therefore the multicast communication in 802.11 is non-reliable in nature.

The second problem of multicast communication in 802.11 networks at Physical (PHY) layer is the efficiency degradation which results from the co existence of multiple stations with different transmission rates in the same multicast group. The performance anomaly problem was first observed for unicast communication by M. Heusse etl. al. [18] in which the performance of all hosts is considerably degraded when some mobile hosts use a lower bit rate than the others. As multiple receivers are involved in a multicast group, therefore the performance can be degraded by choosing one rate over the other given that different receivers operate at different rates. In order to find an easy solution, the 802.11 multicast protocol fixed the transmission rate to a basic rate (for example, 6-24 Mb/s are the basic rates in 802.11a standard [12]) at the PHY layer for multicast communication. The basic rate may change for other standards.

The basic procedure of multicast is described in the baseline wireless LAN MAC 802.11 specification [12]. Only the Access Point (AP) is allowed to send multicast frames in infrastructure Basic Service Set (BSS). The other STAs can only receive the multicast frames. The AP sends the multicast frame after the Delivery Traffic Indication Message (DTIM) to the intended receivers. DTIM is an 8-bit count field in Traffic Indication Message (TIM). It indicates how many Beacon frames (including the current frame) appear before the next DTIM. A DTIM Count of 0 indicates that the current TIM is a DTIM. TIM is included in the beacons sent by AP to tell the station in Power Save Mode (PSM) that the AP has data for them. The STA in PSM send PS-POLL message to AP once it gets TIM in the beacon showing that there is data pending for it at the AP. Thus the AP stores the multicast frames and wait for the PS-Poll messages from STAs which are in the sleep state. Once all the STAs are in active state, the AP broadcasts the multicast frames after DTIM. Each STA is supposed to wake up at DTIM. An example of multicast in BSS is shown in Fig. 2.1.

Similarly, in Independent Basic Service Set (IBSS), the STA who has multicast frame sends a request frame to all the receivers. In IBSS all the STAs whether in PSM or not have to wake up in a window of time called Announcement Traffic Indication Map (ATIM). Each intended receiver of the multicast sends acknowledgement of the multicast request frame and stays awake during the ATIM window. When the transmitting STA gets ACKs from all the receivers, it then broadcasts the message. An example of multicast in IBSS is shown in Fig. 2.2.

2.2 New Extensions to Standard Multicast Protocol

In order to improve the reliability of MAC multicast frames in 802.11, many additional protocols have been added to the new standards. In IEEE 802.11v [19], a new protocol is added called Directed Multicast Service (DMS). The aim of DMS is to achieve reliability for multicast transmission and achieve low jitter characteristics for broadcast and multicast audio/video streams. It

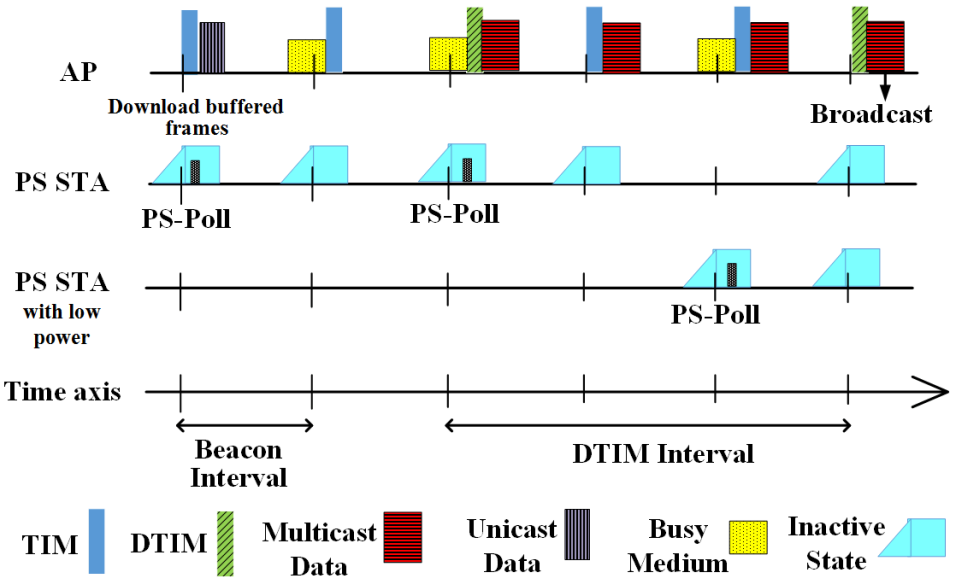

Figure 2.1: Multicast Protocol in BSS

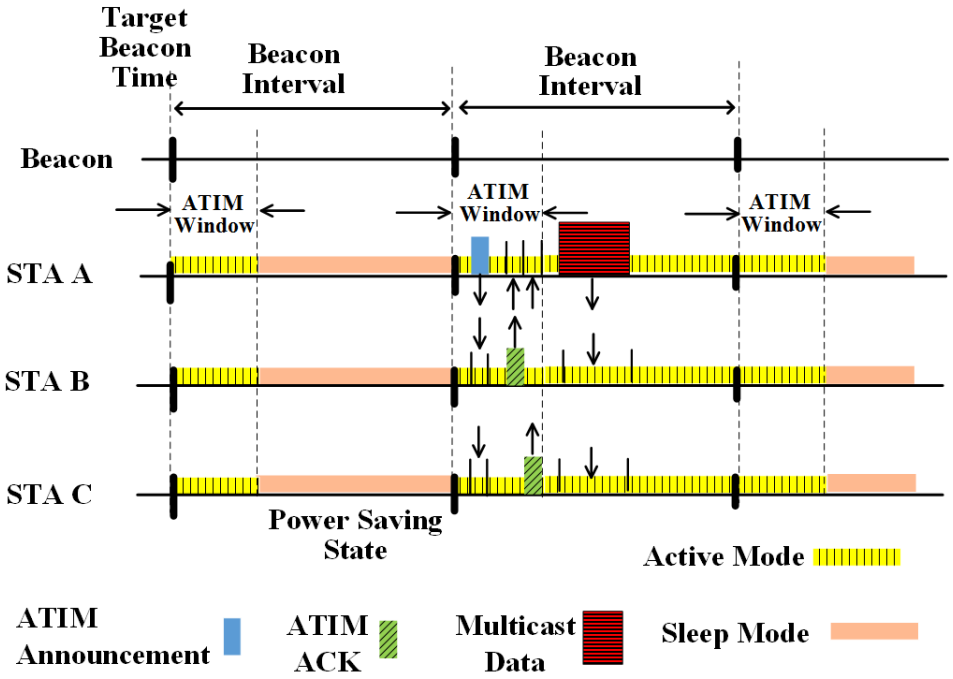

Figure 2.2: Multicast Protocol in IBSS

works simply by converting all the multicast frames into a series of unicast frames destined to each of the intended receivers. In this way the use of MAC-layer Automated Repeat Request (ARQ), Ready to Send (RTS) / Clear to Send (CTS) exchange and higher PHY rates become possible to get the desirable reliability. The multicast frames are processed using the technique of Aggregated MAC Service Data Unit (A-MSDU). An individual receiver address is written in the destination address (DA) field of the MAC header, while the multicast address is written in the DA field of

each A-MSDU sub-frame header. DMS achieves reliability but the protocol becomes very slow when the number of receivers is increased in the multicast group. Thus it is not suitable for larger group communication [2].

The IEEE 802.11aa specifications [20] describe GroupCast Retries (GCR) service to achieve more reliability for one or more multicast frames. The reliability is acquired through Unsolicited Retries (UR) or Block Acknowledgement (BA). It aims to get feedback and admission control for multicast traffic. In GCR with UR, the multicast frames are retransmitted one or more time (up to a specific life limit) to increase the chances of correct reception of the multicast frames by all receivers in multicast group. GCR-UR tries to reduce the loss of multiple multicast frames by accessing the medium in different Transmission Opportunities (TXOP). The advantage of GCR-UR is its low overhead. However there is no granularity to select which flows are GCR protected and which are not. Furthermore, GCR-UR requires the transmission of the multicast packets several times in order to increase the probability of the successful delivery. This policy retains the scalability since the overhead does not depend on the group size. However, the transmission redundancy limits the efficiency of GCR-UR significantly.

On the other hand, GCR with BA exploits the technique of block acknowledgement of 802.11n [21] in order to improve the reliability. The sender of the multicast frames establishes admission control for block acknowledgement with all the receivers in the multicast group. The sender then transmits streams of multicast frames which are also called groupcast data frames. After the transmission, the groupcast sender sends a request for Block ACK to all or a sub set of receivers. The intended receivers reply with Block ACK. In this way the lost frames can be found by the multicast sender and those frames are retransmitted. Thus the reliability of multicast frames is improved. However GCR-BA is not a suitable choice for large multicast groups because it introduces delay in such cases.

2.3 Pseudo-broadcast Multicast

In [22] a pseudo-broadcast method was proposed for receiving a multicast IPTV transmission from a common gateway to various set-top-boxes in different rooms. The authors claim that this way of promiscuous reception of unicast transmission, achieves high reliability and high efficiency as compared to broadcast delivery.

The two claims that are presented in the paper are achieved in the proposed scheme; however there are certain limitations in this mechanism. First the scheme uses the unicast transmission for sending the IPTV delivery to a specified destination which is selected on the basis of the link quality. In this way the contents are retransmitted when failed at the selected unicast destination. Thus it is reliable for this station but what about the failure at the other stations which receive the delivery in promiscuous mode? Secondly, unlike low rate transmission in multicast transmission in 802.11, the promiscuous transmission can use the rate adaptation algorithm as it is unicast. The authors propose the use of measurement request and measurement reply frames in 802.11k [23]

for this kind of information. This results in improving the efficiency.

An inherent problem with promiscuous reception is the extra processing. Every station has to receive every transmission in the air and then process it irrespective of the fact whether it belongs to it or not to make the decision of accepting or rejecting the packets. This will definitely incur extra processing.

The authors intelligently use the control frame to their benefit; however it introduces an undesirable limitation in the protocol. The length of the subtype field is 4 bits in frame control MAC which is used as Pseudo-broadcast ID (PID) for identifying any specific channel. It means only 16 channels can be seen which is not a good restriction in todays world where people are interested in getting hundreds of channels.

Although the arguments are testified by experimental results in which the performance of pseudo-broadcast is compared to unicast and broadcast in terms of frame loss rate and channel idle time. But the frame error rate will be unexpectedly changed if one of the receivers changes the channel quickly. This is because the algorithm chooses a new designated receiver each time a new receiver joins or leaves. As a result, the gateway has to gather information about frame error rate from all receivers even if one user is simply browsing the TV channels.

Similarly, the paper by Peng et.al [24] explored three different methods separately and in combination to improve the quality of multicasting video on wireless local area networks. The first approach is leader-driven multicast (LDM) which monitors the MAC layer unicast (re)transmissions by other receivers. The other two techniques are application-level forward error correction (FEC) using block erasure codes; and negative feedback from selected receivers in the form of extra parity requests (EPR).

Pace et.al in [25] and [26] presented WEVCast system for transmission of multimedia video contents to a large group. It is based on sending video packets to a single Target Node (TN) in unicast mode while the other nodes within the AP coverage area can switch in overhearing mode to automatically eavesdrop the video transmission. In addition, a feedback mechanism, based on RSSI messages periodically sent by the client nodes, has been added and managed by the sender node to dynamically adjust the transmission data rate.

Jean Tourrilhes [27] proposed a robust broadcast to overcome the collision losses for broadcast transmissions by selecting a collision detector node before transmitting multicast data which returns an ACK packet for a multicast packet. However, the complicated mechanism of choosing the station and retransmitting multicast packets must be implemented on the MAC layer.

Likewise a Cisco white paper [28] examines the challenges of delivering business video over Wi-Fi and discuss key technical elements that can help to provide an intelligent, flexible platform for real-time video applications. A multicast-to-unicast capability is implemented in the context of CISCO systems. In the same way [29] and [30], proposed pseudo-broadcast approach to convert the multicast traffic into unicast streams. In [31] Chandra et al. proposed DirCast, where the AP transmits multicast data packet addressed to a unicast receiver while the others listen promiscuously. DirCast uses four techniques which are pseudo-broadcast, association control, destination

control and proactive FEC. As already mentioned previously pseudo broadcast is the transmission of a unicast data packet which is received promiscuously by the other receivers. Chandra et al. consider a situation where there is a number of receivers, each of which can join more than one multicast group and also there is more than one AP. DirCast uses a DirCast server to perform association control that selects the AP that a multicast group member should join with, so that it reduces the air time usage. In fact in their experimental analysis, DirCast always used 2 out of 3 APs to transmit multicast data packets to 12 receivers, decreasing the airtime utilization. However, since they consider a dynamic medium, Chandra et al. also proposed that the DirCast Server should select the Target Client for each multicast group of each AP by observing the loss experienced periodically, whenever a receiver joins a multicast group or any receiver experiences more than 10% packet loss. The last technique i.e. proactive FEC, tackles the fact that the losses experienced by the non-Target Client may not necessarily be correlated with the packet loss experienced by the Target Client. Therefore, the DirCast Server transmits proactively redundant packets so that any receiver can mitigate the loss it experienced.

2.4 Leader Based Multicast

Kuri and Kasera suggested in [32] an ARQ-based approach for reliable multicast protocol at MAC layer in a single channel which is shared among multiple stations simultaneously. It is argued that the wireless links are prone to more errors as compared to wired links. Thus the local error recovery helps in increasing throughput and decreasing delay and bandwidth consumption as compared to sending the retransmission from the original sender. The authors have categorized their work in three protocols each aiming at successful reception of multicast frames by all receivers in multicast group. The first and foremost approach is called Leader Based Protocol (LBP) in which one receiver is elected as a leader. The base station sends RTS to all receivers. The leader replies CTS if it is ready otherwise stays silence. The non-leader receivers do nothing if they are ready. If any of these receivers is not ready, it sends Not CTS or NCTS to the base station. After the CTS frame is heard by the base station, it sends the multicast streams. The leader of the group transmits ACK if the multicast transmissions are successfully received otherwise stays silence. On the other hand, the other receivers keep silence if they receive the multicast frames successfully and send Negative ACK or NACK to the base station in case of failure. If the leader does not get the multicast frames and all other receiver do, the base station will receive nothing as everyone will remain silence in this case. Similarly if the leader and any of the receivers do not get the multicast transmission, the non-leader receiver will sends NACK. The ACK will be collided with one or more NAKs to ensure the sender of the failure.

In addition to LBP, two other protocols are also described namely: Delayed Feedback-Based Protocol (DBP) and Probabilistic Feedback-Based Protocol (PBP). In DBP, the AP sends multicast RTS and starts a timer waiting to receive CTS. On the other hand, each receiver sets a random timer whose value is less than that of AP. If the receiver hears a CTS within its timer, it does not send CTS otherwise it transmits CTS. This protocol tires to reduce the CTS collusion using the random

timers. The second proposed scheme i.e. PBP is similar to DBP with only one difference. Unlike random timers in DBP, the receiver uses a randomly chosen probability to decide whether to send CTS or not.

Although DBP outperforms PBP using shorter mean access time but LBP is comparatively better than DBP and PBP in terms of throughput and channel holding time. The given algorithms try to mitigate the problem of non-reliability by proposing a mechanism for CTS and then minimizing the effects of CTS collision. However the authors have made many assumptions which do not model the real environment, for example: only the multicast traffic is considered. On the contrary there is always other unicast transmission going on in the surrounding environment. In addition, it is assumed that the control packets never get lost which is not true because the wireless medium is a harsh medium and there is always high probability of packet loss due to collision, interference and bad channel conditions.

There are many limitations in Kuri et.als paper. First, the protocols are compared with themselves and not with other protocols in the literature. Secondly, the algorithms are neither tested using simulation results or implemented in hardware. Thirdly, the performance of LBP will degrade in the presence of mobility because once the leader quits, the AP will never know immediately and it will keep sending RTS. This will also incur delay in multicast transmission. Similarly, in DBP, the RTS CTS collision may decrease the performance. In the same way, the parameters L, T and N used in DBP are not optimally determined. Lastly, the election of leader is not proved to be efficient.

S.K Gupta et al [33] proposed a protocol to remove the drawback of LBP in high mobility wireless networks in which a new leader has to be selected whenever the current leader leaves the group due to high mobility. This affects throughput and reliability. The authors proposed an extension called 802.11MX which is based on Negative Acknowledgement (NAK), Negative CTS (NCTS) and tones to minimize the problem of non-reliability.

Although the proposed algorithm contributes towards solving the problem of collision of multiple CTSs in LBP by introducing a narrow-bandwidth sinusoidal signal called tone to send NAK or NCTS instead of NAK or NCTS packets. However the tones need extra hardware and it is not compatible with the current Wi-Fi cards. The obvious benefit of the tone is that it does not matter how many receivers are transmitting the tones at the same time because the collision has no effect on tones.

The main idea of this paper is that the senders sends RTS to all the members of multicast group and then waits for NCTS tone. If it does not hear any NCTS tone, it starts the transmission of multicast data. On the other hand, the receiver transmits NCTS tone if the node is not ready. Similarly the receiver waits to hear NAK tone after sending the multicast data. If there is no NAK, the data is received successfully by all receivers otherwise it retransmits the multicast data. The receiver sends NAK tones if either the timer expires which is set after receiving RTS or the packet received is corrupted.

The major weakness of the paper is the requirement of the extra hardware for generating the

tones which is not a flexible and realistic approach. In addition to the extra cost and complexity, the proposed scheme is neither compatible with the currently deployed Wi-Fi device hardware nor with the base MAC 802.11 protocol. The authors do not take into consideration the fact that the loss of RTS is a false positive alarm for the multicast data sender. If the RTS is lost in the air, a receiver which is not ready for receiving the multicast data will not transmit NCTS tone which is taken by the sender as false positive for multicast transmission. In addition, the paper makes no attempt to consider many other factors that can affect the throughput and reliability. For example packet loss due to the movement of the node from the senders range is not taken into account. Similarly the effect of multi rate nodes is not shown in the simulation results. Taking this into one more level, the simulations are performed only for a single error rate not for different ranges of error rates which is an important factor to be considered.

Similarly, two reliable multicast protocols i.e., leader-based protocol with a sliding window (LBPW) and leader-based protocol with a sliding window and n-fold acknowledgement reduction (LBPR (n)), are proposed in [34]. Firstly, the pipelining technique is added into LBP to form LBPW so as to make frame transmission efficient. Then, an acknowledgement reduction scheme is incorporated into LBPW to form LBPR (n) to alleviate the ACK/NAK implosion problem. A Reliable PLCP-based Multicast Protocol (RPMP) was proposed in [35] that use NAK and adds one additional OFDM symbol in the Physical Layer Convergence Procedure (PLCP) header of the multicast frame instead of using additional control frames.

Authors in [36] focused their experiments on multicast streaming in 802.11g environment and studied the performance of LBM in comparison to standard multicast services. The loss correlation has been determined between a small numbers of WLAN equipped laptops. The results are used to compare video streaming using leader based ARQ schemes and legacy multicast. Unfortunately the paper does not describe how the correlation was calculated making it difficult to verify the results, but have not employed any subjective quality assessment methods. A similar leader based approach was proposed in [37] in addition to two mechanisms to adapt the PHY data rate of multicast flows: the simplest leader-based mechanism (LB-ARF) and the Robust-Rate Adaptive Mechanism (RRAM). Similarly, Nicolas et. al [38] experimentally assessed the viability of employing commercially available IEEE 802.11n hardware to multicast real-time multimedia content, requiring high bandwidth and low delay. The leader based unicast is insufficient to support multicast multimedia in real-time, since there is no guaranteed maximum latency. Min-Te et.al in [39] proposed two protocols namely Batch Mode Multicast MAC (BMMM) and Location Aware Multicast MAC (LAMM) to reduce the average time to complete a multicast/broadcast. This is achieved by decreasing the number of contentions and using the location information of stations. In BMMM the multicast sender transmits RTS to all the receivers in which it instructs the receivers about the order in which they should send the CTS in order to avoid the CTS collisions. In the same way the ACK is only sent when it is requested by the transmitter with the help of a new control message called Request for ACK (RAK). However one of the limitations of the algorithm is that the baseline MAC has to be changed in order to add RAK frame. The second protocol that is LAMM is based on the assumption that all stations have GPS which limits the applications of

the algorithm. The multicast receiver selects a sub set of multicast based on the locations and the transmission is considered successful if it is received by all these intended receivers otherwise not. The authors have analyzed that the contention phases are reduced with the use of the proposed protocols. Although the simulation results show a better successful delivery rate with the density of neighbours and message generation probability however the request for sequential CTS and the addition of RAK may incur delay in the multicast transmission. In addition, the presence of other unicast transmissions may decrease the performance of the protocol.

In [40] Zhao et.al. proposed that application layer error recovery schemes like ARQ and forward error correction incur more delays as compare to the MAC layer error correction schemes due to fast feedback and retransmission. An enhanced mechanism is suggested by authors to overcome the two main drawback of LBP. The main idea of BLBP is to send a beacon frame before the transmission of multicast data. The other working of BLBP is similar to LBP. The authors claim beacon to guide the non-leader receivers by setting timers and receiving sequence number of the multicast data frame. In this way the unnecessary retransmissions can be reduced which leads to better performance in terms of less channel holding time and less multicast delay in high data rates as compared to LBP. The results are evaluated and validated by simulations as well as analytical analysis.

The BLBP improves the two main limitations of LBP. Firstly the LBP is unreliable for non-leader receivers because if the entire frame is lost in the air, the non-leaders do not know about this and therefore cannot send NACK. This problem is removed in the BLPB by setting a timer at all the non-leader receivers as soon as they get the beacon. If the data frame is lost, the timers will expire and the non-receivers will send NACK. The second problem of BLP is its poor performance in high data rate because the receiver sends NACK if the current frame is in error irrespective of the fact whether it has already received or not. This problem is solved by intruding sequence number in the beacon frame. However the authors ignore the fact that the beacon frames may collide or lost due to many potential problems of wireless medium. The performance of the BLPB may degrade in such cases.

The two major problems of the algorithm are its non-compatibility with the base MAC protocol and some of the impractical assumptions. Firstly the addition of new beacon needs changes in the base MAC protocol because normally beacon is not sent before the transmission of multicast data. Secondly, the channel is considered error free for control messages i.e. RTS, CTS, ACK and beacon frames which is not a realistic approach. In addition to the two major drawbacks, the performance of BLBP is not very effective in low data rate. One other limitation is that all stations in simulations and analysis are 24 Mbps. The effect of algorithm for multi-rate stations is not evaluated in the paper. Similarly, no other leader election mechanism is considered except the simplest process of making the first station joining the group to be the leader.

In [41], a leader was preselected to send ACK to multicast frames, to avoid collisions among multiple ACK frames. If a non-leader client fails to receive a frame, it sends a negative ACK frame to corrupt the ACK frame from the leader, to trigger a retransmission from the sender. It was shown through experiment that LBP outperforms the standard link-layer multicast if the leader

is properly selected. However, as discussed earlier, LBP may lead to unnecessary retransmissions since non-leader clients do not know whether they have received an incorrect frame.

Li and Herfet in [40] introduced Beacon-driven Leader Based Protocol (BLBP) to guarantee a low Packet Loss Ratio (PLR) under strict delay constraints for video multicast over a Gilbert-Elliott (GE) channel. A Hybrid Leader Based Protocol (HLBP) was proposed in [42] that transmits the original data packets using raw broadcast and retransmits parity packets using an improved BLBP which is based on block feedback. A comparison was presented in [43] among LBP, BLBP and HLBP. BLBP needs the minimum number of redundancy transmissions among all pure ARQ based schemes while HLBP needs the near-minimum number of redundancy transmissions among all schemes. Due to the simplicity and efficiency, BLBP is a good choice for IPTV multicast delivery.

In [44] a cross-layer auto rate selection multicast mechanism was proposed for multi-rate wireless LANs, namely auto rate selection for multicast (ARSM). It adapts the data transmission to the varying conditions of the channel and takes into account the characteristics of various applications. Similarly the [45] introduced the LBM which is based on receiving ACKs from a leader in successes and NAKs from other stations in failures. A multicast sender can retransmit erroneous data, adapt transmission rate, and adjust contention window size.

Two mechanisms were proposed in [46] namely: Semi-reliable multicasting (SRM) and Probing-based auto-rate fall back (PARF). SRM selects a leader who sends feedback information to lessen the reliability problem of multicast frames while PARF allows the multicast source to adjust the bit rate depending on the link conditions of multicast recipients. However its performance statistics do not defer substantially from the ones reported for the previous approaches (LBP used together the ARF protocol). The main drawback of most proposals reported in the literature to date is that they do not provide a complete solution to overcome the main error sources, i.e., channel access conflicts and channel varying operating conditions.

The authors in [47] proposed (Leader Based Multicast Service)LBMS that consists of a leader-based transmission and feedback mechanism for multicasting by extending the IEEE 802.11v [19] standard. However, the selection of the leader(s) or subset of the receivers to provide feedback, can compromise service reliability LBMS.

2.5 Rate Adaptive Schemes

The original IEEE 802.11 supported a single base rate, typically 2 Mbps, whereas the multi-rate enhancement enables the data transmission at various rates. The rate to be used is selected by taking into account the wireless channel conditions, given by the signal-to-noise ratio (SNR). Since the multi-rate enhancements are implemented into the PHY layer, the MAC mechanisms should be adapted in order to fully exploit them. The Auto Rate Fallback (ARF) protocol is the best known commercial implementation of the IEEE 802.11 MAC making use of this feature [48]. Under the ARF protocol, after the reception of ten consecutive ACKs, the next higher mode is

selected for future data frames. If the delivery of the 11th frame is unsuccessful, it immediately falls back to the previously supported mode. During other cycles with less than ten consecutive ACKs, it switches to a lower rate mode after two successive ACK failures. Since the ARF protocol selects the data rate taking into account the channel conditions between the AP and a given mobile terminal (MT), it is only suitable for point-to-point communications. In the case of multicast communication it is more difficult to determine the highest data rate to be used since the channel conditions between the AP and each one of the MTs in the multicast group may differ and no feedback is available. In most current set-ups, it is left to the network administrator to set up the data rate to be used by the multicast service. This rate is then used to provide network connectivity to all the MTs covered by the AP. It is obvious that, in order to ensure full coverage, the rate to be used is determined by using the channel conditions between the AP and the MT exhibiting the worst channel conditions. Furthermore, since the coverage of the AP is inversely proportional to the transmission data rate, the administrator should then select the proper data rate according to the distance between the AP and the worst MT. As the distance increases, the data rate has to be reduced in order to compensate for the increased range that the AP has to cover [46].

Moreover, as shown in [49], the performance of an IEEE 802.11 WLAN is severely affected when operating at such low PHY data rates. This simple approach does not efficiently support the point-to-multipoint communications service. Similarly, the authors in [50] presented RTS/CTS based rate adaptive MAC protocol called the Receiver-Based AutoRate (RBAR) protocol in which the rate adaptation mechanism is in the receiver instead of in the sender. The source sends RTS. The receiver of the RTS frame calculates the transmission rate to be used by the upcoming data frame transmission based on the SNR of the received RTS frame and on a set of SNR thresholds calculated with an a priori wireless channel model. The rate to use is then sent back to the source in the CTS packet. The RTS, CTS, and data frames are modified to contain information on the size and rate of the data transmission to allow all the nodes within the transmission range to correctly update their Network Allocation Vector (NAV). However RBAR has several limitations:

- The threshold mechanism used in each receiver to pick the best possible rate requires a calculation of the SNR thresholds based on an a priori channel model.
- The algorithm assumes that the SNR of a given packet is available at the receiver, which is not generally true: some (but not all) 802.11 devices provide an estimation of the SNR by measuring the energy level prior to the start of the reception of a packet and during the reception of the packet. The RTS/CTS protocol is required even though no hidden nodes are present.
- The interpretation of the RTS and CTS frames and the format of the data frames are not compatible with the 802.11 standard. Thus, RBAR cannot be deployed in existing 802.11 networks.

Mathieu Lacage et al. [51] proposed an Adaptive ARF (AARF) algorithm for low latency systems that improves upon ARF to provide both short-term and long-term adaptation. The step

up parameter is doubled every time the algorithm tries to increase the bit rate and the subsequent packet fails.

The importance of transcoding as proposed by Chiou et al. [52] and Chen et al. [53]-[54] lies in the fact that when a referenced frame is in error, the error will propagate from one frame to another, highlighting the advantage of modifying the application-layer parameters, especially increasing the intra-frame rate in order to improve the video quality, despite the increase in bandwidth consumption. However, they did not propose the adaptation of a whole frame but of the most important macroblocks within a frame, a classification evaluated at the server.

In [55] the authors proposed a scheme that takes into account the varying channel conditions of multiple users, and dynamically allocates available bandwidth between source coding and channel coding. In particular, source coding parameters (intra update and quantization) and application-layer FEC code rate are chosen jointly to optimize a multicast performance criterion, based on feedbacks from all multicast receivers.

A rate adaptation algorithm was proposed in [56] that utilizes RTS/CTS control frames to enable receivers to perform channel estimation and rate selection while taking advantage of feedback collisions to deliver this information to multicast transmitter. The transmitter sends RTS frame to indicate the beginning of a multicast transmission. Each member measures the RSS of the received RTS frame. In response to the successfully received RTS frame, each member simultaneously sends a variable length dummy CTS frame. The variability of CTS frame length depends on the selected modulation scheme. The simultaneous transmissions of CTS frames will surely cause a collision at transmitter's interface. A transmitter will take advantage of this collision by sensing the channel and measuring the collision duration. After collision is over, depending on collision duration, transmitter can predict the lowest data rate request and will transmit data frame accordingly. However its performance is related to the size of MCS set. When the size is small, such as 4 in IEEE 802.11b, the multi-rate multicast protocols work well. However, in 802.11n, there are 76 MCS schemes, and then protocols like [56] cannot work well.

In [57], Villalon et al. have proposed an auto-rate selection mechanism for multicasting (ARSM). ARSM dynamically selects a multicast rate based on the feedback information pertaining to channel conditions perceived by mobile stations. ARSM also solves the fairness and the packet loss problems by utilizing LBP. However, ARSM requires the introduction of new MAC control frame formats and the modification of the PHY (PLCP) header as well. This makes it incompatible with the 802.11 standard. Similarly, Park et al. [58] proposed SARM (SNR-based Auto Rate for Multicast) which is a rate adaptation mechanism for multicasting multimedia content. It uses an auxiliary signalling method to obtain the channel quality for each mobile node and adapts the transmission rate based on the SNR of the node experiencing the worst air-channel. It makes use of Peak Signal to Noise Ratio (PSNR), basically used to compare quality of receiving to transmitting videos, to estimate quality. However, PSNR can only be measured once the video traffic has arrived at receivers, so this approach is not appropriate for controlling admission in real-time.

2.6 Other Schemes

2.6.1 Error Recovery Schemes

The ERS of 802.11 i.e. Automatic Repeat reQuest (ARQ) is not feasible in multicast, since there is no acknowledgement or request of packet-retransmission in multicast communication. Therefore, multicast is inherently vulnerable to the transmission failures caused by wireless channel errors. To overcome this deficiency, many Forward Error Correction (FEC) schemes have been proposed in the literature. FEC at the application layer is a promising alternative for handling losses in multicast services. The basic idea of FEC is that redundant information is sent a-priori by the source station, in order to be used by the receivers to correct errors/losses without contacting the source. Since CRC-based error detection at the link layer results in the removal of the corrupted packets, many FEC-based protocols try to recover these packets [59]. It is one of the very first implementations of FEC for wired computer communication, which implemented an FEC using Vandermonde matrices that can increase scalability for applications using multicast. However, such a scheme introduces overhead since extra parity packets are now transmitted by the source station. The overhead introduced is the number of parity packets to be sent for k source packets. The number of parity packets, m, can be determined as shown in eq. (2.1).

$$m = \frac{kP_E}{1 - P_E} \tag{2.1}$$

where PE is the Packet Error Rate (PER). Note that, the level of the overhead depends on the packet error rate, PE, in the network. Thus, the higher is the packet error rate, the more the parity packets that must be transmitted by the server, and therefore the more the overhead and the less the FEC rate, which is the ratio of source packets to the total number of packets as shown in eq. (2.2).

$$\frac{k}{k+m} = 1 - P_E \tag{2.2}$$

Unfortunately, FEC is computationally expensive and has additional energy requirements. However, better performance results can be obtained when using FEC in conjunction with re-transmissions to deliver the necessary reliability which is called Hybrid-ARQ (HARQ).

Alay et al. [60] proposed a joint transmission rate and FEC adaptation algorithm to maximize the multicast performance. The basic idea behind the proposed system is that all the multicast receivers periodically send PER information to the AP. Based on the received PER information, the AP identifies the worst channel and adjusts the transmission rate and the FEC based on this PER. The source first transmits k data packets and after receiving feedback from the receivers, transmits the maximum requested number of parity packets, always creating new parity packets at every retransmission request. The transmission of parity packets instead of the retransmission of data packets is called code combining [61]. Chou et al. [62] also proposed transmitting delayed parity packets exactly after transmitting the data packets using different multicast groups up to the delay bound. Another variant included the use of layered FEC, where each FEC layer contains parity

packets related to one video layer [63], considering hierarchical video encoding. The receiver then decides which data and FEC layers it receives. Even though this scheme was proposed for the MBone, layered FEC encoding was also implemented in wireless multicasting systems [63, 64, 65, 66, 67, 68, 69].

In [70] the authors proposed an adaptive H-ARQ MAC layer protocol where different levels of FEC encodings are used depending on the channel conditions. It is up to each receiver to notify the multicast transmitter of the required FEC encoding rate by using a modified RTS/CTS exchange protocol. The authors performed R-S encoding on the data payload, so that the protocol can be integrated with legacy multicast. However using control frames which cannot be understood by legacy multicast does not necessarily prohibit the integration with legacy devices, especially if these are used only for handshake purposes allowing the AP to transmit a multicast data packet unmodified. M. Schaar et al. [71] evaluated different error control and adaptation mechanisms available in the different layers for robust transmission of video, namely MAC retransmission strategy, application-layer forward error correction, bandwidth-adaptive compression using scalable coding, and adaptive packetization strategies. Subsequently, they proposed an adaptive cross-layer protection strategy for enhancing the robustness and efficiency of scalable video transmission by performing trade-offs between throughput, reliability, and delay depending on the channel conditions and application requirements.

Besides distinguishing between the priority of packets according to the importance of the frame they originate from, Xu et al. [65] also proposed three algorithms to decide whether the reliability should be enhanced via FEC only, FEC and retransmission of data packets or retransmission of data packets. Which of the three algorithms is employed depends on the average number of lost packets experienced relative to the number of data packets and redundant parity packets. The ERS is applied to the packets of those frames which Xu et al. term as QoS-essential frames i.e. the I-frames and some or all of the P-frames.

Similarly, [72] presents an experimental study of a proxy service to support collaboration among mobile users. Specifically, the paper addressed the problem of reliably multicasting web resources across wireless local area networks, whose loss characteristics can be highly variable. The software architecture of the proxy service is described, followed by results of a performance study conducted on a mobile computing testbed. An adaptive forward error correction mechanism was proposed, which adjusts the level of redundancy in response to packet loss behaviour, can quickly accommodate worsening channel characteristics in order to reduce delay and increase throughput for reliable multicast channels.

In order to be able to distinguish between packet losses due to congestion and the dynamic nature of the wireless medium, Tang and McKinley [73] require a bitmap to be fed back to the source using the NAK, which shows which packets were lost. They assume that the packet losses experienced by the entire multicast group are due to buffer overflow at the AP and hence should not affect the proactive parameter adaptation. This scheme however has the drawback that it requires feedback from every receiver and hence the scheme must find an optimum way how all the receivers who experience a loss can inform the source without causing feedback implosion,

transmitting at the same time avoiding collisions and do not cause an excessive increase in the delay to transmit the next video frame. Combining FEC and ARQ schemes using a multiple number of retransmission rounds and NAKs to retransmit either data packets or redundant packets at the Real-time Transport Protocol (RTP) level via Adaptive Hybrid Error Correction (AHEC) [74] is another means of increasing reliability and the QoS at the receivers end. However, limited multicast topologies with small groups of multicast receivers connected directly to the source were considered.

2.6.2 Cooperative Relaying Schemes

In a regular Wi-Fi network, the stations communicating with AP often have different signal qualities, resulting in different transmission rates. This induces a phenomenon known as the rate anomaly problem [75], in which stations with lower signal quality transmit at lower rates and consume a significant majority of airtime, thereby dramatically reducing the throughput of stations transmitting at higher rates.

The notion of opportunistic repeating for 802.11 WLANs is proposed in [76]. The idea is to have wireless links dynamically switch between direct transmission and two-hop mesh packet forwarding. The authors called the system SoftRepeater, which enables stations (known as repeaters) with good signal strength and high transmission rates to opportunistically act as relays for stations (known as clients) with poor connectivity to the AP and low transmission rates. This can only be achieved by having the repeater alternately switch between the infrastructure mode (for communication with the AP) and the ad hoc mode (for communication with the client). However, in SoftRepeater the clients perform only passive measurements.

Jie Xiong et al. [76] presented PeerCast, a wireless multicast protocol that engages clients in cooperative relaying. Instead of broadcasting to all the clients at the bottleneck rate, the AP selects a higher rate to deliver a batch of packets to the majority of clients. Then, the AP chooses a suitable subset of these clients to relay the packets to the weaker ones. Since the channel quality between a strong and weak client can be significantly better than that between the AP and the weak client, the relayed transmissions can also occur at higher rates. Multiple transmissions at higher data rates can finish quicker than a single transmission at the low (bottleneck) rate. The authors showed that multicast throughput and reliability can both be improved.

Similarly in [77] the authors presented PULLCAST, a cooperative protocol for multicast systems, where nodes receive video chunks via multicast from a streaming point, and cooperate at the application level, by building a local, lightweight, P2P overlay that support unicast recovery of chunks not correctly received via multicast. PULLCAST sends 1-hop hello messages to build a local neighborhood where chunks can be retrieved sending unicast messages to pull a chunk from a neighbor that has it. Although the scheme uses P2P for improving multicast performance in wireless networks but it does not reduce the server load.

Network coding (NC) [78] was recognized as an efficient approach for information dissemination, widely applied to file sharing [79] and data storage [80]. In [81], the network coding

theory was further utilized to improve the performance of multicasting. Specifically, with network coding, instead of forwarding native packets, intermediate forwarding nodes will linearly combine the received packets to get a coded packet, and forward the coded packet to other nodes. The coefficients for linear combination, which form a coefficient vector, will be carried together with the coded packet. For any node, if the coefficient vectors of the received coded packets can form an invertible square matrix, the original native packets can be re-constructed. [82] is the first work that verifies the feasibility of network coding in wireless communications systems. By a practical testbed implementation and study, it is demonstrated that significant performance gain can be achieved by NC.

Cooperative diversity may prove useful in multicasting. Transmitting the same data packet simultaneously from different nodes that are acting as relays in order to divide the nodes into two groups of differing channel quality i.e. those which can receive the data directly from the source and those which can only recieve the data from the relays, has been proposed by Alay et al. in [83, 84, 85]. If the multicast group members are receiving scalable-encoded video the relays may forward only the base layer as published by Alay et al. focused on broadcast on ad hoc networks also discussed how this technique i.e. transmitting the same data packet cooperatively could, not only increase the transmission range but also make the transmission range greater than the interference range, increasing the reliability of the transmission.

2.7 Conclusion and Limitations

As the above discussion shows, multicast in IEEE 802.11 has many problems which can be broadly categorized into two main issues namely: lack of reliability and absence of efficiency. A tremendous amount of literature has already investigated the multicast MAC for standard Wi-Fi wireless networks. It can be categorized into many classes but we have followed a methodological order as the authors in [86] also followed. As we presented in subsection 2.2, the IEEE has published many amendments in its original 802.11 standard to mitigate the issue in multicast by introducing DMS, GCR-UR, and GCR-BA protocols. However the main issues with these protocols are:

- Scalability
- Delay problems
- Less Efficiency

On the other hand, the pseudo-broadcast schemes (subsection 2.3) are based on promiscuous reception of unicast. Thus the protocols in this category are highly scalable as only one receiver sends feedback to the multicast transmitter and the others listen promiscuously. In addition the rate adaptation and contention windows adjustment are easier for multicast transmitter. However, in general these protocols suffer from the following weaknesses:

- The security of targeted user is compromised.

- Every user in multicast group must be informed of the target nodes MAC and IP address.
- Each user must know how to perform MAC spoofing and the IP address alias to its receiver.
- If the target node/receiver leaves the multicast group without informing the AP, then the other receivers will experience 100% loss because the AP will, at one point or another, stop forwarding the unicast data packet to a node which is no longer associated.

Similarly, some of the LBM protocols in subsection 2.4 such as LBP, DBP, PBP, LBP 802.11MX, LBPW, LBPW(n), BLBP, LB-ARF, HLBP, ARSM, SRM, LBMS try to improve the reliability to some extent and some of them such as LBPW, LBPW(n), RPMP, LB-ARF, RRAM, HLBP, ARSM, PARF, LBMS address the issue of efficiency as well. The main challenges with the LBM schemes are:

- Careful leader selection can increase the reliability in terms of delivery.
- The number of contention phases should be minimized.
- As far as possible, new control frames should not be introduced.
- The protocol should be designed for a single interface to enable seamless integration with the existing standard.
- The time spent in control frame exchange as compared to data transmission must be minimized.
- The protocol should ensure unicast-multicast fairness in the presence of reliable multicast.
- The comparative throughputs of unicast and multicast flows must be adjustable to provide required degree of fairness. In other words, the protocol should be able to provide user requested degree of fairness.

As far as the ERS category is concerned, the protocols proposed for FEC at the application layer play a pivotal role in handling losses in multicast services. In addition, the concept of unequal error protection over different layers combined with SVC improves the delivery rate in a situation where the bad reception of a weak receiver forces all the other receivers to listen to its requests and retransmissions. The following points can be summarized from the study of different protocols in ERS:

- Since the wireless medium is of broadcast nature, as long as there are receivers within a BSS requesting delayed FEC packets or retransmission in receiver controlled schemes, the other receivers that have successfully decoded the k data packets cannot receive more data packets.

- Using application layer FEC does improve the video quality when compared to transmitting only data packets, however the improvement in PSNR of those frames which experience a bursty packet loss is minimized, showing that when analysing packet losses and designing ERS, the bursty nature of the wireless medium should be tackled. Therefore independent of whether one uses a source controlled solution or a receiver-driven approach, interleaving should be utilized as well to mitigate the effect of bursts.
- Transmitting parity packet results in the largest number of received packets instead of re-transmitting the lost data packets.
- Another important point is the fact that the data should be modified as little as possible
- Some of the proposed technique introduces new types of frames, to get feedback from receivers which may cause incompatibility of legacy 802.11 stations.

Likewise, the protocols proposed in RAS help in adapting to the channel conditions that improves the efficiency and QoS experienced at the multicast receivers. The following points can be concluded from the review of rate adaptation protocols:

- The transmitter must take into account the fact that each receiver experience different losses.
- The intra-frame rate must be selected in accordance with the packet loss.
- The transmitter must ensure an acceptable QoS or QoE by selecting the base layer parameters according to the worst channel quality that can be considered in the target service area.
- An appropriate rate adaptation must be chosen in order to optimize the bitstream switching.
- Transcoding affects the channel usage time, memory requirement and processing time. This face must be taken into account while designing a multicast protocol for real-time streaming.
- The problem with these adaptation schemes over IEEE 802.11 WLAN networks is that feedback from all or a considerable number of receivers are required. Hence it is important to study the overhead induced in order to transmit such feedback, the necessary frequency in order to adapt quickly to the dynamic nature of the wireless medium and whether this feedback results in limiting either the multicast group size or the number of receivers that use a feedback channel, due to playout delays.

Last but not the least, the protocols discussed in CRS can not only increase the reliability, but they also achieve higher data rate transmission and increase the coverage range. After reviewing the protocols in subsection 2.6.2, the main points are summarized as follows.

- One of the most critical design parameters of relaying protocols is how does one select and manage the appropriate relaying node(s).

- Independent of the purpose of the relay node implementation i.e. whether for retransmission of lost packets or for throughput and coverage range augmentation, a loss model of cooperative multicasting should include spatial correlation.
- A thorough analysis of the effect of spatial correlation is crucial since the loss experienced by a relay node maybe the same as that observed by its neighbours and hence the multicast group receivers will depend on the source for reception of the data packet.
- The number of relays can limit the performance of the system.
- Special care must be taken while designing CRS in case of applications that cannot tolerate delay.

2.8 Summary

This chapter presented a comprehensive literature review of state of the art protocols in multicast in WD and standard WiFi 802.11 networks. We categorized the multicast protocols into different groups based on the underlying schemes. We observed that some of the current protocols use a single scheme, while others use a combination of schemes and methods. In order to present a comprehensive comparison, we list a brief description, benefits, and limitations of each protocol in Table 2.1. The literature review revealed that more research needs to be carried out to improve the reliability and efficiency of multicast protocols in WD 802.11 networks.

Table 2.1: Summary of multicast schemes

Name	Description	Benefits	Limitations
SM	AP sends multicast frames after DTIM. There is no ACK.	Easy Simple	Fully non-reliable Non-efficient
DMS	Converts multicast frames into unicast. Uses RTS/CTS AMDSU.	Semi-reliable Lower jitter effects	Slow with large number of receivers.
GCR-UR	Multicast frames are retransmitted one or more times. The medium is accessed using different TXOP.	Reliability increases. Allows admission control. Low overhead.	Efficiency degrades due to transmission redundancy limit.
GCR-BA	Multicast transmitter establishes admission control for BA with all receivers. Sender sends multicast frames and then request for BA.	Provides feedback. Allows admission control.	Introduces delay in larger groups.

PBS	Multicast to unicast conversion. One targeted STA while others turn into promiscuous mode.	Highly scalable. Rate adaptation is easy.	Non-secure for targeted STA. Non-reliable for others. 100% loss in the case when the targeted STA leaves.
LBM	One STA act as a leader. Positive feedback includes RTS, CTS and ACK b/w AP and leader. Negative feedback includes NCTS and NACK by others.	Reliability is increased. Efficiency is also improved.	Additional control frames. Fairness of other unicast stations is decreased.
ERS	Add parity bits. ARQ, FEC, HARQ. Layered FEC.	Reliability is increased. Scalable video transmission. Increase efficiency of delay intolerant apps.	Overhead in terms of parity bits. Extra control frames, backward compatibility issues.
RAS	Change the transmission rate with respect to channel conditions.	Efficiency is increased. Multi-rate stations are supported.	An effective feedback is required from all receivers otherwise the performance degrades. Includes overhead.
CRS	STAs with good signal strength act as relays for others.	Achieve higher data rate transmission. Increase coverage range and security.	Selection of non-optimal relay can degrade the performance. Incurs delay

"The fundamental problem of communication is that of reproducing at one point either exactly or approximately a message selected at another point.n."

Claude Shannon (1916 – 2001)

3

Collision Reduction Methods

3.1 Introduction

In this chapter, we focus on the fundamental problem of reliability in multicast communication in the context of WD networks by analysing and proposing algorithms that can reduce collision. In the first half of the chapter, the performance of Standard Multicast (SM) and Leader Based Multicast (LBM) protocols is explored for WD networks. Then an Enhanced Leader Based Multicast (ELBM) protocol is presented which reduces collision and interference in multicast data transmission by improving the channel access mechanism and selecting an optimal representative multicast receiver, therefore, it enhances the reliability of multicast transmission. We have tested the performance of all the three protocols through simulations. The simulation results show that the ELBM increases throughput as well as improve packet delivery ratio of multicast data by almost two times as compared to SM and LBM.

In the second half of the chapter, an analytical performance model of the early collision detection is presented for WD networks. The analytical model, which is known as Early Packet Loss Detection (EPLD), is derived by careful consideration of the MAC layer in terms of backoff counter, successful transmission time, and time spent in collision. The simulation and analytical results of the EPLD protocol are compared with the standard protocol, which is based on the DCF protocol. The EPLD algorithm surpasses the standard algorithm by an average of almost 12-15% in terms of system throughput under different configurations.

3.2 Leader Based Multicast Protocol

The idea of LBM in WD networks is similar to other leader-based approaches that have been used for traditional multicast as discussed in Chapter 2. However, unlike traditional LBM protocols, a GO is the coordinator as well as the multicast data sender in WD network instead of an AP. In a multicast group, there

is usually one GO and few clients which receive multicast data from the GO. In addition, the GO is also surrounded by an AP in the case of one BSS and many other Unicast Stations (USTA). We assume that the USTAs communicate with the AP. As a result, a LBM protocol for WD network faces more challenges in terms of collision from other USTAs and/or AP. The problem of interference can largely affect LBM protocol in the case of a single BSS for WD network and will cause more packet loss in the case of multiple BSSs.

3.2.1 LBM Protocol at GO

We present a modified LBM protocol in the context of WD networks. The protocol selects a CTS representative, which we will call CTS-R for the sake of simplicity in rest of the chapter. The CTS-R is one of the clients which is responsible for sending CTS to GO when it receives RTS from the GO. It is assumed that the multicast data is generated at GO which is sent to the clients in the multicast group. The LBM protocol at GO works as follows:

1. GO chooses that client as CTS-R client who joins the group first.
2. GO sends RTS to CTS-R client
3. CTS-R client sends CTS to GO
4. GO sends multicast data

Moreover, step 2 and 3 are repeated until the RTS and CTS messages are successfully sent. If an RTS packet collides or interferes with the data or control packets of the AP or USTA, the GO sends RTS again. The process is repeated until a CTS message is received successfully from the CTS-R or a maximum limit of RTS message threshold is achieved.

A GO is the initiator of the multicast transmission. Algorithm 1 shows the pseudo code for LBP that runs at GO. The algorithm illustrates the procedure of CTS-R selection, RTS/CTS exchange method and the mechanism for sending multicast data by GO. Similarly, a flow chart is shown in Fig. 3.1 which captures the implementation point of view of LBM protocol. Algorithm 1 and Fig. 3.1 together define the overall working of LBM protocol in the WD networks.

3.3 Enhanced Leader Based Multicast(ELBM) Protocol

In this section we present the proposed algorithm which is known as ELBM protocol for WD networks [87]. It is assumed that the group is already formed which can be achieved by any one of the three group formation techniques namely: 1) Standard method 2) Autonomous method 3) Persistent method [3]. Likewise, we do not put any constraints on other schemes that can help in efficient group formation. We assume that only one multicast group consisting of GO and its clients exist and that the multicast group shares the same channel with the AP and other unicast stations (referred to as USTAs). The protocol works as follows:

1. GO chooses one of its clients as representative client (CTS-R) for sending CTS. CTS-R is chosen using an optimal method discussed later.
2. GO sends RTS to CTS-R using an enhanced RTS/CTS scheme
3. CTS-R sends CTS to GO
4. GO sends multicast data using an improved access mechanism

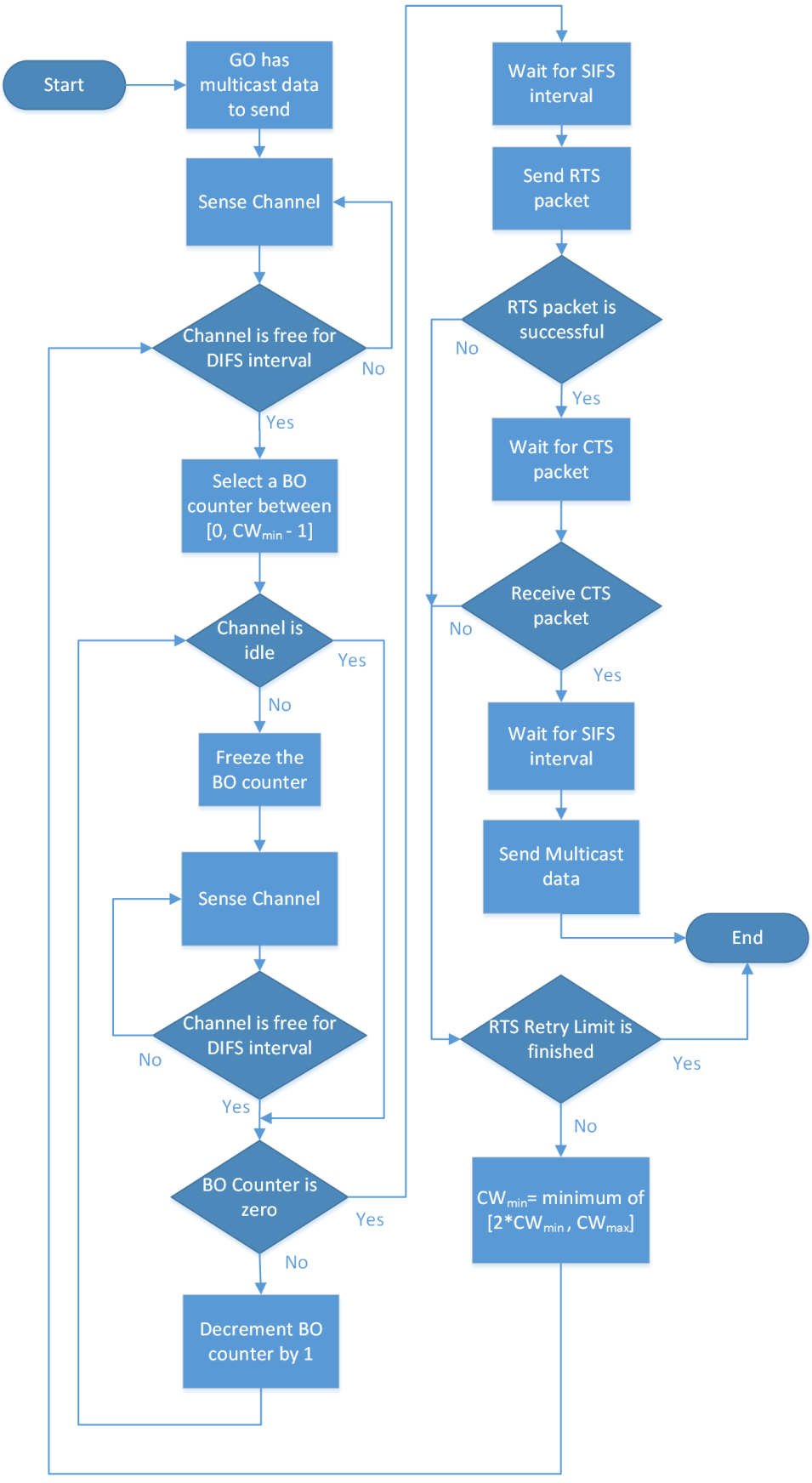

Figure 3.1: Leader Based Multicast Protocol

Algorithm 1 LBM Protocol at GO

Input: $N, MData, TimeOut$
▷ where N is the number of clients in the multicast group
▷ $MData$ indicates the multicast data generated at GO
▷ $TimeOut$ indicates the time for the maximum threshold of RTS messages

1: **for** $i = 1$: to N **do**
2: **if** $i ==$ client who has spent the longest time in the group **then**
3: $CTS\text{-}R \leftarrow i$
4: Exit the loop
5: **end if**
6: **end for**
7: Run DCF protocol
8: $CTS \leftarrow 0$
9: Send RTS packet to $CTS\text{-}R$
10: **while** $CTS == 0$ **and** $TimeOut \neq 0$ **do**
11: $TimeOut \leftarrow TimeOut - 1$
12: **if** GO receives CTS packet from $CTS\text{-}R$ **then**
13: $CTS \leftarrow 1$
14: **end if**
15: **end while**
16: **if** $CTS == 1$ **then**
17: send $MData$ to N clients
18: **else**
19: Go to step 7
20: **end if**

It is worthwhile to note that there is no acknowledgement (ACK) transmission by any multicast receiver including CTS-R. In order to improve reliability of multicast without resorting to any ACK mechanism, we introduce the following three features in ELBM:

1. Optimal selection of CTS-R
2. Improved Channel Access Mechanism
3. Enhanced RTS/CTS method

3.3.1 Optimal Selection of CTS-R

The GO chooses that client as its CTS-R who is closest to the AP among all its clients in the multicast group. The rationale behind this is twofold: first it minimizes the interference of hidden nodes and second it maximizes the effective coverage of CTS frame transmission. Most unicast stations in a BSS communicate with the AP for most of the times. We consider unicast stations to be laptops, mobile phones, tabs or other devices that communicate with AP for accessing the internet, downloading a file, streaming multimedia files and so on. Since most of the communications of unicast stations are with AP, a client which is closer to the AP can hear more number of unicast stations as compared to those clients which are far from the AP. Thus the nearest client to the AP is the best candidate to be chosen as the CTS-R as it can broadcast the CTS message to more USTAs, which will reduce the collision to some extent. The underlying method for choosing the CTS-R is discussed later in this chapter.

3.3.2 Improved Channel Access Mechanism

When a GO intends to send multicast data to USTAs in a multicast group, first of all, it accesses the channel using the DCF protocol and then sends an RTS packet to the CTS-R. After this, the GO enters into a wait state and remains in the waiting state until a CTS packet is received from the CTS-R or an ACK message is heard either from a USTA or an AP. If the transmission of the RTS and CTS packets are successful, the GO will send its multicast data. On the other hand if the transmission of an RTS or a CTS packet fails, the GO will not send the multicast data. It is considered that all the clients are synchronized with the GO in a multicast group. Thus an RTS packet sent by the GO can only collide or interfere with data or control packets of the AP or USTAs. Consequently, when the RTS transmission fails, implying an on-going transmission by other USTA or AP, the GO waits until the AP or USTAs complete the transmission. It is also assumed that the unicast transmission is performed without RTS/CTS exchange. Once the unicast transmission is successful, it is followed by an ACK packet from the AP or USTAs. Although, the ACK packet is not destined to GO but we can decode this information from the header of the received packet. The information is used to decide whether the received packet is a control packet or not based on its header. Finally, as soon as the GO receives the CTS or ACK packet, it waits for a Short Inter Frame Space (SIFS) interval and then transmits multicast data.

3.3.3 Enhanced RTS CTS method

The GO sends an RTS packet and then waits for a CTS or an ACK packet. We loosely define two types of collision/interference in the context of the proposed algorithm.

3.3.3.1 Collision due to nearby node

When two or more stations, which are in the same transmission range of each other, access the channel at the same time, collision occurs due to nearby node. For example, when GO and USTA in Fig. 3.4 access the channel at the same time, their packets collide. In this case the GO and the USTA are not hidden nodes to each other.

3.3.3.2 Collision due to hidden node

The hidden nodes cannot detect the transmission of each other, and they can transmit while the other node transmits, which is called collision due to hidden node. For example, when GO and USTA are hidden nodes to each other as shown in Fig. 3.5, so that the USTA cannot successfully decode the RTS packet sent by the GO and it sends its unicast data while CTS-R sends an CTS packet. In this case, unicast data interferers with the transmission of the CTS packet.

Moreover the collision/interference cannot only be caused by hidden node senders, but also via other sources of RF signals in the relevant band, e.g. microwave ovens, etc. However, we consider only the two types of collision.

Let us, consider all possible cases in the following subsections. It is assumed that in Case-1 3.3.4 and Case-2 3.3.5, there is no hidden node while in Case-3 3.3.6 and Case-4 3.3.7, a USTA and GO are hidden nodes to each other.

3.3.4 Case-1: Successful RTS and successful CTS

This is the ideal case in which a GO successfully sends an RTS packet to a CTS-R client in a multicast group which is followed by a successful transmission of a CTS packet by CTS-R as shown in Fig. 3.2.

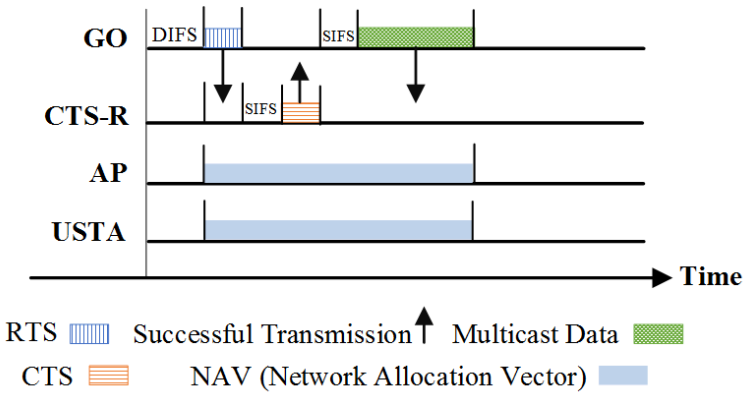

Figure 3.2: A case where RTS and CTS both are successful

3.3.5 Case-2: Unsuccessful RTS (Collision due to nearby node)

When an RTS packet collides with a control or data packet of an AP or a USTA. In this case, the GO does not resend an RTS packet but it waits for an ACK packet from the AP or any of USTAs. This scenario is depicted in Fig. 3.3.

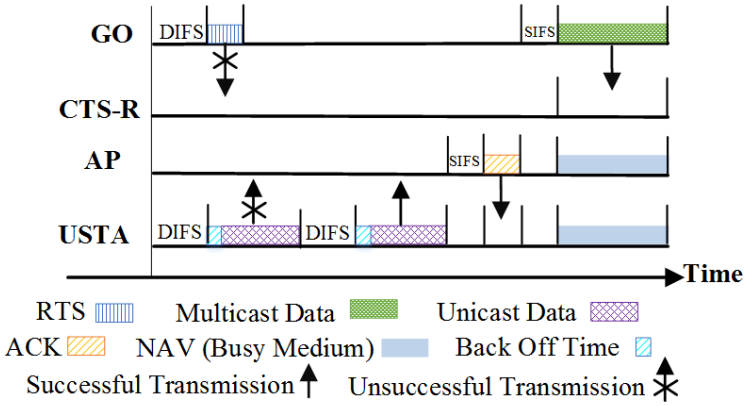

Figure 3.3: A case where RTS is unsuccessful

3.3.6 Case-3: Successful RTS and Unsuccessful CTS (Collision due to hidden node)

There may be situation where an RTS packet is successful but a CTS packet collides with packets of USTAs. In such a situation, the RTS and CTS packets are not retransmitted but the GO waits for an ACK packet from the AP. Figure 3.4 shows the timing diagram of such scenario.

3.3.7 Case-4: Unsuccessful RTS or unsuccessful CTS (Collision/Interference due to nearby or/and hidden node)

This is the case in which a GO competes with an AP, whcih transmits data to USTA, for accessing the channel as shown in Fig. 3.5. The USTA will send an ACK packet to the AP. In addition, the USTA is hidden to the GO and hence the GO cannot detect the on going transmission of data between the AP and the USTA. However, this does not make a serious problem because an ACK packet is usually transmitted at the most robust modulation scheme and coding rate, so that even though GO cannot decode data sent by

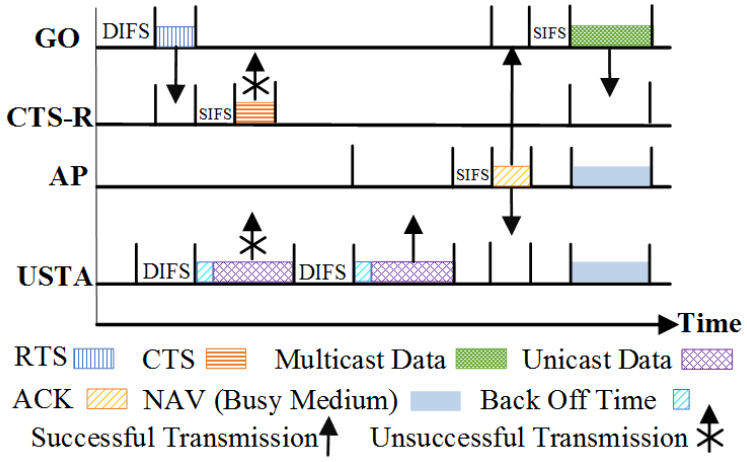

Figure 3.4: A case where RTS is successful but CTS is unsuccessful

USTA but it can correctly decode an ACK packet sent by USTA (with high probability).

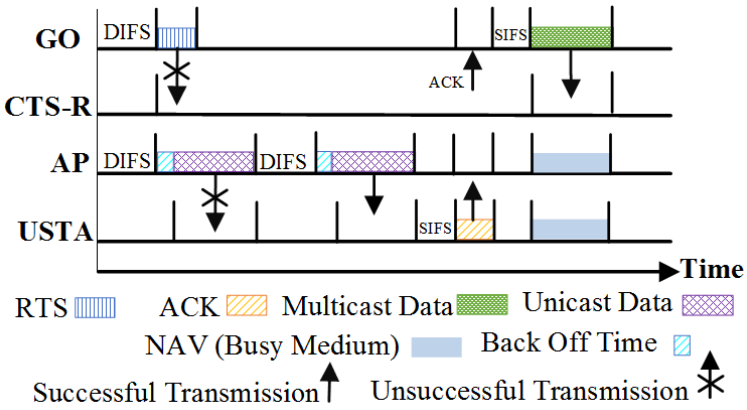

Figure 3.5: A case where RTS or CTS is unsuccessful and USTA sends ACK

In this way, ELBM effectively copes with collision and interference by USTAs and/or AP and assures the transmission opportunity of GO without significant overhead, which contributes to the reliability of multicast transmission by GO. Moreover, it is important to note that the ELBM protocol needs to be implemented only at GO and it does not require any modification at clients. The pseudo code of ELBM is illustrated in Algorithm 2 whereas Fig 3.6 shows the overall flow of ELBM from the implementation viewpoint.

3.3.8 Distance of Client from AP

In the ELBM protocol, the GO determines the CTS-R based on the distance between the AP and its clients. For this purpose, it can make use of many techniques to estimate the distance of clients from the AP, such as Time of Arrival (TOA), Time Difference of Arrival (TDoA), or techniques based on Received Signal Strength Indicator (RSSI) [88], [89], [90]. In the proposed algorithm, every client stores ToA, TDoA, or RSSI values from the beacon signal periodically transmitted by the AP, and sends this information to GO during the group formation method.

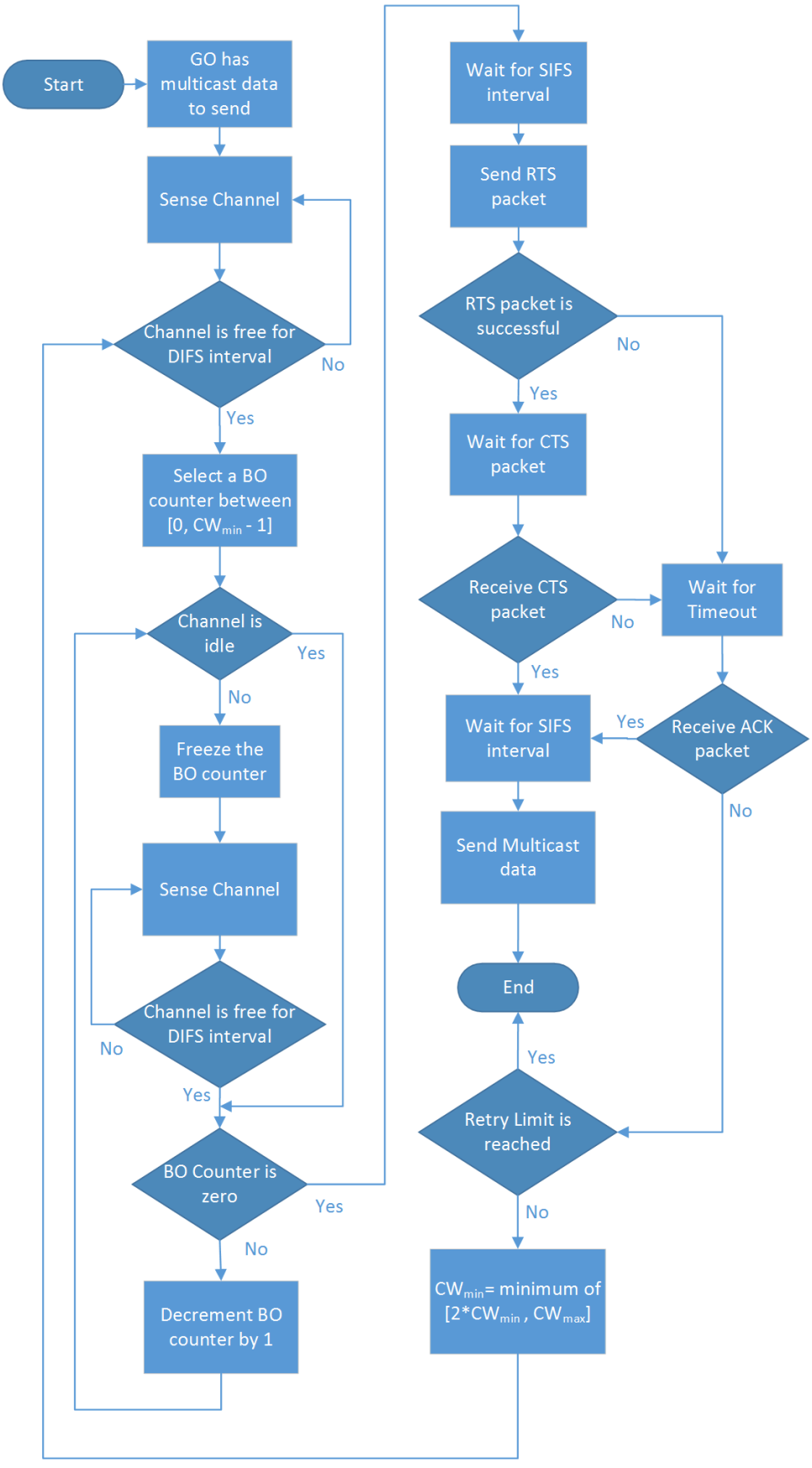

Figure 3.6: Enhanced Leader Based Multicast Protocol

Algorithm 2 ELBM Protocol at GO

Input: $N, MData, TimeOut$
▷ where N is the number of clients in the multicast group
▷ $MData$ indicates the multicast data generated at GO
▷ $TimeOut$ indicates the time for the maximum threshold of RTS messages

1: **for** $i = 1$: to N **do**
2: $d_i \leftarrow$ distance of client i from AP
3: **if** $d_i == 1$ **then**
4: $d_{min} \leftarrow d_i$
5: $CTS\text{-}R \leftarrow i$
6: **else if** $d_i < d_{min}$ **then**
7: $d_{min} \leftarrow d_i$
8: $CTS_{state} \leftarrow 0$
9: **end if**
10: **end for**
11: $CTS_{state} \leftarrow 0$
12: $ACK_{state} \leftarrow 0$
13: Send RTS packet to $CTS\text{-}R$
14: **while** $CTS_{state} == 0$ **and** $ACK_{state} == 0$ **and** $TimeOut \neq 0$ **do**
15: $TimeOut \leftarrow TimeOut - 1$
16: **if** GO receives CTS packet from $CTS\text{-}R$ **then**
17: $CTS_{state} \leftarrow 1$
18: **end if**
19: **if** GO receives ACK packet from AP **then**
20: $ACK_{state} \leftarrow 1$
21: **end if**
22: **end while**
23: **if** $CTS_{state} == 1$ **or** $ACK_{state} == 1$ **then**
24: send $MData$ to N clients
25: **else**
26: Go to step 17
27: **end if**

3.4 Early Packet Loss Detection (EPLD)

3.4.1 Description

The MAC layer of IEEE 802.11 is based on CSMA/CA (Carrier Sense Multiple Access with Collision Avoidance) in which the collision is detected at the receiver. The receiver stays silent in the case of collision and sends an ACK in the case of successful transmission. However the loss may not be due to collision only. In fact, there are two reasons of a packet loss in 802.11. The first reason is collision between two or more packets transmitted at the same time and the second reason is loss due to weak signal reception at the receiver [16]. A number of metrics can be used to detect collision and weak signal loss. This include Received signal strength (RSS), Bit error rate (BER), Error rate per symbol (EPS), Symbol error rate (SER), and Symbol error burst length (S-Score) [16]. Once collision is detected then the receiver does not send an ACK for the packet. The transmitter waits for the ACK for a specified amount of time and if the ACK

is not received for the packet in that time, the transmitter will resend the packet again until a maximum retransmission limit is reached [91].

The problem with the traditional MAC access in WD networks is that a substantial amount of time is wasted in collision. In order to reduce the time of collision, CSMA/CN (Collision Notification) protocol was proposed in [92] for 802.11 networks. In CSMA/CN, the receiver detects the collision earlier and immediately sends a unique collision notification to the transmitter. The transmitter listens to the collision notification on a separate antenna and aborts the transmission as soon as the collision notification is detected. Similarly the authors in [93] presented Partial Packet Recovery (PPR) scheme which reduces the retransmission of a full packet by using SoftPHY hints and retransmits only those bits which are in error. PPR can improve the capacity in a timevarying wireless channel, however its performance is degraded if an inappropriate bit rate is selected for an individual transmission. In a similar way, Nilsson et al. [94] presented yet another algorithm to detect the collision earlier for multicast transmission in 802.11. The algorithm sends an early multicast collision detection packet and works in an ideal Extended Service Set (ESS) with no hidden stations.

3.4.2 System Model

We consider a single hop fully connected WD group in which there is one GO and n clients. Every station in the group, be it GO or any client, consists of at least two antennas. One antenna is used for transmission/reception of data frames while the other one is used for listening for a collision notification frame from the receiver as shown in Fig. 3.7. When higher order MIMOs are used, we will reserve one antenna for collision notification frame. For example, in the case of uplink traffic, when a client sends data to the GO, the client listens on the other antenna for a collision notifications from the GO while transmitting the data frame. On the other hand, the receiver (GO in uplink mode) continuously detects the collision while the data frame is being received. The collision detection process is out of the scope of this paper. The details of the collision detection mechanism as well as the pattern of the collision notification frames can be found in [92]. It is assumed that each client can sense transmission from every other client in the same group. All clients operate in saturated mode i.e., they always have data to send to the GO. A data transmission is considered successful if it is followed by an ACK from the GO, otherwise it is retransmitted. The wireless channel is assumed ideal i.e., a frame is failed only due to collision that occurs when two or more clients access the shared channel simultaneously. Thus the packet loss which results from weak signal is not considered in this paper.

3.4.3 Analytical Model

We consider a single hop fully connected WD group in which there is one GO and n clients. It is assumed that each client can sense transmission from every other client in the same group. All clients operate in uplink saturated mode i.e., they always have data to send to the GO. A data transmission is considered successful if it is followed by an ACK from the GO, otherwise it is retransmitted. The wireless channel is assumed ideal i.e., a frame is failed only due to collision that occurs when two or more clients access the shared channel simultaneously.

We consider the Markov model of [95] that represents the DCF as two stochastic processes namely: $b(t)$ and $s(t)$ to model the backoff time counter and the backoff stage, respectively. Without the loss of generality, let CW_{min} and CW_{max} represent minimum and maximum contention windows, respectively. Let m indicates maximum backoff stage such that $CW_{max} = 2^m CW_{min}$. Let CW_i represents the contention window of a STA at ith backoff stage i.e., $CW_i = 2^i CW_{min}$ where $i \in [0, m]$. Thus $b(t)$ takes any random value from $[0, CW_i]$ where i is modelled by $s(t)$. For the sake of simplicity, we represent $CW_{min} = W$.

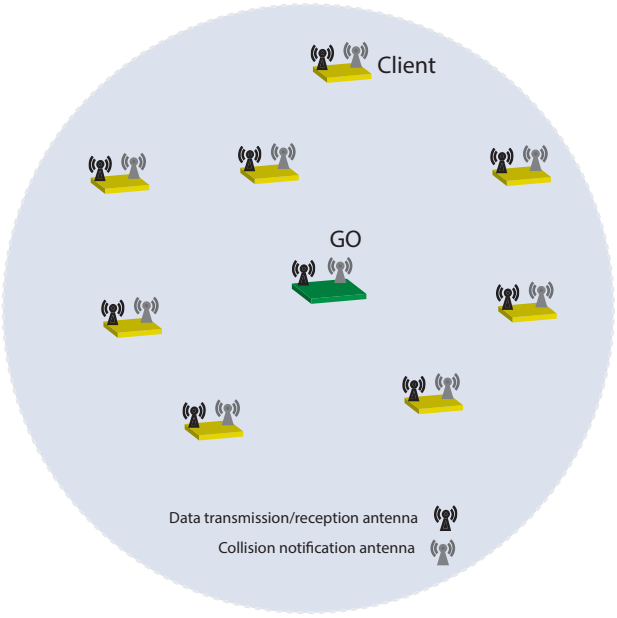

Figure 3.7: WD Group with one GO and n clients

The key approximation is that collision probability is constant regardless of retransmission stage. This is a reasonable approximation as long as W and n get larger.

During a randomly selected slot, a client senses the channel in one of the three states namely: idle state (no transmission activities), busy due to successful transmission, or busy due to collision. Suppose a client attempts to transmit a frame in a randomly chosen slot with probability τ. The system considers a Binary Exponential Backoff (BEB) mechanism which doubles the contention window on collision. If p represents the collision probability; then τ is given by eq. (3.1) [95].

$$\tau = \frac{2(1-p)}{(1-2p)(W-1) + pW(1-(2p)^m)} \tag{3.1}$$

The probability of collision p can be calculated from the fact that collision occurs if at least one of the remaining $n-1$ clients starts transmission. Therefore, if $1-\tau$ is the probability that exactly one STA is idle then $(1-\tau)^{n-1}$ is the probability that $n-1$ STAs are idle. It follows that the probability that at least one of $n-1$ clients transmits is given in eq. (3.2)

$$p = 1 - (1-\tau)^{n-1} \tag{3.2}$$

Transmission probability τ and collision probability p can be calculated numerically by solving eq. (3.1) and eq. (3.2) using a numerical method, such as fixed point iteration. In addition, it can be proved that this system of non linear equations has a unique solution [95]. We have used Maple 15 [96] to solve eq. (3.1) and eq. (3.2).

We are interested in calculating throughput S of the system which is expressed as a ratio of average payload information transmitted in a slot per average duration of a slot as listed in eq(3.3).

$$S = \frac{E[D]}{E[T]} \tag{3.3}$$

where $E[D]$ is the expected value of data transmitted successfully in a randomly selected slot while $E[T]$ is the average length of a time slot as listed in eq. (3.4) and eq. (3.9).

$$E[D] = P_{tr} P_s E[L] \tag{3.4}$$

where P_{tr} denotes the probability that there is at least one transmission in the considered time slot. On the other hand, P_s is the probability that the given transmission is successful and $E[L]$ denotes the average length of payload data. Consequently, P_{tr} can be calculated for n contending stations as shown in eq. (3.5).

$$P_{tr} = 1 - (1 - \tau)^n \tag{3.5}$$

Similarly, P_s can be calculated from the fact that a transmission is successful if and only if exactly one client transmits given that at least one STA transmits among n clients, as listed in eq. (3.6).

$$P_s = \frac{n\tau(1-\tau)^{n-1}}{1-(1-\tau)^n} \tag{3.6}$$

Accordingly, $E[D]$ is calculated from eq. (3.5) and eq. (3.6). In order to calculate $E[T]$, let us denote T as a random variable that indicates a randomly selected time slot. Moreover T takes any of the following three values as shown in eq. (3.7).

$$T = \begin{cases} \sigma & \text{if the medium is idle} \\ T_s & \text{if successful transmission} \\ T_c & \text{if there is collision} \end{cases} \tag{3.7}$$

where σ is the duration of an empty slot while T_s and T_c are the average time when the channel is busy due to successful transmission and collision, respectively. The corresponding probability for these three cases can be calculated as illustrated in eq. (3.8).

$$f_T(t) = \begin{cases} 1 - P_{tr} & \text{if } T = \sigma \\ P_{tr} P_s & \text{if } T = T_s \\ P_{tr}(1 - P_s) & \text{if } T = T_c \end{cases} \tag{3.8}$$

Using eq. (3.7) and eq. (3.8), $E[T]$ can be calculated as

$$E[T] = \sum_{\forall t, T} T f_T(t) \tag{3.9}$$

The normalized throughput S is calculated by using eq. 3.4 and eq. (3.9) in eq. (3.3). Similarly, T_s and T_c are calculated in eq. (3.10) and eq. (3.11), respectively.

$$T_s = T_{DIFS} + T_{DATA} + T_{SIFS} + T_{ACK} + 2\rho \tag{3.10}$$

$$T_c = T_{DIFS} + T_{trans-DATA} + T_{SIFS} + T_N + 2\rho \tag{3.11}$$

where T_{DIFS}, T_{SIFS}, and ρ indicate the during of DIFS timer, SIFS timer, and the propagation delay, respectively as listed in TABLE 3.1. Similarly $T_{DATA}, T_{trans-DATA}, T_{ACK}, T_N$ indicate the transmission time of a complete data frame, the data frame transmitted until a collision is detected, ACK frame and

Table 3.1: MAC and PHY Parameters

Parameter	Value	Parameter	Value	Parameter	Value
Slot time (σ)	9 μs	CW_{min}	16	T_{DIFS}	34 μs
L_{macH}	34 bits	CW_{max}	1024	T_{SIFS}	16 μs
$T_{VHT-STF}$	4 μs	T_{SYMS}	3.6 μs	T_{STF}	8 μs
$T_{VHT-SIG-A}$	8 μs	T_{L-SIG}	4 μs	T_{LTF}	8 μs
$T_{VHT-SIG-B}$	4 μs	T_{SYML}	4 μs	N_{tail}	6 bits
$T_{VHT-LTF}$	4 μs	$N_{service}$	16 bits	ρ	1 μs

collision notification frame, respectively.

In the same way, T_{DATA} and T_{ACK} are calculated in eq. (3.12-3.13).

$$T_{DATA} = T_{LEG-PREAMBLE} + T_{L-SIG} + T_{VHT-SIG-A} + T_{VHT-PREAMBLE} + T_{VHT-SIG-B} + T_D \quad (3.12)$$

$$T_{ACK} = T_{LEG-PREAMBLE} + T_{L-SIG} + T_{VHT-SIG-A} + T_{VHT-PREAMBLE} + T_{VHT-SIG-B} + T_A \quad (3.13)$$

T_N depends on the consideration and implementation of the length of the collision notification frame as discussed in [92]. Since the function of the notification frame is similar to a negative acknowledgement, therefore we assume that it contain the same fields and have the same length as a regular ACK frame in WD 802.11ac network. Hence our analytical model considers $T_N = T_{ACK}$.

Similarly $T_{trans-DATA}$ depends on the time when the receiver detects the collision if there is any.

$$T_{trans-DATA} = \begin{cases} \lambda_s T_{slot} & \text{collision detected at the start} \\ \lambda_e T_{DATA} & \text{collision detected in the end} \end{cases} \quad (3.14)$$

where λ_s indicates the probability that the collision occurs and is detected at the very start of the packet whereas λ_e indicates the probability that the collision is detected at end of the packet. It depends on two things: first when does the collision occur? and second when is the collision detected? If collision occurs at the start of the packet and the receiver is able to detect it right away then this the best case. On the other hand, if the receiver is not able to detect the collision, or the collision occurs at the end then the performance of the early packet loss detection will not be different than that of the traditional DCF. Instead of finding the performance at the extreme limits, we choose more sensible and practical approach which is the expected value of $T_{trans-DATA}$ i.e., $E[T_{trans-DATA}]$ as shown in eq. (3.15).

$$E[T_{trans-DATA}] = \lambda_s T_{slot} + \lambda_e T_{DATA} \quad (3.15)$$

Under a uniform probability distribution, $\lambda_s = \lambda_e = \frac{1}{2}$. The details of different fields of a VHT packet used in eq. (3.12-3.15) are discussed Appendix A.

3.5 Simulation Environment

We evaluate the performance of the proposed algorithm with the help of a time driven simulator which we have developed in Matlab. It models the DCF 802.11 with the MAC and PHY parameters listed in Table 3.1 [95]. The simulation time is set to 1 million time slots, where the duration of each time slot is $1\mu s$ as listed in Table 3.1. Because the propagation delay is very small and it will not be a major factor that affects the performance, we have assumed no propagation delay. Each simulation was run 40 times and then the average was taken.

The implementation of a WiFi Direct network in NS3 is a non-trivial task because NS3 does not provide any support to group formation, the capability of Group Owner and client, and other features of WiFi Direct technology. Thus coding everything from the scratch will be time consuming. Moreover, we need to implement the individual field level simulation of the PHY packets which requires a complete system level implementation of all blocks in the transmitter and receiver, especially the new features of 802.11ac. NS3 does not provide any well-known libraries which can help in achieving our aims. Most of algorithms in the thesis have been developed from a complete system levels point of view i.e., transmitter, communication channel, and receiver. We have used six profile channel models (TGn Channel A-F), which are not supported by NS3. On the other hand, all these tasks can be achieved in Matlab because Matlab is very flexible and provides helpful documentation. In addition, the availability of WLAN, communication system, and signal processing toolboxes helps in the overall system level implementation. Moreover, we have developed the system in incremental fashion which is easily applicable in Matlab and not in NS3. Initially, the MAC layer was implemented using the DCF in Matlab and later on the PHY layer and six channel profiles were built on the top of it.

In order to test the validity of the algorithm, two test cases were considered, namely:

- Standard test case
- Complex test case

3.5.1 Standard Test Case

The standard test case consists of one AP, one GO, two P2P clients, and two USTAs in a single BSS as shown in Fig. 3.8. The USTAs send unicast data to AP while GO sends multicast data to clients. All unicast transmissions use the standard DCF 802.11 to access the channel while multicast transmission uses three methods namely SM, LBM and ELBM to access the channel. The GO and clients do not participate in unicast transmission. Similarly, AP and USTAs do not participate in multicast transmission. Because unicast and multicast transmissions share the same channel, therefore collision and interference can occur between unicast and unicast or unicast and multicast transmissions. For the sake of simplicity, we consider saturated unicast and multicast transmissions which implies that USTAs and GO always have data to send. All stations are deployed in a square area of 100x100 m^2 in which AP is located in the centre of the square. The transmission range of each station is 50 m; it follows a two-ray ground propagation model with Omni directional antenna. The transmission ranges of AP abd GO are shown by solid and dotted lines, respectively. As shown in Fig. 3.8, USTA-H is a hidden node from the perspective of the GO.

3.5.2 Complex Test Case

The complex test case consists of one AP, one GO, two clients and two sets of unicast stations (USTA-D and USTA-H) as shown in Fig. 3.9. USTA-D are the unicast stations which are not hidden nodes to GO

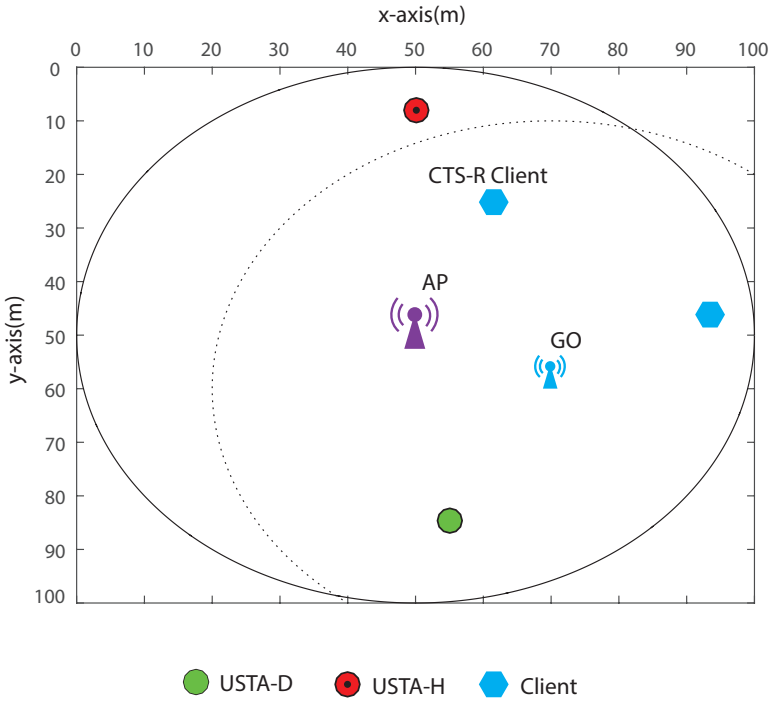

Figure 3.8: Standard test case scenario

and can hear the direct communication by GO, whereas USTA-H are the unicast stations which are hidden nodes to GO. All the assumptions of the standard test case will also apply to the complex test case.

3.5.3 Performance Parameters

We use two performance metrics to measure the performance of the proposed protocol, as described in the following subsections.

3.5.3.1 Packet Delivery Ratio

Packet Delivery Ration (PDR) is defined as the ratio of the number of packets delivered successfully to the number of total packets sent. The PDR of a station i, denoted by PDR_i, is calculated in eq. (3.16).

$$PDR_i = \frac{N_i}{N_{total}} \tag{3.16}$$

where N_i and N_{total} indicate the number of successful packets and the number of total packets sent by station i, respectively.

3.5.3.2 Throughput

Throughput at the MAC layer is defined as the number of bits transmitted successfully in a given time. The individual throughput, S_i of a station i is calculated in eq. (3.17).

$$S_i = \frac{N_i \times L}{T} \tag{3.17}$$

where L indicates the length of the packet (bits) and T indicates the total time (sec). In order to calculate the gain and loss of the protocol, we calculate multicast PDR, multicast throughput of GO, and average PDR and throughput of USTA-D and USTA-H. Our results confirm that the mechanism works well in the

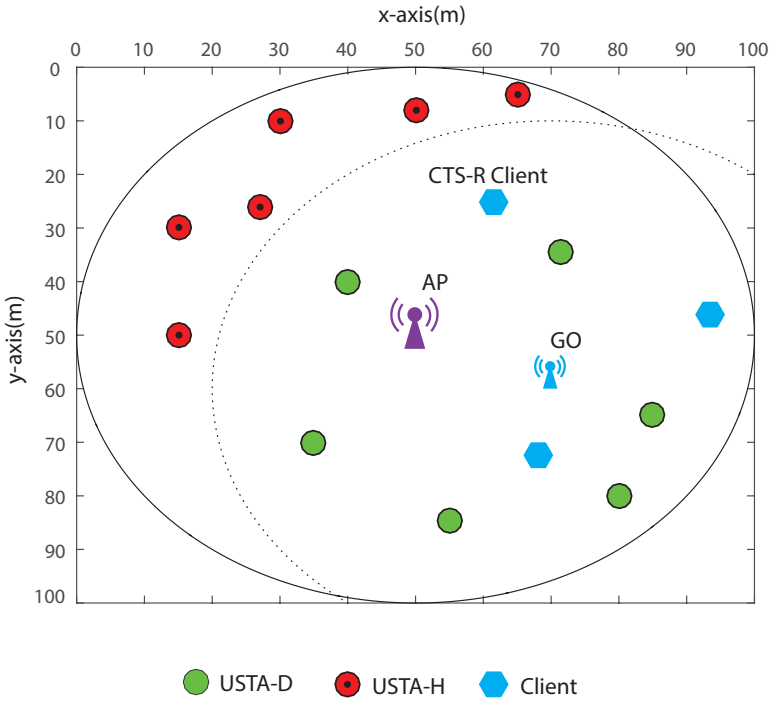

Figure 3.9: Complex test case scenario

given test cases. However, the performance of the protocol can not be predicted for other test cases, which are different than the standard test case 3.5.1 and the complex test case 3.5.2.

3.6 Simulation Results and Discussions

3.6.1 Standard Test Case

In this section, we present and discuss the results for standard test case of Fig. 3.8. Firstly, we intend to show that the system is stable under the given configuration. This can be achieved from the consistent results of multicast PDR of GO over a certain time. Figure 3.10 shows that PDR remains constant for SM, LBM and ELBM. As shown in Fig. 3.11, PDR of multicast data is almost 90% for SM, 95.5 % for LBM and 100% for ELBM. This is because of the different levels of collisions and interference within the three protocols. In the case of SM, multicast packet of GO can collide as well interfere with unicast packets of USTA-D and USTA-H. On the other hand, collision is reduced in the case of LBM. however, a hidden node such as USTA-H can cause an interference. Therefore, there is a marginal improvement in PDR of LBM. On the other hand, ELBM minimizes both collision and interference of unicast data with multicast data, thereby surpassing both SM and LBM.

We observe a similar trend in the case of multicast throughput as shown in Fig. 3.12. Multicast throughput of ELBM is increased by about 72% and 45% as compared to that of SM and LBM, respectively. This is due to reducing multicast collision, minimizing interference of hidden node, and decreasing the effects of RTS/CTS collision. We also investigate the effects of the proposed method on unicast data. As Fig. 3.13 shows, the average PDR of USTA-D and USTA-H is 76.5% for SM, 74.5% for LBM and 75.5% for ELBM. A similar trend can be seen for unicast throughput of USTA-D and USTA-H as shown in Fig. 3.14. The reason for this trade-off in ELBM and SM is the addition of RTS/CTS in the case of ELBM.

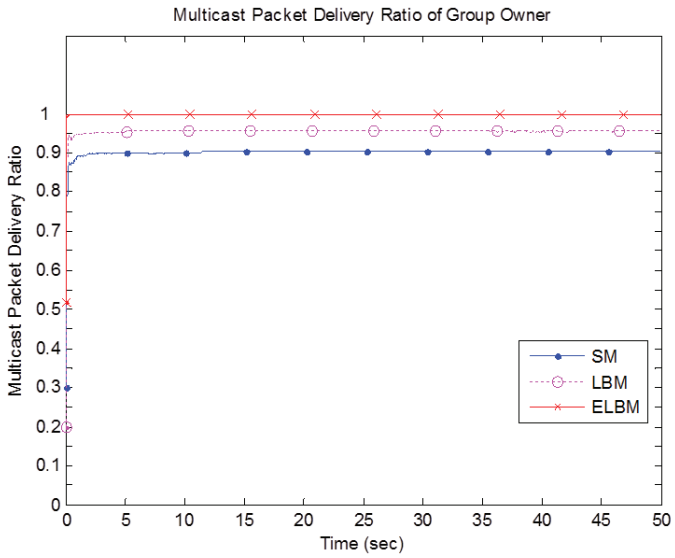

Figure 3.10: Multicast PDR of multicast packets at GO

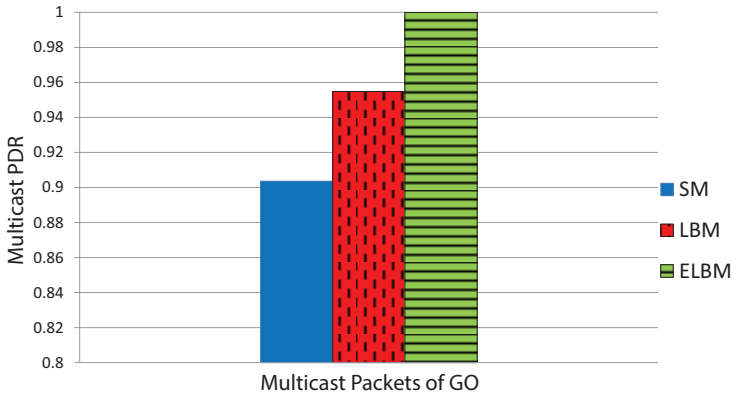

Figure 3.11: Multicast PDR of multicast packets at GO

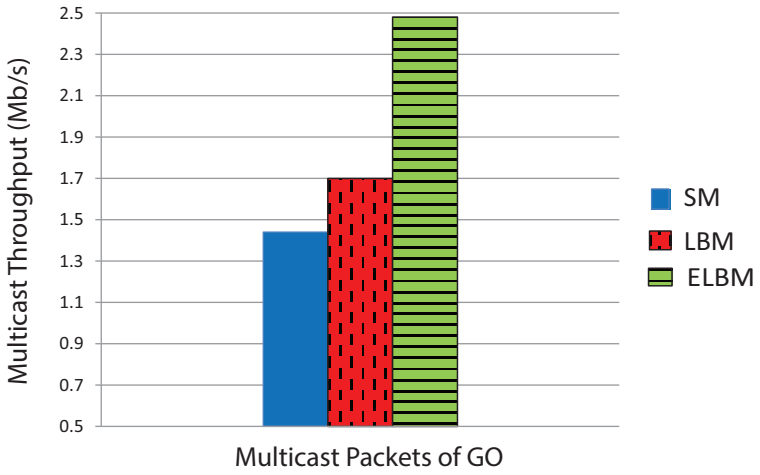

Figure 3.12: Multicast Throughput of multicast packets at GO

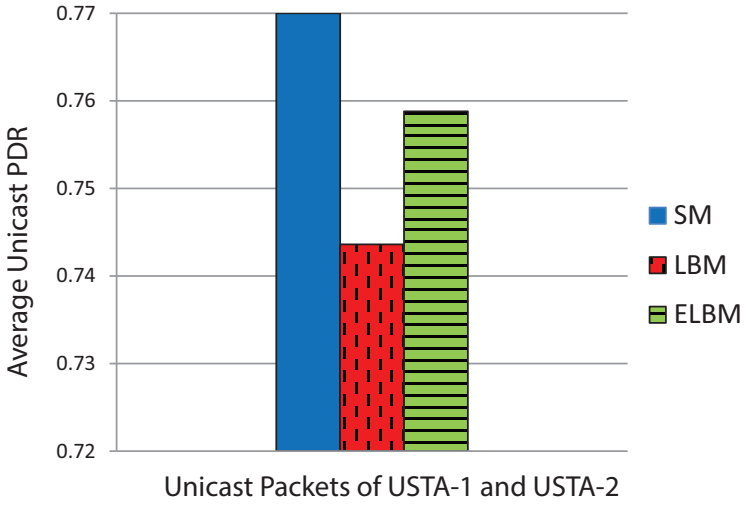

Figure 3.13: Average unicast PDR of USTA-D and USTA-H

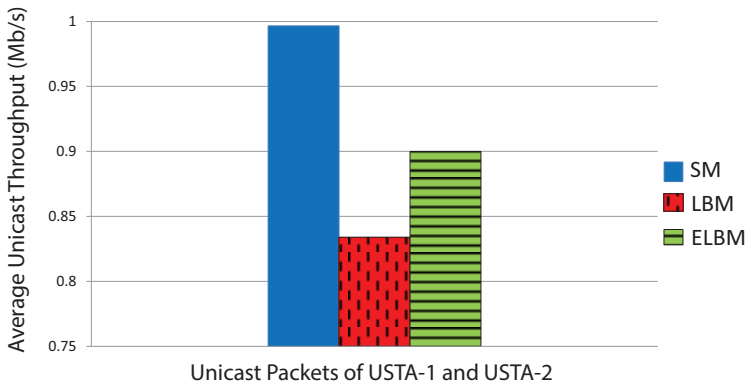

Figure 3.14: Average unicast Throughput of USTA-D and USTA-H

However, a comparison between the gain and loss in terms of PDR and throughput shows improvement. ELBM achieves 10% gain for multicast PDR at the cost of 2% loss in unicast PDR as compared to SM. Likewise it achieves 72% gain in multicast throughput and about 10% loss in unicast throughput as compared to SM. On the other hand ELBM outperforms LBM both in PDR and throughput for both unicast and multicast transmissions.

We also showed the advantages of ELBM over LBM in terms of overhead i.e., RTS and CTS packets. As shown in Fig. 3.15, PDR of RTS packets is improved from 96% to 97%, whereas PDR of CTS packets is increased from about 99.5% to 100% for the case of ELBM protocol as compared to LBM protocol.

3.6.2 Complex Test Case

We repeated the simulations for different number of USTAs such that the number of USTA-D is equal to that of USTA-H as shown in Fig. 3.9. We observe that PDR of multicast data of GO decreases for SM and LBM as the number of USTAs increases but it remains almost constant in the case of ELBM protocol as shown in Fig. 3.16. The reason is the reduction of collision from USTA-D and interference from USTA-H for ELBM. In the case of ELBM, PDR of multicast data of GO is increased by 40% and 19% as compared to SM and LBM, respectively.

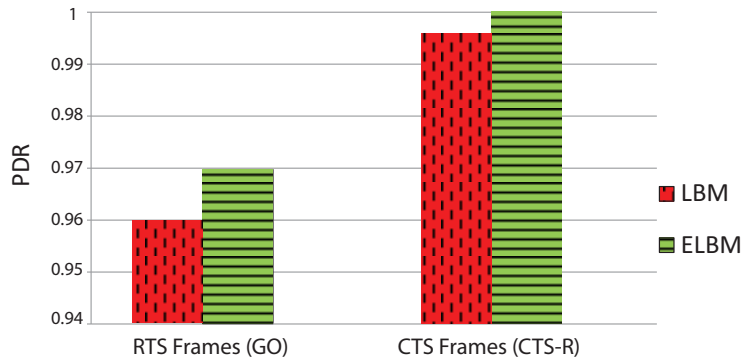

Figure 3.15: PDR of RTS (GO) and CTS (CTS-R)

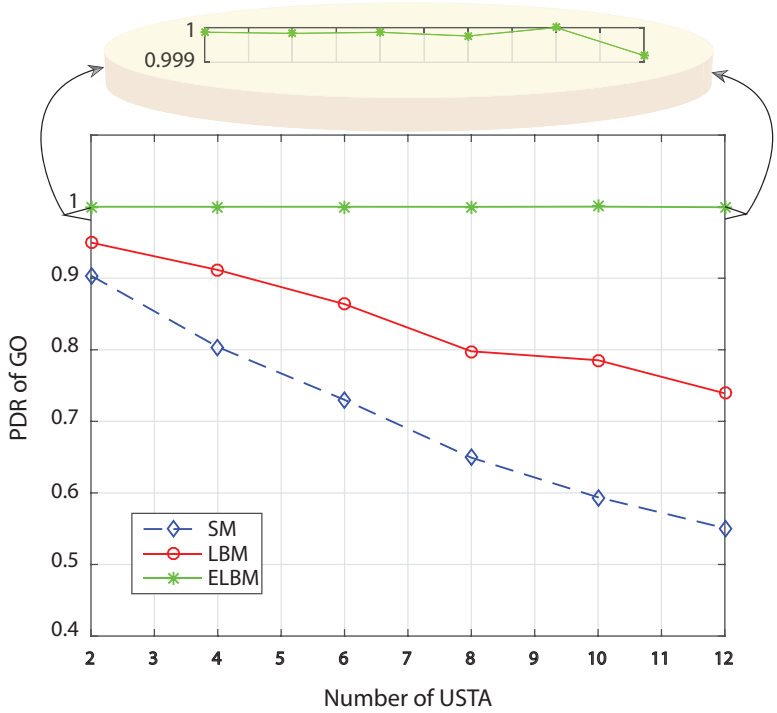

Figure 3.16: Multicast PDR of multicast packets at GO

As shown in Fig. 3.17, multicast throughput decreases as the number of USTAs increases for all protocols however the rate is much lower for ELBM as compared to SM and LBM. The multicast throughput of ELBM is higher by almost double and 1.8 times than those of SM and LBM respectively.

Similarly, average PDR of unicast stations is lower for ELBM as compared to SM when there is smaller number of USTAs but it is improved for ELBM than SM when the number of USTAs is increased as shown in Fig. 3.18. The reason for this change is the loss of packets due to collision and interference. Thus on average the PDR of USTAs is decreased by less than 1% for ELBM as compared to SM. On the other hand, average PDR of ELBM is better than that of LBM by about 1.8%. In the same way, average throughput of USTAs is lower for ELBM than LBM when the number of USTAs is smaller but it is reversed as the number of USTAs is increased as shown in Fig. 3.19. The average unicast throughput of USTAs is decreased by 1% for ELBM as compared to SM. However, average unicast throughput is improved by 4% for ELBM

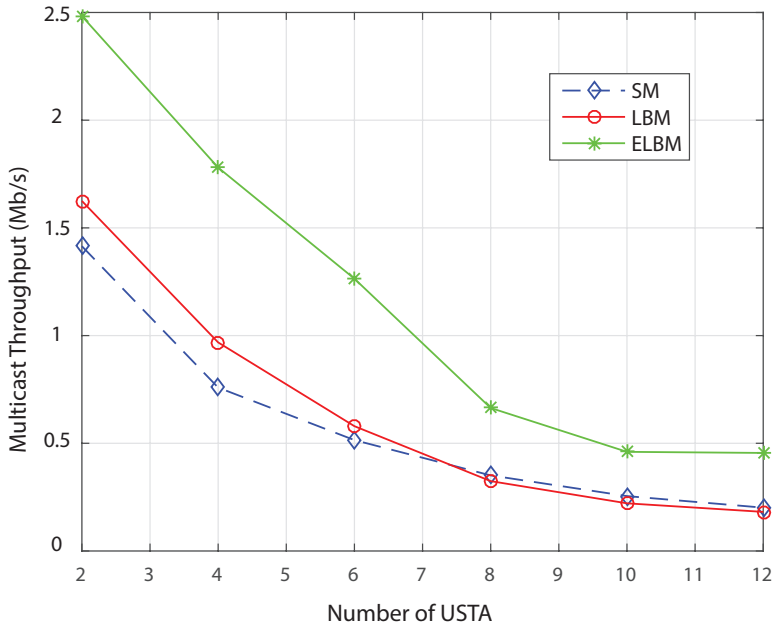

Figure 3.17: Multicast Throughput of multicast packets at GO

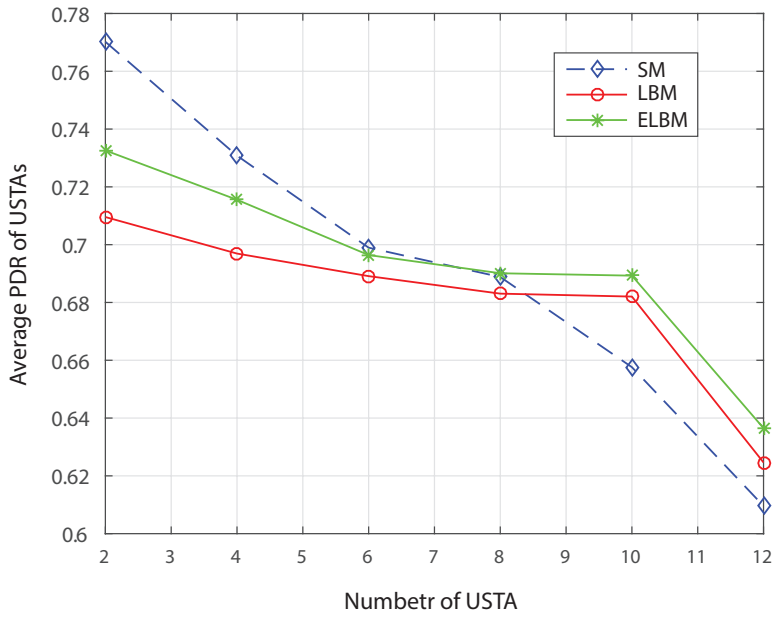

Figure 3.18: Average unicast PDR of USTA1 and USTA2

as compared to LBM due to avoidance of interference in case of ELBM protocol. Lastly, we show the advantages of ELBM over LBM in terms of overhead. As Table 3.2 illustrates, percent PDR of RTS/CTS of ELBM is greater than that of LBM. This is due to enhanced RTS/CTS method and optimal selection of CTS-R for ELBM.

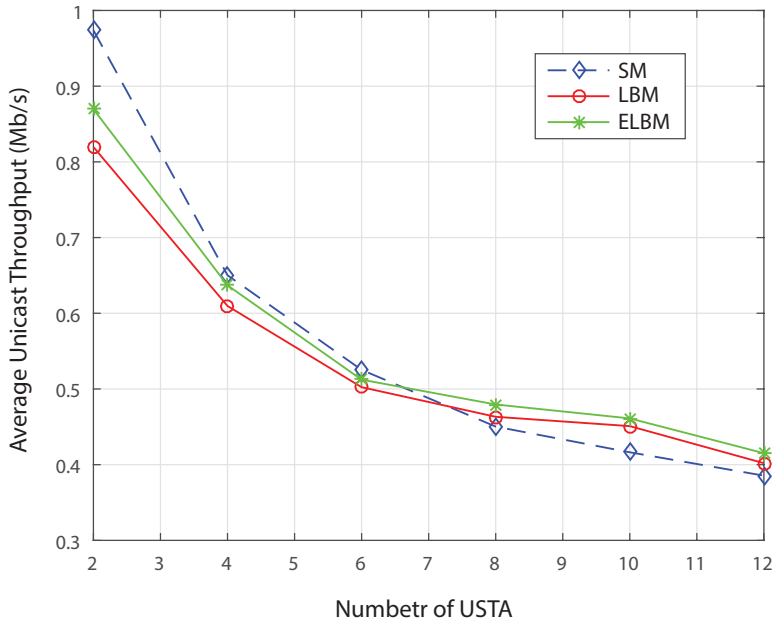

Figure 3.19: Average unicast Throughput of USTA1 and USTA2

3.7 Results and Discussions for EPLD Model

In order to examine the performance of the EPLD scheme, we have used Maple to solve the equations and Matlab for simulation. The values of different parameters of the MAC and PHY layers are illustrated in TABLE 3.1. We compare the simulation and analytical results of the EPLD model with the standard method, which is the DCF protocol of WD 802.11ac networks [11] without early packet collision detection in terms of system throughput. We use the parameters values mentioned in TABLE 3.1 unless it is exclusively mentioned for a specific experiment. The number of clients is set to 10 for all all cases except the case where the throughput is calculated as a function of number of clients. Similarly, the data rate and packet length are fixed at 13 Mb/s and 1500 bytes, respectively unless otherwise mentioned. Furthermore, we consider a 2x2 MIMO-OFDM system with 20 MHz channel bandwidth. We have obtained the results for different configurations to investigate the proposed EPLD analytical method from a wider perspective.

It is important to note that the analytical model presented is applied to the SM and the proposed early

Table 3.2: Percent PDR of RTS/CTS for LBM and ELBM

Number of USTAs	**PDR of RTS Packets (%)**		**PDR of RTS Packets(%)**	
USTA-H + USTA-C	**LBM**	**ELBM**	**LBM**	**ELBM**
2	96.52	96.86	99.69	100
4	92.60	93.67	99.57	99.98
6	89.29	90.19	99.06	99.93
8	78.88	80.22	98.60	99.80
10	77.25	79.64	98.57	99.74
12	75.60	78.88	97.90	98.89

packet loss detection model. The results discussed below are based on the observation of the SM and the proposed early packet loss detection. However, the early packet loss detection model can be equally applied to the LBM and ELBM.

Figure 3.20 shows the system throughput for EPLD method and the standard protocol for different payload size. The proposed analytical model provides higher throughput as the payload size increases as compared to the standard method. This is because the standard protocol spends more time in collision when the payload size increases. On the other hand, EPLD reduces the time of collision and the notification is sent earlier instead of waiting until the end of the payload size. As shown in Fig. 3.20, the throughput of the standard and proposed methods are 6.7 Mb/s and 7.3 Mb/s, respectively when payload size is 500 bytes. Thus the EPLD protocol increases the throughput by 8.92%. Similarly, the throughput of the standard and proposed methods are 9.5 Mb/s and 10.7 Mb/s respectively for a payload size of 2000 bytes, which is an improvement of 12.63%.

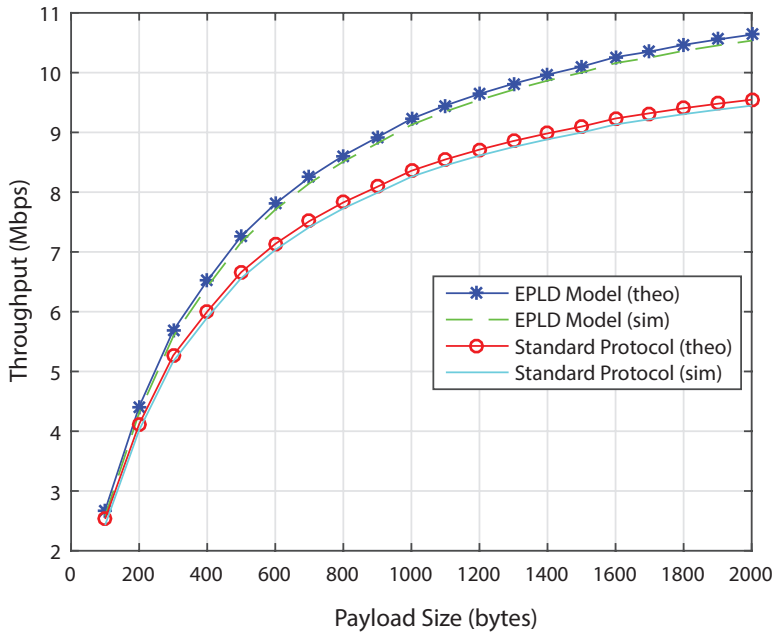

Figure 3.20: Total Throughput with different payload size

Similarly, EPLD model largely improves the throughput when the number of clients is increased. As shown in Fig. 3.21, the system throughput increases from 9.8 Mb/s to 10.6 Mb/s when the number of clients is five for the proposed method as compared to standard method. Therefore, the improvement is 8.16% in the case of EPLD method. On the other hand, for 20 clients, the throughput of the proposed method is improved by 14.19% i.e., from 8.4 Mb/s to 9.6 Mb/s as compared to the standard method.

We also investigate the performance of the EPLD protocol for different data rates as shown in Fig. 3.22. To this end, we use a range of data rates derived from the MCS of a 2x2 MIMO system under 20 MHz channel bandwidth as illustrated in TABLE 3.3. As Fig. 3.22 shows, the throughput of the proposed method is almost 8.33% better than that of the standard method for R_8.

Similarly, the system throughput increases as we increase the minimum contention window because it reduces the probability of collision. The throughput is shown in Fig. 3.23 for different values of the minimum contention contention window i.e, $W = \{2, 4, 8, 16, 32, 64\}$ for the standard and EPLD methods. We notice that system throughput of the EPLD protocol (9.1 Mb/s) is 18.18% higher than that of the standard protocol (7.7 Mb/s) when the minimum contention window is 8. This trend also continues for other sizes

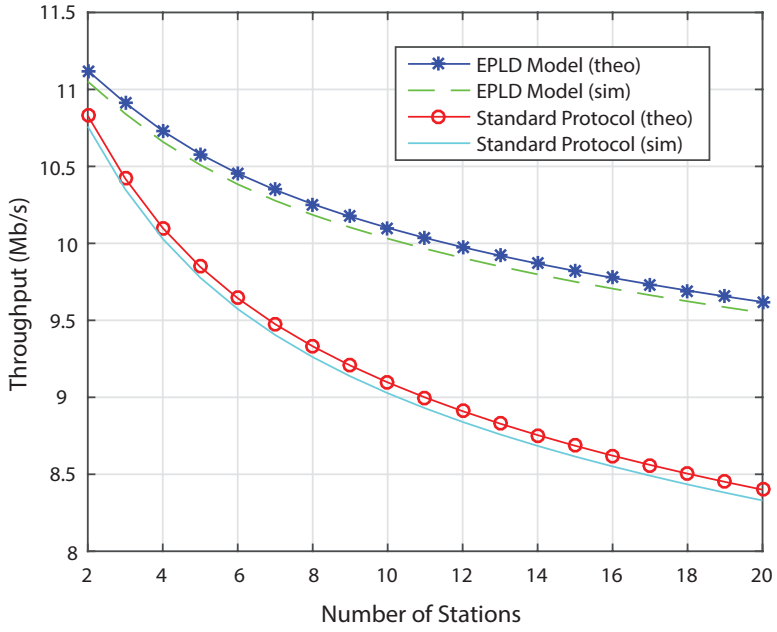

Figure 3.21: Total Throughput with different number of clients

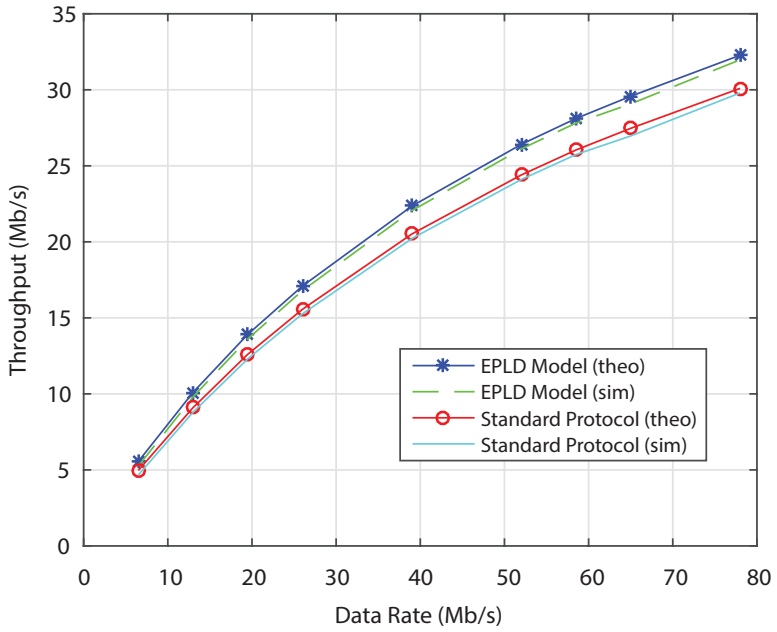

Figure 3.22: Total Throughput with different data rate

of the minimum contention window. Lastly, we calculate the system throughput for different contention

Table 3.3: Data Rates of VHT under a 20 MHz bandwidth Channel

Data Rate	R_0	R_1	R_2	R_3	R_4	R_5	R_6	R_7	R_8
Mb/s	6.5	13	19.5	26	39	52	58.5	65	78

stages i.e., $m = \{1, 2, 3, 4, 5, 6, 7\}$. As shown in Fig. 3.24, the system throughput of the EPLD model is almost 12% higher on average than that of the standard protocol.

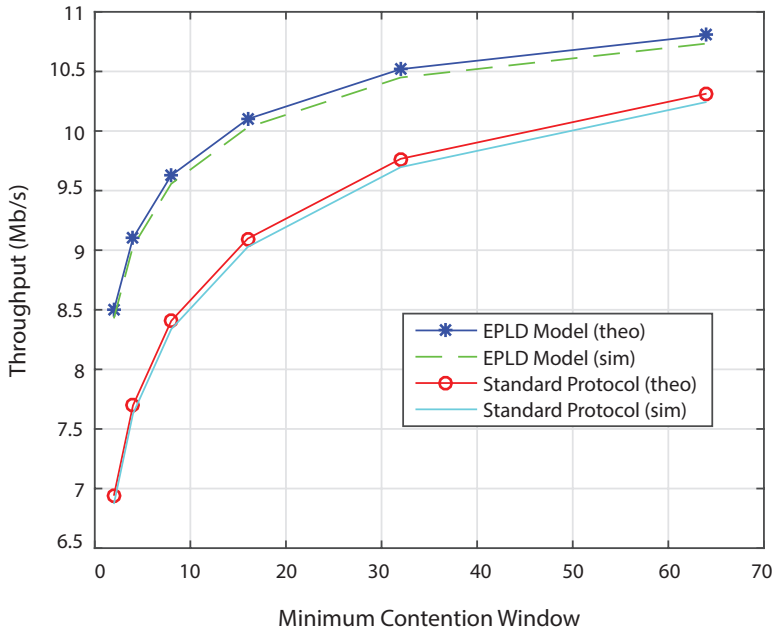

Figure 3.23: Total Throughput with different size of contention window

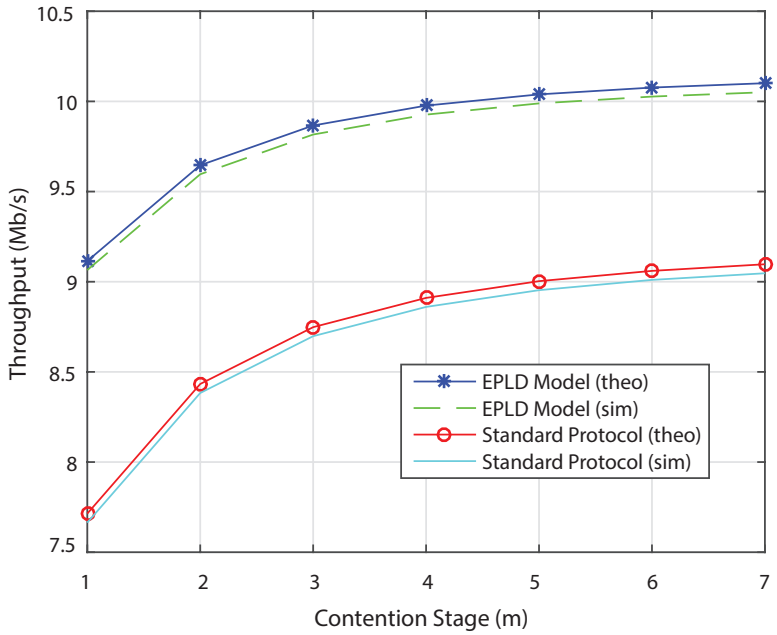

Figure 3.24: Total Throughput with different contention stage

3.8 Summary

In this chapter, we have investigated the problem of reliable multicast for WD and proposed a new algorithm called ELBM. ELBM improves reliability by reducing collision and interference from AP and other stations due to an improved channel access method, efficient CTS-R selection and enhanced RTS/CTS mechanism. The simulation results show better PDR and improved throughput for ELBM as compared to SM and LBM. In addition, an analytical model, EPLD was proposed to investigate the performance of early detection of packet loss in WD networks. For this purpose, the EPLD model considered the DCF backoff counter,

successful transmission time, and the time spent in collision at the MAC layer. The analytical results of the early packet loss detection protocol were compared with the standard protocol. The results showed that the system throughput of EPLD is better than the standard algorithm under different configurations. The application of the EPLD model to LBM and ELBM can be carried out in future research.

"Pure mathematics is, in its way, the poetry of logical ideas."

Albert Einstein (1879 – 1955)

4

Analytical Models for Very High Throughput with/out Hidden Stations

This chapter proposes two analytical models to evaluate the performance of Very High Throughput (VHT) for WD 802.11ac with/out hidden stations.

The first analytical model (4.1) formulates VHT at the MAC and PHY layers of 802.11ac followed by a system model of TGn MIMO multipath fading channel in the absence of hidden nodes. The model takes into account the key features of the MAC layer, such as transmission probability, contention window and transmission stage. Similarly, the new critical attributes of the 802.11ac PHY, such as modulation and coding schemes, spatial streams, and channel bandwidth are considered under TGn MIMO channel models. The simulation and theoretical results identifies important trends and trade-offs between system throughput and (MAC + PHY) features as a function of number of contending stations and payload size. It is observed that the system throughput of 802.11ac networks is significantly improved due to the addition of new PHY features. However, the system may degrade upto 50% in terms of symbol reception in the case of a high error-prone MIMO channel. Similarly, based on the Packet Error Rate (PER) analysis, appropriate channel models are suggested for given configurations to achieve better performance.

The second analytical model (Section 4.2), which is known as Vidden, formulates VHT of WD 802.11ac in the presence of hidden stations. The current analytical models in the literature do not accurately calculate the system throughput for high data rates, which is mainly due to ignoring the composite effects of hidden stations and/or the correct backoff time on system throughput. To this end, Vidden is proposed, which stands for ***V***HT ***i***n the presence of hi***dden*** stations. It carefully calculates the collision probability by taking into account both the contending as well as the hidden stations. Furthermore, closed-form formulas are derived to precisely calculate the geometric backoff time, successful transmission time and the time spent in the collision. The accuracy of the Vidden model is validated by simulation results. The system throughput obtained from the Vidden model closely follows the simulation results as compared to the extended Bianchi model [97].

4.1 VHT Model Without Hidden Nodes

The 802.11ac is a new standard by IEEE which achieves VHT [11] by using the new standard uses enhanced frame aggregation techniques at the MAC layer, whereas wider channel bandwidths, higher order Modulation and Coding Schemes (MCS), more complex MIMOs, and a Multi User (MU)-MIMO at the PHY layer.

We formulated the MAC and PHY layers of VHT in the absence of hidden nodes in Section 3.4.3 in chapter 3. We intend to analyse the throughput of WD under different configurations of new features of 802.11ac, such as different MIMOs, bandwidths, and MCSs. The following are the three key features which lead to VHT in 802.11ac.

1. More Spatial Streams (SS)
2. Higher Modulation and Coding schemes
3. Wider channel bandwidth

4.1.1 More Spatial Streams

802.11ac has increased the number of SS from 4 in 802.11n up to 8 at the PHY layer in a MIMO OFDM system. There are three main advantages of using more MIMO in 802.11ac, which are as follows.

i. Extending the range

ii. Improving reliability

iii. Achieving higher throughput

In addition to SU-MIMO, 802.11ac WAVE-2 also supports down link MU-MIMO in which an AP can send multiple data frames in the form of an Aggregated MAC Protocol Data Unit (A-MPDU) to multiple receivers at the same time. In practice, the current 802.11ac devices support three SS in WAVE-1 and four SS in WAVE-2 of 802.11ac. However, a total of 8 SS can be supported in the upcoming products [11, 98].

4.1.2 Modulation and Coding Schemes

A more advanced modulation i.e., 256 QAM has been added to 802.11ac standard which increases the number of bits per sub-carrier of OFDM as compared to a 64 QAM. As a result, the PHY data rate increases up to 33% as compared to the previous 802.11 standards. On one hand it significantly increases data rate; on the other hand, however, it requires higher Signal to Noise Ratio (SNR) for receivers to correctly demodulate the symbols. Similarly, 802.11ac supports a range of coding rates such as $\frac{1}{2}$, $\frac{2}{3}$, $\frac{3}{4}$, and $\frac{5}{6}$ [11].

4.1.3 Wider Channel Bandwidth

The IEEE standard 802.11ac increase the channel bandwidth due to its operation in 5 GHz band. In addition to 20 MHz and 40 MHs channels that were already available in 802.11n, wider channels of 80 MHz and 160 MHz have been added in 802.11ac. Furthermore a 160 MHz channel is established with two contiguous or non-contiguous 80 MHz channels [11].

4.1.4 Channel Model for 802.11ac

In order to evaluate the impact of the channel on the MAC and PHY layers of 802.11ac , we consider a set of channel models which are designed for IEEE 802.11 WLAN [99]. Each model is applicable to a specific

Table 4.1: Parameters of TGn Channel Models of 802.11ac

Channel name	User-case scenario	D_{BP} (m)	No of taps	σ_{RMS}	σ_{Max}	No of clusters	Conditions	K (dB)	Fading std. dev. (dB)
A	Flat Fading	5	1	0	0	1	LOS	0	3
							NLOS	$-\infty$	4
B	Residential	80	2	5	9	15	LOS	0	3
							NLOS	$-\infty$	4
C	Residential/ small office	200	2	5	14	30	LOS	0	3
							NLOS	$-\infty$	4
D	Typical office	390	3	10	18	50	LOS	3	3
							NLOS	$-\infty$	6
E	Large office	730	4	20	18	100	LOS	6	3
							NLOS	$-\infty$	6
F	Large space indoor/outdoor	1050	6	30	18	150	LOS	6	3
							NLOS	$-\infty$	6

environment with a set of 6 profiles, labelled A to F. All these profiles cover different scenarios as listed in TABLE 4.1. Each channel model has a path loss model including shadowing, and a MIMO multipath fading model, which describes the multipath delay profile, the spatial properties, the K-factor distribution shown as Rician K-factor in TABLE 4.1, and the Doppler spectrum [100].

Each channel model has a certain number of taps which are associated with specific delays. Furthermore, each channel model is comprised of a certain number of clusters. A cluster is made up of a set of taps. The number of taps, Root Mean Square (RMS) delay (σ_{RMS}), maximum delay (σ_{Max}), the number of clusters and standard deviation of shadow fading both in the case of Line of Sight (LOS) and Non Line of Sight (NLOS) for each model are listed in TABLE 4.1. The LOS K-factor is applicable only to the first tap while all the other taps K-factor remain at $-\infty$ dB. The following set of spatial properties are defined for each cluster.

i. Mean Angle of Arrival (AoA)

ii. Mean Angle of Departure (AoD)

iii. Angular Spread (AS) at transmitter

iv. AS at receiver

These parameters determine the transmit and receive correlation matrices associated with each tap delay. The LOS component can only be present on the first tap. If the distance between the transmitter and the receiver is greater than d_{BP}, which is the break-point distance or distance of the first wall (i.e., distance of

transmitter from the first reflector), then the LOS component is not present. The d_{BP} for all channel models (A-F) are listed in 5^{th} column of TABLE 4.1.

We consider a path loss model, which takes into account the free space loss L_{FS} (log-distance model with a path-loss exponent of 2) up to d_{BP} and log-distance model with the path-loss exponent of 3.5 after d_{BP} [101]. For each of the models, a different break-point distance d_{BP} is chosen. The path loss model $L(d)$ is defined in eq. (4.1).

$$L(d) = \begin{cases} L_{FS}(d) & \text{if } d \leq d_{BP} \\ L_{FS}(d_{BP}) + 35log10(d/d_{BP}) & \text{if } d > d_{BP} \end{cases} \tag{4.1}$$

where d is the distance between transmitter and receiver. The other parameters of the path loss model are listed of TABLE 4.1. The standard deviations of log-normal (Gaussian in dB) shadow fading are also included in 10^{th} column in TABLE 4.1. The values were found to be in the range between 3 and 14 dB [102].

Similarly, the zero-mean Gaussian probability distribution is given by eq. (4.2).

$$p(x) = \frac{1}{\sqrt{2\pi\sigma}} e^{[\frac{x^2}{2\sigma^2}]} \tag{4.2}$$

We are interested in modelling the MIMO channel of 802.11ac. Thus, the correlation between transmit and receive antenna is an important aspect of the MIMO channel. To this end, we follow a procedure based on the transmitter and receiver correlation matrices [103] to calculate the MIMO channel matrix H for each tap, at one instance of time, in the A-F delay profile models. The channel matrix H is derived as a sum of two matrices namely: a fixed LOS matrix with constant entries, and a Ryleigh NLOS matrix with variable entries as shown in eq. (4.3).

$$H = \sqrt{P}\left(\sqrt{\frac{K}{K+1}} H_F + \frac{1}{K+1} H_V\right) \tag{4.3}$$

where P indicates the power of each tap which is obtained by summing all the power of LOS and NLOS powers, and K is the Ricean K-factor. Eq. (4.3) can be expressed for any number of transmitter and receiver for MIMO. If there are T input antennas at the transmitter and R output antennas at the receiver then H_F and H_V in eq. (4.3) can be represented as shown in 4.4 and eq. (4.5).

$$H_F = \begin{bmatrix} e^{j\phi_{11}} & e^{j\phi_{12}} & \dots & e^{j\phi_{1T}} \\ e^{j\phi_{21}} & e^{j\phi_{22}} & \dots & e^{j\phi_{2T}} \\ \vdots & \vdots & \ddots & \vdots \\ e^{j\phi_{R1}} & e^{j\phi_{R2}} & \dots & e^{j\phi_{RT}} \end{bmatrix} \tag{4.4}$$

$$H_V = \begin{bmatrix} X_{11} & X_{12} & \dots & X_{1T} \\ X_{21} & X_{22} & \dots & X_{2T} \\ \vdots & \vdots & \ddots & \vdots \\ X_{R1} & X_{R2} & \dots & X_{RT} \end{bmatrix} \tag{4.5}$$

where $e^{j\phi_{ij}}$ indicates the constant elements of the LOS matrix (H_F) and X_{ij} indicates the element of the variable NLOS Rayleigh matrix (H_V) between i^{th} receiving and j^{th} transmitting antennas. It is assumed that X_{ij} is a complex Gaussian random variable with zero mean and unit variance.

In order to correlate an X_{ij} element of the matrix H_V, the following method is used as shown in eq.

(4.6).

$$[X] = [R_{rx}]^{\frac{1}{2}}[H_{iid}][R_{tx}]^{\frac{1}{2}} \tag{4.6}$$

where R_{rx} and R_{tx} are the receive and transmit correlation matrices, respectively, whereas, the H_{iid} is a complex Gaussian random variable. All the Gaussian random variables used in the formulation are considered to be identically independent with zero mean and unit variance. In addition, R_{tx} and R_{rx} are given by eq. (4.7) and eq. (4.8).

$$[R_{tx}] = [\rho_{txij}] \tag{4.7}$$

$$[R_{rx}] = [\rho_{rxij}] \tag{4.8}$$

where ρ_{txij} indicate complex correlation coefficients between i^{th} and j^{th} transmitting antennas, and ρ_{rxij} indicates the complex correlation coefficients between i^{th} and j^{th} receiving antennas.

Alternatively, X in eq. (4.6) can also be calculated using other approaches such as Kronecker product of the transmit and receive correlation matrices to calculate X as shown in eq. (4.9) [103].

$$[X] = ([R_{tx}] \otimes [R_{rx}])^{\frac{1}{2}}[H_{iid}] \tag{4.9}$$

It can be seen that H_{iid} is an array in this case instead of a matrix, which is further represented by R_{tx} and R_{rx} matrices as listed in eq. (4.10) and eq. (4.11).

$$R_{tx} = \begin{bmatrix} 1 & \rho_{tx12}{}^{*} & \cdots & \rho_{tx1T}{}^{*} \\ \rho_{tx21} & 1 & \cdots & \rho_{tx2T}{}^{*} \\ \vdots & \vdots & \ddots & \vdots \\ \rho_{txR1} & \rho_{txR2} & \cdots & 1 \end{bmatrix} \tag{4.10}$$

$$R_{rx} = \begin{bmatrix} 1 & \rho_{rx12}{}^{*} & \cdots & \rho_{rx1T}{}^{*} \\ \rho_{rx21} & 1 & \cdots & \rho_{rx2T}{}^{*} \\ \vdots & \vdots & \ddots & \vdots \\ \rho_{rxR1} & \rho_{rxR2} & \cdots & 1 \end{bmatrix} \tag{4.11}$$

The values of complex correlation coefficient ρ are calculated from power angular spectrum (PAS), AS, mean AoA, mean AoD, and individual tap powers [99, 104]. Consequently, for the Uniform Linear Array (ULA), the complex correlation coefficient at the linear antenna array is expressed as shown in in eq. (4.12).

$$\rho = R_{XX}(D) + jR_{XY}(D) \tag{4.12}$$

where $D = 2\pi d/\lambda$ (λ shows the wavelength in metre), whereas, R_{XX} and R_{XY} are the cross-correlation functions between the real parts and between the real part and imaginary part, respectively as shown in eq(4.13) and eq. (4.14).

$$R_{XX}(D) = \int_{-\pi}^{\pi} \cos(D\sin\phi)PAS(\phi)d\phi \tag{4.13}$$

$$R_{XY}(D) = \int_{-\pi}^{\pi} \sin(D\cos\phi)PAS(\phi)d\phi \tag{4.14}$$

The correlation coefficient matrices are calculaetd in three ways namely: uniform, truncated Gaussian, and truncated Laplacian PAS shapes [99].

Table 4.2: Parameters of a VHT Frame 802.11ac

Parameter	Value (μs)	Parameter	Value	Parameter	Value (μs)
Slot time	9	CW_{min}	16	T_{SYMS}	3.6
T_{DIFS}	34	m	5	T_{SYML}	4
T_{L-SIG}	4	$m\prime$	7	T_{SIFS}	16
$T_{VHT-STF}$	4	L_{MAC}	34 bits	T_{STF}	8
$T_{VHT-SIG-A}$	8	N_{VHTLTF}	1	T_{LTF}	8
$T_{VHT-SIG-B}$	4	N_{tail}	6 bits	T_{SIFS}	16
$T_{VHT-LTF}$	4	$N_{service}$	16 bits	ρ	1

4.1.5 Simulation Environment

We have implemented the MAC and PHY layers of 802.11ac in matlab with the given parameters as defined in [11]. TABLE 4.2-4.6 list the parameters, which are used in the theoretical analysis as well as the simulation setup. We do not consider a frame aggregation scheme for the sake of simplicity. To simulate different features of the PHY, we summarize the MCSs into four tables i.e., TABLES 4.3-4.6 for 20 MHz, 40 MHz, 80 MHz, and 160 MHz channels, respectively. The values of MCSs are chosen such that a wide range of modulation and coding schemes is covered.

We consider various modulation schemes namely: Quadrature Phase Shift Keying (QPSK), 16-QAM (Quadrature Amplitude Modulation), 64-QAM, and 256-QAM. The coding rate (R) is chosen as $\frac{1}{2}, \frac{2}{3}, \frac{3}{4}$, and $\frac{5}{6}$. In the same way, the number of SS (N_{SS}) is selected to be 1, 2, 4, and 8. The data rate is calculated from eq. (3.12) in Chapter 3, whereas ACK rate is fixed at basic rate as per eq. (3.13) Chapter 3. Each simulation is run 40 times and then average is calculated to show stable results.

In order to implement a TGn channel in matlab, we use the parameters from TABLE 4.1. In addition, we use OFDM with MIMO channel at transmitter and receiver for the PHY layer and channel analysis of 802.11ac.

Table 4.3: MCS for 20 MHz Channel

MCS	Modulation	R	N_{ss}	N_{DBPS}	N_{ES}	Data rate (Mbps) GI = 800 ns	Data rate (Mbps) GI = 400 ns
1	QPSK	1/2	1	52	1	13	14.4
			4	208	1	52	57.8
			8	416	1	104	115.6
3	16-QAM	1/2	1	104	1	26	28.9
			4	416	1	104	115.6
			8	832	1	208	231.1
5	64-QAM	2/3	1	208	1	52	57.8
6	64-QAM	3/4	1	234	1	58.5	65
7	64-QAM	5/6	1	260	1	65	72
8	256-QAM	3/4	1	312	1	78	86.7

Table 4.4: MCS for 40 MHz Channel

MCS	Modulation	R	N_{ss}	N_{DBPS}	N_{ES}	Data rate (Mbps)	
						GI = 800 ns	GI = 400 ns
1	QPSK	1/2	1	108	1	27	30
			2	216	1	54	60
			4	432	1	108	120
			8	864	1	216	240
3	16-QAM	1/2	1	216	1	54	60
			2	432	1	108	120
			4	864	1	216	240
			8	1728	1	432	480
5	64-QAM	2/3	1	432	1	108	120
9	256-QAM	5/6	1	720	1	180	200

Table 4.5: MCS for 80 MHz Channel

MCS	Modulation	R	N_{ss}	N_{DBPS}	N_{ES}	Data rate (Mbps)	
						GI = 800 ns	GI = 400 ns
1	QPSK	1/2	1	234	1	58.5	65
			4	936	1	234	260
			8	1872	1	468	520
3	16-QAM	1/2	1	468	1	117	130
			4	1872	1	468	520
			8	3744	2	936	1040
5	64-QAM	2/3	1	936	1	234	260
8	256-QAM	3/4	1	1404	1	351	390
			4	5616	3	1404	1560
			8	11232	6	2808	3120

4.1.6 Results and Discussions

We calculate aggregate throughput for different number of STAs and payload size.

4.1.6.1 Wider Channels

In order to evaluate the effect of wider channels on system throughput, we calculate total throughput for 20 MHz, 40 MHz, 80 MHz, and 160 MHz channels. We simulate a scenario which uses QPSK with $N_{ss} = 4$, and $GI = 400\ ns$. The payload size is fixed at 1500 bytes. As shown in Fig. 4.1, the total throughput decreases for all the cases of channel bandwidths as the number of STAs increases. However, the total throughput increases when a wider channel bandwidth is used. As compared to the case of a 20 MHz

Table 4.6: MCS for 160 MHz Channel

MCS	Modulation	R	N_{ss}	N_{DBPS}	N_{ES}	Data rate (Mbps)	
						GI = 800 ns	GI = 400 ns
1	QPSK	1/2	1	468	1	117	130
			4	1872	1	468	520
			8	3744	2	936	1040
3	16-QAM	1/2	1	936	1	234	260
4	16-QAM	3/4	1	1404	1	351	390
5	64-QAM	2/3	1	1872	1	568	520
			4	7488	4	1872	2080
			8	14976	8	3744	4160
8	256-QAM	3/4	1	2808	2	702	780
			4	11232	6	2808	3120
			8	22464	12	5616	6240

channel bandwidth, the total throughput is increased by more than 10, 20, and 30 Mb/s in the cases of 40, 80, and 160 MHz channel bandwidth, respectively. It is important to note that the comparative raise in total throughput is not proportional to the increase of channel bandwidth, i.e., less than one quarter increase of channel bandwidth. The theoretical (num) results also show a similar trend.

Similarly, we observe the effects of available channel bandwidth on throughput as a function of payload size. For this purpose, we use a modulation of 16 QAM with one SS i.e., $N_{ss} = 1$, and $GI = 800\ ns$. In the case of 20/40/80/160 MHz channel, the coding rate of 16QAM can be 1/2 or 3/4 (see Table IV-VII). The number of STAs is 20 (i.e., $n = 20$) in this set up. Fig. 4.2 illustrates that total throughput increases by nearly 10 Mbps as the channel width is doubled.

4.1.6.2 Modulation Schemes

The choice of a particular modulation scheme can greatly affect the system throughput. To observe this result, we fix the number of SS to 1 in a 20 MHz channel with $GI = 800\ ns$ and payload size of 1500 bytes. We calculate throughput for different modulation schemes. As illustrated in Fig. 4.3, QPSK gives the lowest throughput while 256 QAM produces the highest total throughput. The improvement is 20 Mpbs from QPSK to 256 QAM. It is also worth noting that the total throughput is greatly affected by different modulation techniques under different payload sizes. To examine this, the number of STAs is fixed to 20, while $N_{ss} = 1$ with QPSK in a 40 MHz channel and $GI = 800\ ns$. Fig. 4.4 represents that the total throughput increases as the payload size is increased. In addition, the higher order modulation schemes produce higher throughput. The difference of throughput between different modulation schemes is increased with increase in payload size. For instance, when payload size reaches 2000 bytes, there is an elevation of 10 Mbps for each modulation scheme (i.e., QPSK, 16 QAM, 64 QAM and 256 QAM).

4.1.6.3 Multiple Spatial Streams

Similarly, in order to observe the impact of different number of transmitting antennas on total throughput, we consider a user case of 16 QAM with 40 MHz channel, $GI = 800\ ns$ and fixed payload size of 1500

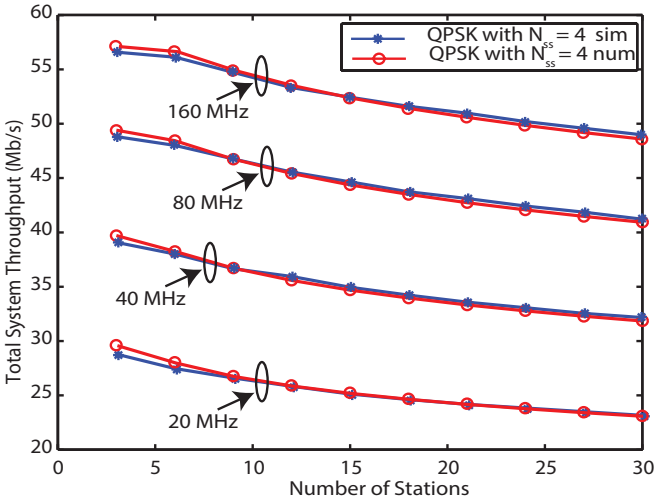

Figure 4.1: Throughput for different channels as a function of number of STAs

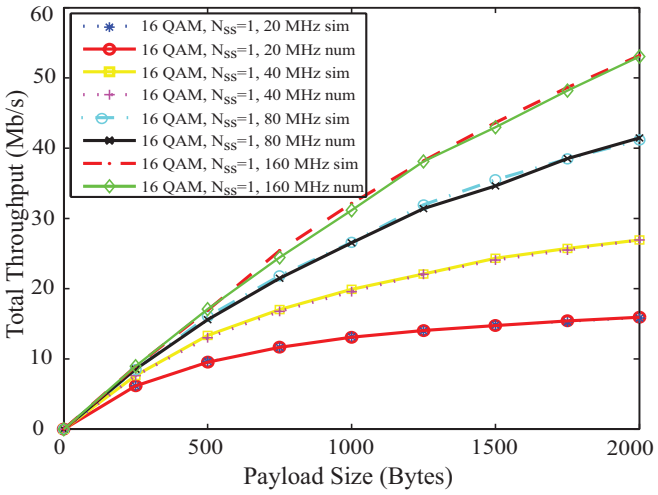

Figure 4.2: The effects of wider channels on throughput for different payload size

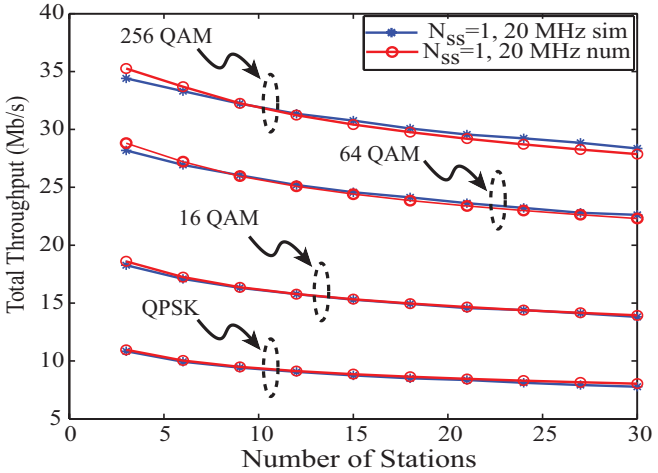

Figure 4.3: Throughput of different modulation schemes for different STAs

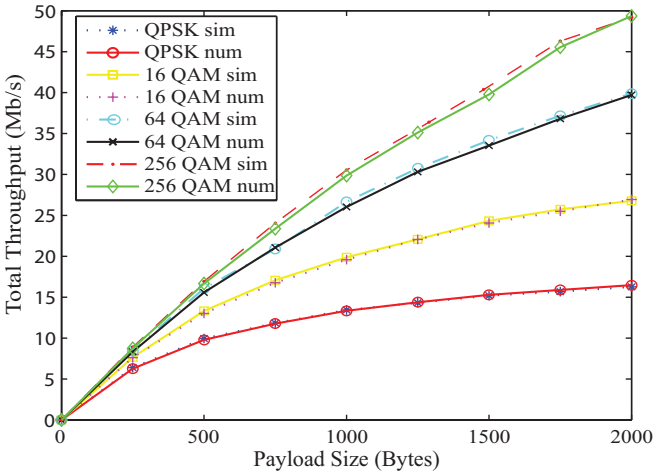

Figure 4.4: Throughput for different modulations as a function of payload size

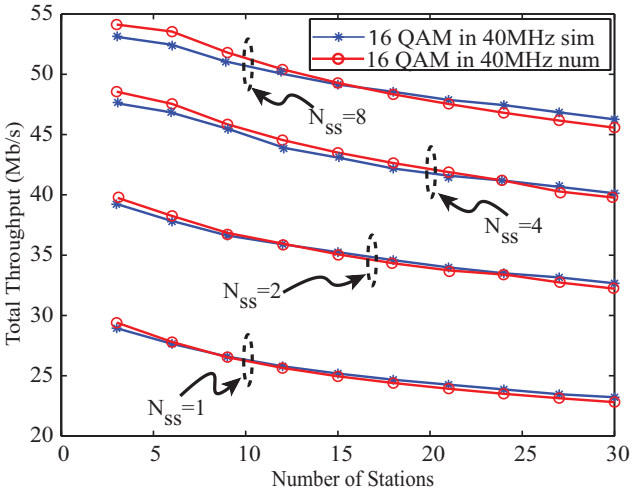

Figure 4.5: The effects of SS on throughput for different number of STAs

bytes. Although 802.11ac may support 1 to 8 SSs, however, for the sake of simplicity and comprehension, we consider $N_{ss} = \{1, 2, 4, 8\}$. As shown in Fig. 4.5, the total throughput decreases as we increase the number of STAs for all SSs. Nonetheless, the overall throughput for a particular number of SS increases by 10 Mbps as the number of SS is doubled. Likewise Fig. 4.6 illustrates the total throughput for different antenna streams. The modulation used is QPSK with $GI = 800\ ns$ in a 40 MHz channel with 20 STAs. As can be seen in Fig. 4.6, the total throughput increases as we increase the payload size. In particular, the total throughput increases by almost 10 Mbps for every $2N_{ss}$.

4.1.6.4 Coding Rate

The relationship between total throughput and different number of STAs is examined under various coding rates, such as $R = \{\frac{2}{3}, \frac{3}{4}, \frac{5}{6}\}$. The other parameters are set as $N_{ss} = 1$, modulation = 64 QAM, and $GI = 400\ ns$ in a 20 MHz channel. Given the aforementioned setup, Fig. 4.7 shows that the total system throughput increases by 1 Mbps as we choose the next available higher coding rate. The impact of coding rate on total throughput as a function of payload size is illustrated in Fig. 4.8. We choose 16 QAM in a 160 MHz channel with $N_{ss} = 1$. The number of STAs is 20 while $GI = 800ns$. The total throughput

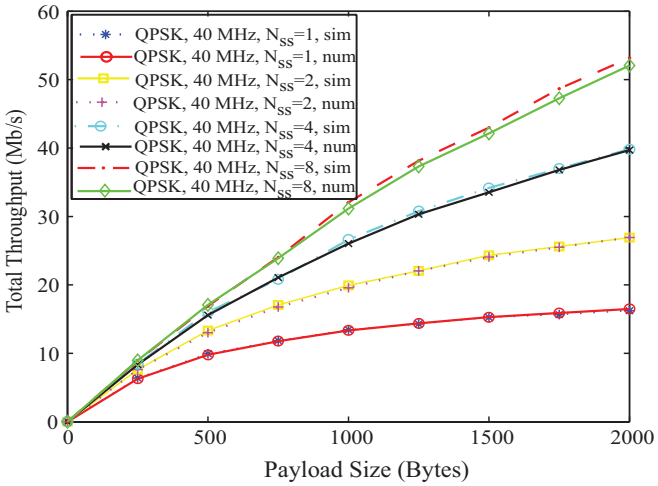

Figure 4.6: Throughput for different antenna streams with variable payload size

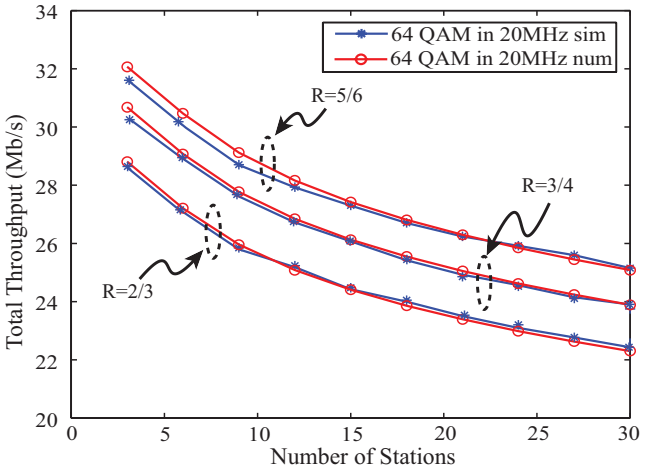

Figure 4.7: Throughput in different coding rate (R) for different STAs

comparatively increases by 4 Mbps for $R = \frac{3}{4}$ than $R = \frac{1}{2}$ for a payload size of 1500 bytes. However, the throughput raises upto 9 Mbps for $R = \frac{3}{4}$ as compared to $R = \frac{1}{2}$, when the payload size increases to 2000 bytes. Fig. 4.8 indicates that a particular coding rate can tremendously affect total throughput under a variable frame size.

4.1.6.5 Analysis under TGn Channel

As illustrated in TABLE 4.1, each TGn channel has a different profile. In order to investigate the impact of a channel on MCS, we simulate 802.11ac under channel D and see the performance in terms of Symbol Error Rate (SER). For this purpose, we use an OFDM system under a 40 MHz MIMO multipath Rayleigh fading channel. Accordingly, a 128 point Fast Fourier Transform (FFT) is used with 128 subcarriers for a 40 MHz.The bandwidth of each sub carrier is 312.5 KHz for OFDM in 802.11ac. Out of 124 subcarriers, the 114 subcarriers (-58 to 2 and 2 to 58) are used for data and pilot (timing and synchronization). The indices used for pilot subcarriers are -53, -25, -11, 11, 25, and 53. The subcarriers -1, 0, and, -1 are used as a Direct Current (DC) component while the remaining 11 subcarriers are used as left (6) and right (5) guard bands.

The SER of the system is calculated for a BPSK, QPSK, 16-QAM, 64-QAM and 256-QAM modulation

Table 4.7: PER levels for a range of SNR of SISI-OFDM 802.11ac WLAN system

TGn Channel	Parameter	Initial Value	Intermediate Value	Final Value
A	SNR (dB)	0-7	8-34	35-50
	PER (%)	100	91.66-2	0
B	SNR (dB)	0-7	8-25	26-50
	PER (%)	100	91.66-2	0
C	SNR (dB)	0-13	14-26	27-50
	PER (%)	100	68.75-2	0
D	SNR (dB)	0-7	8-25	26-50
	PER (%)	100	91.66-8	6
E	SNR (dB)	0-11	12-40	41-50
	PER (%)	100	91.66-3.2	2
F	SNR (dB)	0-13	14-20	21-50
	PER (%)	100	68.75-14.10	11.70

Table 4.8: PER levels for a range of SNR of 2x2 MIMO-OFDM 802.11ac WLAN system

TGn Channel	Parameter	Initial Value	Intermediate Value	Final Value
A	SNR (dB)	0-14	15-34	35-50
	PER (%)	100	78.57-12.79	11.82
B	SNR (dB)	0-9	10-34	35-50
	PER (%)	100	91.66-4	2
C	SNR (dB)	0-17	18-33	34-50
	PER (%)	100	91.66-2.32	2
D	SNR (dB)	0-15	16-28	29-50
	PER (%)	100	78.57-1.8	2
E	SNR (dB)	0-16	17-36	37-50
	PER (%)	100	78.57-3.4	6.1
F	SNR (dB)	0-15	16-33	34-50
	PER (%)	100	91.66-19.29	18.03

schemes under different Energy per Symbol (E_s/N_o) for OFDM transceiver under a 40 MHz 2x2 MIMO TGn D channel as shown in Fig. 4.9. The SER decreases as E_s/N_o increases for all modulation schemes. However, in lower E_s/N_o, the SER of BPSK is much lower as compared to other modulation schemes. Similarly, QPSK shows lower SER at higher noise as compared to other high order modulation schemes. A similar trend can be seen for a 16-QAM and 64-QAM as compared to a 256-QAM. Thus, in an error-prone channel conditions, 802.11ac suffers from almost 50% SER for 256-QAM as compared to BPSK as shown in Fig. 4.9.

Table 4.9: PER levels for a range of SNR of 4x4 MIMO-OFDM 802.11ac WLAN system

TGn Channel	Parameter	Initial Value	Intermediate Value	Final Value
A	SNR (dB)	0-20	21-43	44-50
	PER (%)	100	91.66-32.35	28.94
B	SNR (dB)	0-24	25-35	36-50
	PER (%)	100	91.66-4.2	0
C	SNR (dB)	0-24	25-35	36-50
	PER (%)	100	91.66-1	0.8
D	SNR (dB)	0-19	20-27	28-50
	PER (%)	100	84.61-0.26	0.20
E	SNR (dB)	0-16	17-28	29-50
	PER (%)	100	84.61-6.3	5.8
F	SNR (dB)	0-18	19-33	34-50
	PER (%)	100	84.61-10.78	9.32

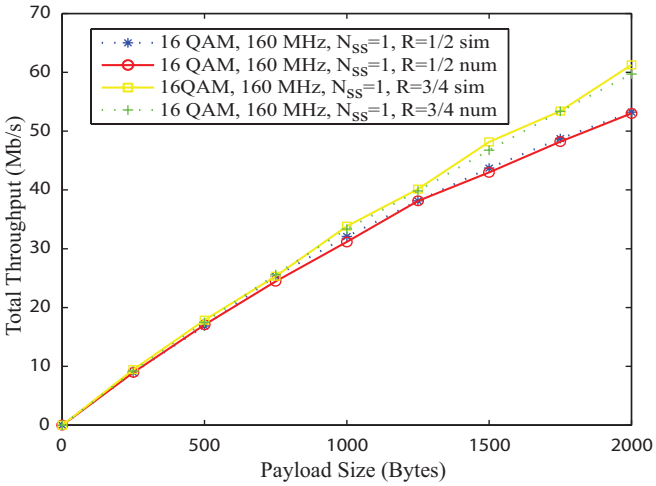

Figure 4.8: Throughput of different coding rate for different payload

Next, we consider the impact of all TGn channels i.e., (A to F) TABLE 4.1 on the performance of 802.11ac network. For this purpose, we fix all other parameters except the number of of transmit and receive antennas. This will help in observing an accurate estimation of a 1x1, 2x1, and 4x4 MIMO changes on the performance of 802.11ac network under different TGn channels. We use the MIMO OFDM system with 64 point FFT, 20 MHz channel, 64-QAM, a coding rate of 1/2 (i.e., MCS = 3) as illustrated in TABLE 4.3. The packet length is set to 1500 bytes. We calculate the Packet Error Rate (PER) to asses the performance of MIMO OFDM 802.11ac under different channels. We sent 1000 packets for each Signal to Noise Ratio (SNR) point that ranges from 0 dB to 50 dB. The distance between the transmitter and receiver is set to 10 m. We also add Additive White Gussian Noise (AWGN) in order to make a realistic estimation of the wireless channel.

We observe that the PER and SNR can be divided into three different levels when the SNR of a channel

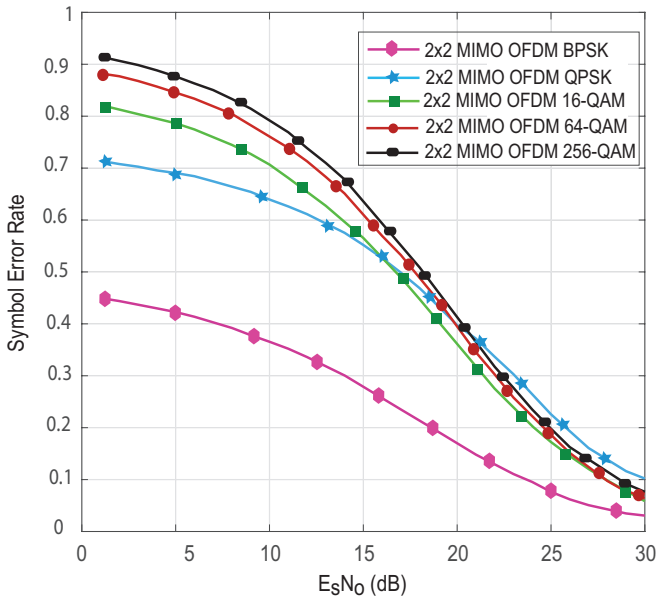

Figure 4.9: Symbol Error Rate vs. EsNo for different Modulation schemes

is changed from 0 dB to 50 dB for all the six channel models in 1x1, 2x2 and 4x4 MIMOs. This trend can also be seen in a different configurations of transmit and receive antennas as shown in Fig. 4.10-4.15. Let the three levels are referred to as *initial level*, *intermediate level*, and *final level*. The PER is explained with the help of Fig. 4.10-4.15 and TABLE 4.7-4.9. As shown in Fig. 4.10-4.15 and TABLE 4.7-4.9, the PER remains constant at *initial* and *final levels* while it drops down over a range of SNR values at *intermediate level* for all the channel models under 1x1, 2x2 and 4x4 MIMOs. The range of SNR values for the three levels changes differently for the six channel models under different MIMO configurations.

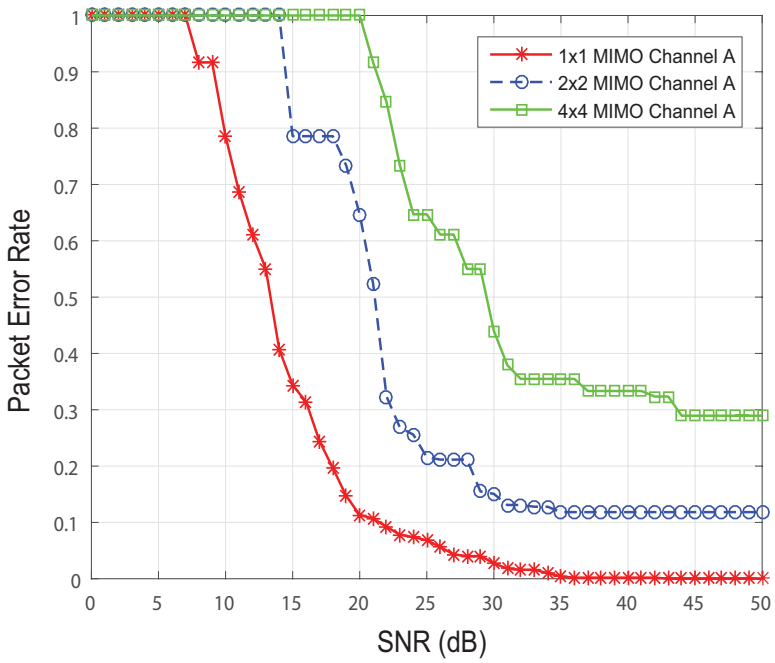

Figure 4.10: Packet Error Rate vs. SNR of Channel A under different MIMO configurations

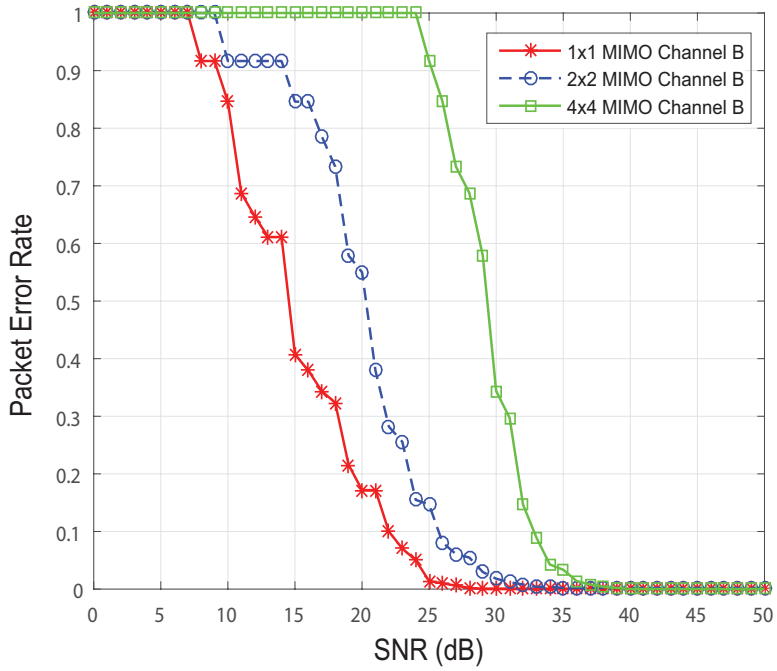

Figure 4.11: Packet Error Rate vs. SNR of Channel B under different MIMO configurations

As illustrated in TABLE 4.7-4.9, the PER is 100% at *initial level* for all the channels and all the cases, which indicates that the system performance is worst at *initial level*. However, the range of SNR points at *initial value* increases as we increase the number of transmit and receive antennas. For example: the average range of SNR (average of A-F) is 0 to 9.6 dB (TABLE 4.7) , 0 to 14.3 dB (TABLE 4.8), and 0 to 20.1 dB (TABLE 4.9) for 1x1, 2x2, and 3x3 MIMOs, respectively. It shows that the performance of 1x1 MIMO is better than that of 2x2 MIMO and 4x4 MIMO. Similarly, the performance of a 2x2 MIMO is better than that of 4x4 MIMO in terms of packet reception at lower SNR values. In the same way, the PER remains constant at *final level* for all channel models and all MIMO configuration. However, the values of PER and the range of SNR are different for different channels under different MIMOs. For example at *final level*, the PER and SNR of channel model A remains 0%, 11.82%, and 28.94% at 35-50 dB, 35-50 dB, and 44-50 dB for 1x1 MIMO, 2x2 MIMO, and 4x4 MIMO configurations, respectively. A similar trend can be seen for other channels. On the other hand for *intermediate level*, the PER drops down from higher values to lower values over a range of SNR points. The slop and trend of each drop is different for different channel models and different MIMO configurations.

Based on the simulation results, we find interesting performance patterns for 802.11ac under different channel models. As shown in Fig. 4.10-4.15 and TABLE 4.7, the PER of 802.11ac is 100% at *initial level* and 0% *final level* for channel models A, B, and C under 1x1 MIMO. The PER is 2% and 6% for channel models D and E, respectively. However, the PER is 11.70% in case of channel model F which is the worst performance for 1x1 MIMO for a given configurations.

Similarly, under 2x2 MIMO, the system performs best for channel models B, C and D, where the PER remains at 2% at *final level* for these three channel models as shown in Fig. 4.10-4.15 and TABLE 4.8. However, the system performance degrades to some extent for channel models A, E, and F where the PER is 11.82%, 6.1%, and 18.03%, respectively. The PER for channel model F is the maximum (18.03%) as compared to other models. Channel model B relatively provides better results under 2x2 MIMO as shown in Fig. 4.10-4.15. The PER of 802.11ac network remains lower for channel models B, C, and D under 4x4

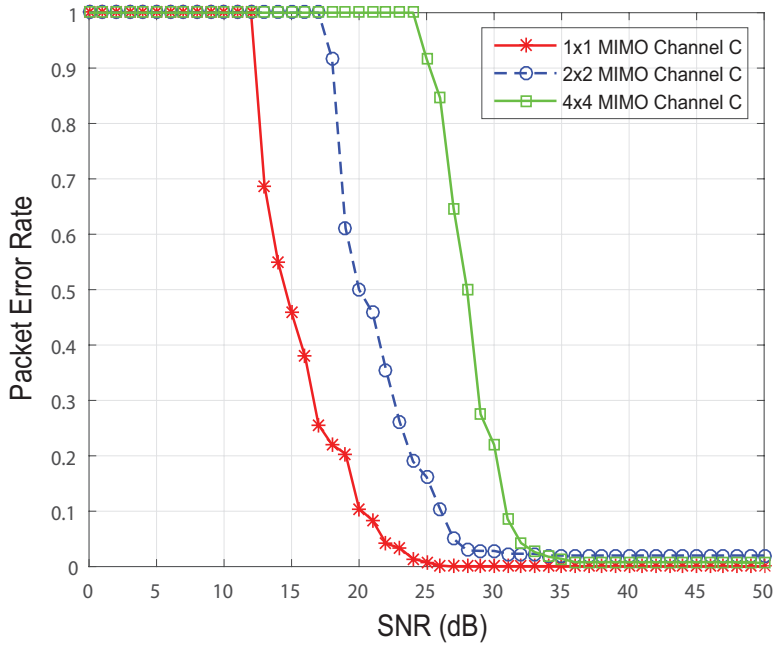

Figure 4.12: Packet Error Rate vs. SNR of Channel C under different MIMO configurations

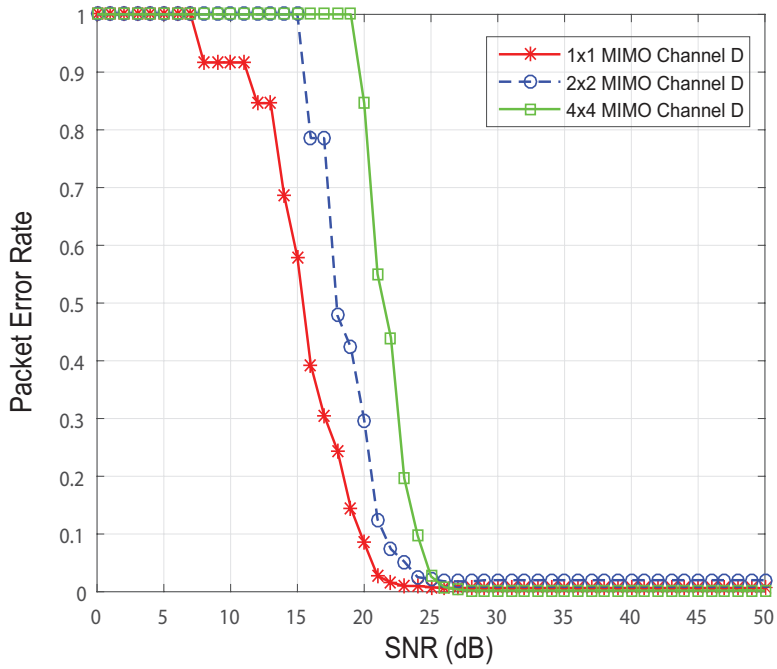

Figure 4.13: Packet Error Rate vs. SNR of Channel D under different MIMO configurations

MIMO as illustrated in Fig. 4.10-4.15 and TABLE 4.9. In this case, the performance is worst for channel model A in which PER remains 28.94% at *final level*. The system achieves relatively better performance for channel model D as compared to the other channel models under 4x4 MIMO configuration. This can be seen in TABLE 4.9, where the PER is 0%, 84.61%-0.26%, and 0.20% for *initial*, *intermediate*, and *final levels*, respectively.

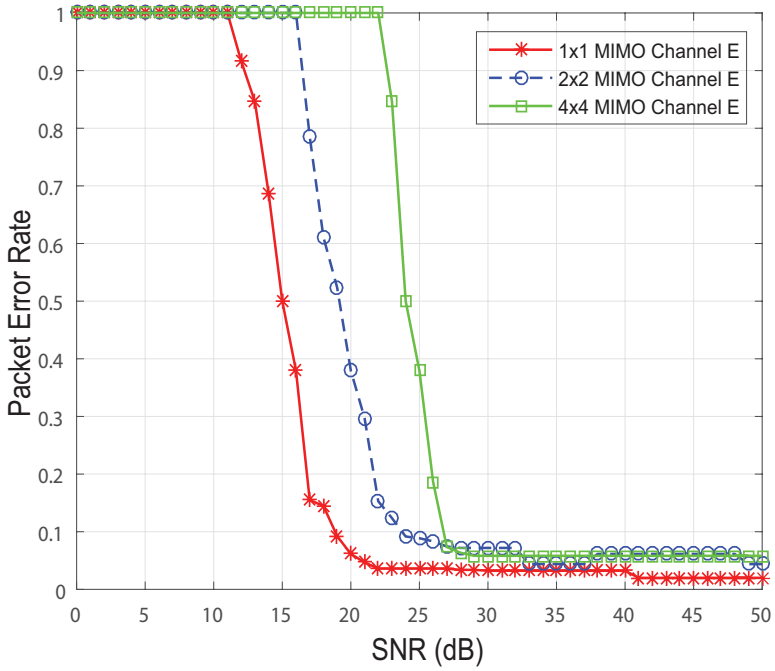

Figure 4.14: Packet Error Rate vs. SNR of Channel E under different MIMO configurations

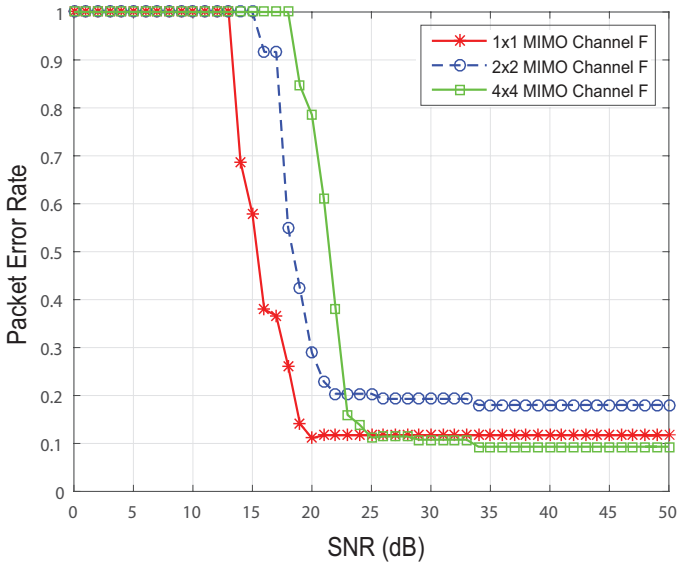

Figure 4.15: Packet Error Rate vs. SNR of Channel F under different MIMO configurations

4.2 VHT Model With Hidden Nodes: Vidden

We propose an analytical model, known as Vidden, to calculate the system throughput of VHT 802.11ac in the presence of hidden stations. Vidden is based on the Bianchi model; however it takes into account the hidden stations in calculating collision probability, backoff time, collision time and transmission time. Vidden is also the name of a trail, which stretches from the Mount Ulriken to the Mount Floyen in the town of Bergen, Norway. The height of the Vidden trail is such that it gives a comprehensive view of the

area's natural beauty. Likewise, we believe that our analytical model Vidden provides a comprehensive performance of VHT 802.11ac

4.2.1 System Model

We use a two dimensional Markov model [95] as shown in Fig. 4.16 to analyse the DCF in terms of two random variables namely: contention window (X) and contention stage (Y) such that $X \sim [0, 2^k W - 1]$ and $Y \sim [0, m-1]$, where k, W, and m indicate the current backoff stage, minimum contention window, and maximum number of backoff stages, respectively. Let n be the total number of stations (STAs), n_c the contending STAs, and n_h the hidden STAs in WLAN, where $n = n_c + n_h$[1]. Without the loss of generality, let $x_{i,k}$ indicate the contention window of an STA i at contention stage k. Let $\Omega = \{1, 2, ..., n\}$, $C = \{1, 2, ..., n_c\}$, and $H = \{1, 2, ..., n_h\}$, where $C \subseteq \Omega$, $H \subseteq \Omega$, and $C \cup H = \Omega$. The n_c and n_h STAs may belong to the same Basic Service Set (BSS) in the case of a single Access Point (AP) and may also belong to different BSSs in the case of more than one AP. It is assumed that the time (t) is divided into discrete slots and all operations occur at the start of the slot. Let an STA attempt to send data in a randomly chosen slot with transmission probability τ. The transmission may collide with the frames of $n_c - 1$ contending STAs and/or n_h hidden STAs with a collision probability, say p. On the other hand, the data transmission can be successfully received by the AP with a probability $1 - p$, which is always followed by an Acknowledged (ACK) frame. We assume that the ACK frame is always successfully transmitted, which is a reasonable assumption keeping in mind the small size of the ACK frame and its fast channel access mechanism under the DCF protocol. We also assume that packet loss is only due to collision and thus the losses due to weak signals are ignored in this letter. For the purpose of simplicity, we further consider a saturation mode for all STAs, where an STA always stays in one of the four states namely: decrementing backoff, frozen backoff, successful transmission, and collision. An STA enters a binary exponential backoff period before accessing the channel in which the contention window is doubled on each collision until an ACK is received or a maximum number of retries (m') is reached. The contention window X remains at $2^m W - 1$ after $m' - m$ retries and is frozen as long as the medium is busy. The transmission probability is calculated in eq. (4.15) [95].

$$\tau = \frac{2(1-p)}{(1-2p)(W-1) + pW(1-(2p)^m)} \tag{4.15}$$

The probability of collision p of an STA i (where $i \in C$) at contention stage k depends on the contention window $x_{i,k}$ of $n_c - 1$ contending STAs and the contention window $x_{i,k}$ and T_v of the n_h hidden STAs. As shown in Fig. 4.17, T_v indicates the collision vulnerable period for a transmitting STA i i.e., a period in which the frame sent by an STA i can collide with the frames of at least one of the n_h hidden STAs. When the MAC layer of an STA i receives data from the higher layers, it senses the medium. If the medium is free for a DCF Inter-Frame Spacing time (T_{DIFS}), it randomly chooses $x_{i,k}$ in a current time slot, say t according to the contention stage k and the number of retries as shown in Fig. 4.16. The STA i then decrements $x_{i,k}$ at each slot and transmits its frame at slot t' as shown in Fig. 4.17. The t' is calculated in eq. (4.16).

$$t' = T_{DIFS} + x_{i,k} + t \tag{4.16}$$

The data frame of STA i can collide with other frames if at least one of the following scenarios take place:

i $x_{j,k} = 0$ at time slot $t' \; \exists \{j \mid j \in C \wedge j \neq i\}$

ii $x_{j,k} = 0$ in a time interval $\left[t', t' + T_v\right] \; \exists \{j \mid j \in H\}$

[1] STA A is contending STA for STA B if A and B are in the same transmission range otherwise A and B are hidden STAs to each other.

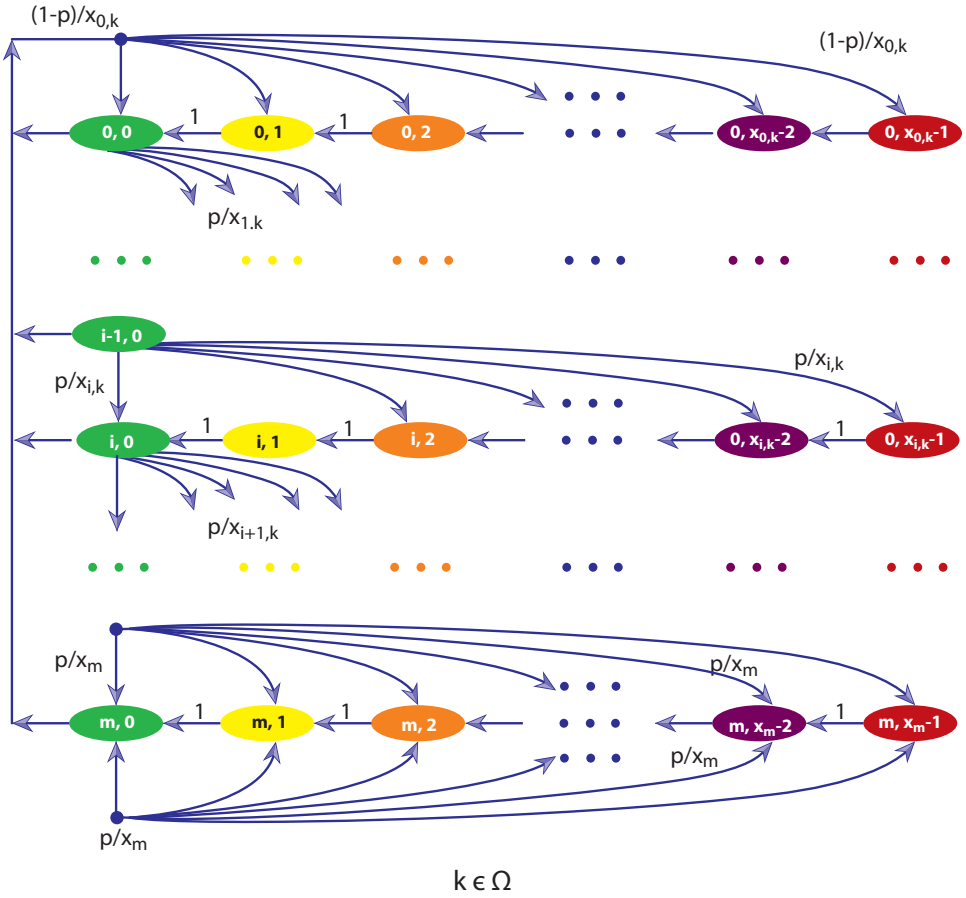

Figure 4.16: 2D Markov model of DCF 802.11ac

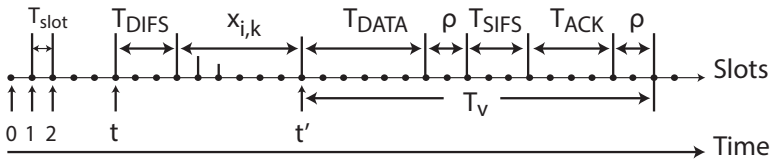

Figure 4.17: Timing diagram of an STA i at contention stage k

T_v is calculated in eq (4.17).

$$T_v = T_{DATA} + T_{ACK} + T_{SIFS} + 2\rho \tag{4.17}$$

where T_{DATA}, T_{ACK}, T_{SIFS} and ρ indicate the transmission time of the data frame, the transmission time of the ACK frame, the Short Inter Frame Space (SIFS) time, and propagation delay of DCF, respectively. If $1-\tau$ is the probability that exactly one STA is idle and $(1-\tau)^{n-1}$ is the probability that $n-1$ STAs are idle, then the collision probability for an STA can be calculated in eq (4.18).

$$p = 1 - \left[(1-\tau)^{n_c-1}\right]\left[\left((1-\tau)^{n_h}\right)^{T_v}\right] \tag{4.18}$$

The two non-linear equations, i.e., eq. (4.15) and eq. (4.18) can be numerically solved using a fixed point iteration to calculate p and τ after substituting eq. (4.17) in eq. (4.18). We used Maple 15 [96] to calculate the values of p and τ. Let P_{tr} and P_s be the probability that there is at least one transmission in a given time slot and the probability of success, respectively. For an STA i where $i \in C$, P_{tr} and P_s can be calculated in

Table 4.10: Data Rates of VHT under a SISO 20 MHz bandwidth Channel

Data Rate	R_0	R_1	R_2	R_3	R_4	R_5	R_6	R_7	R_8
Mb/s	6.5	13	19.5	26	39	52	58.5	65	78

eq. (4.19-4.20).

$$P_{tr} = 1 - \Big[(1-\tau)^{n_c}\Big]\Big[(1-\tau)^{n_h}\Big] \tag{4.19}$$

$$P_s = \frac{n\tau\Big[(1-\tau)^{n_c-1}\Big]\Big[(1-\tau)^{n_h}\Big]}{1 - \Big[(1-\tau)^{n_c}\Big]\Big[(1-\tau)^{n_h}\Big]} \tag{4.20}$$

The system throughput S is derived in eq. (4.21).

$$S = \frac{E[D]}{E[T]} \tag{4.21}$$

where $E[D]$ indicates the average number of bits transmitted successfully in an average time $E[T]$. E[D] and E[T] are calculated in eq. (4.22-4.23).

$$E[D] = P_{tr}P_sE[L] \tag{4.22}$$

$$E[T] = (1-P_{tr})T_{slot} + P_{tr}E[X]T_{slot} + P_{tr}P_sT_s + P_{tr}(1-P_s)T_c \tag{4.23}$$

where $E[L]$ denotes the average length of payload data in bits; T_{slot}, T_s, T_c, and $E[X]$ indicate slot time, the time spent in successful transmission, the time spent in collision and the average backoff time in seconds, respectively.

As per the DCF mechanism, the probability of choosing a contention window is uniformly distributed over $0, 1, ..., W-1$ in the first attempt. Similarly, the contention window for attempt k is uniformly distributed over $0, 1, ..., (2^{k+1}W-1)$. Thus the average backoff time $E[X]$ can be formulated in eq. (4.24).

$$E[X] = \frac{(1-p)W}{2} + \frac{p(1-p)2W}{2} + \frac{p^2(1-p)2^2W}{2} + ... + \frac{p^m(1-p)2^mW}{2} + \frac{p^{m+1}2^mW}{2} \tag{4.24}$$

where m indicates the maximum contention stage. Similarly, T_s and T_c are calculated in eq. (4.25) and eq. (4.26), respectively.

$$T_s = T_{DIFS} + T_{DATA} + T_{SIFS} + T_{ACK} + 2\rho \tag{4.25}$$

$$T_c = T_{DIFS} + T_{L-DATA} + T_{ACK-TOut} + \rho \tag{4.26}$$

where $T_{ACK-TOut}$ and T_{L-DATA} indicate the time out for ACK frame and the transmission time of the longest frame among frames in collision, respectively. We assume homogeneous traffic in this letter, thus T_{L-DATA}=T_{DATA} whereas $T_{ACK-TOut}$ is calculated in eq. (4.27).

$$T_{ACK-TOut} = T_{ACK} + T_{SIFS} + \rho \tag{4.27}$$

Similarly T_{DATA} and T_{ACK} are calculated in Appendix A.

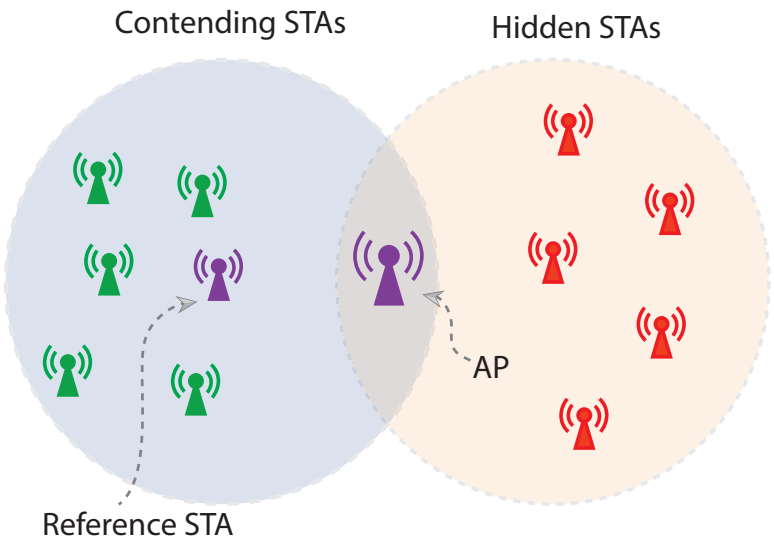

Figure 4.18: Network Architecture

4.2.2 Performance Evaluation and Results of Vidden

We evaluate the performance of the Vidden model by comparing its system throughput to the simulation results of a time driven simulator and the theoretical results of the extended Bianchi model [97]. The time driven simulator is implemented in Matlab (R2015b) following the specifications of the MAC and PHY layers of VHT 802.11ac. The simulation time is divided into discrete time slots each of 1 μs duration, and the simulation time is composed of 1 million slots. We have used Maple (ver. 15) [96] to solve the analytical equations. A complete list of parameters, which are used for simulation and analytical results, are summarized in Table 4.2. The network architecture consists of an AP and different STAs. The AP is placed in the centre of the network and STAs are randomly distribute around AP in such a way that the STAs make two groups namely: contending STAs and hidden STAs as shown in Fig. 4.18. We use a Single Input Single Output (SISO) with 20MHz bandwidth, however the simulation and analytical results can be equally extended for different MIMOs and wider bandwidths. We use the MCS of SISO under 20MHz [11]. We represent the data rate obtained from MCS_i as R_i, such that $0 \leq i \leq 8$, which are listed in Table 4.10.

The system throughput is calculated under four different configurations namely: varying payload size with n_c=1, n_h=1, varying payload size with n_c=5, n_h=5, varying data rate with n_c=1, n_h=1, and varying data rate with n_c=5, n_h=5. Fig. 4.19-4.20 show the system throughput for varying payload size using R_4. As shown in Fig. 4.19, the system throughput increases as we increase the payload size, however the more we increase the payload size, the greater the deviation is from simulation results for the extended Bianchi model. This is due to the collision and backoff time introduced due to hidden node. The system throughput of the extended Bianchi model is almost 1.7 Mb/s greater than that of the simulation results at 1500 bytes as shown in Fig. 4.19. On the contrary, the system throughput obtained from the Vidden model is almost similar to that of the simulation results with less than 1% difference. Similarly, the system throughput attained from the extended Bianchi model diverges more than three times from the simulation results in the case of n_c=5, n_h=5 as represented in Fig. 4.20. However, the results of the Vidden model are only 2% different than the simulation results for the same scenario. More hidden nodes increase the collision which is not modelled by the extended Bianchi model.

Similarly, the performance of the Vidden model and the extended Bianchi model for different date rates in the case of n_c=1, n_h=1 are shown in Fig. 4.21. The extended Bianchi model follows the simulation

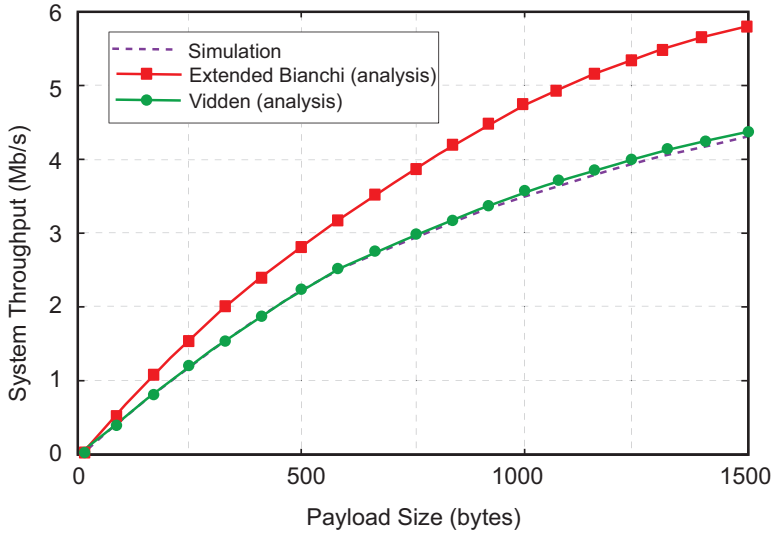

Figure 4.19: System throughput with different payload size ($n_c = 1, n_h = 1$)

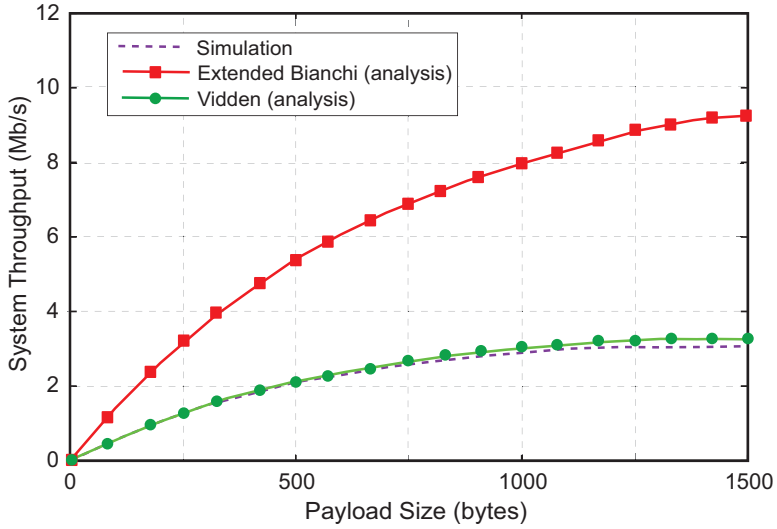

Figure 4.20: System throughput with different payload size ($n_c = 5, n_h = 5$)

results at lower data rates. However, the results start deviating after 13 Mb/s and the deviation magnifies more at higher data rates. For example, the results of the extended Bianchi model changes by almost 45% as compared to simulation results at R_9 as shown in Fig. 4.21. Similarly, in the case of n_c=5, n_h=5, the results of the extended Bianchi model deviates from simulation results by almost 100% as illustrated in Fig. 4.22. On the other hand, the vidden model closely follows the system throughput of the simulation results both for n_c=1, n_h=1 and n_c=5, n_h=5 for different data rates as shown in Fig. 4.21 and Fig. 4.22, respectively. Because we made some assumptions to simplify our analysis, it leads to a little difference (98% confidence interval) between the Vidden model and the simulation results.

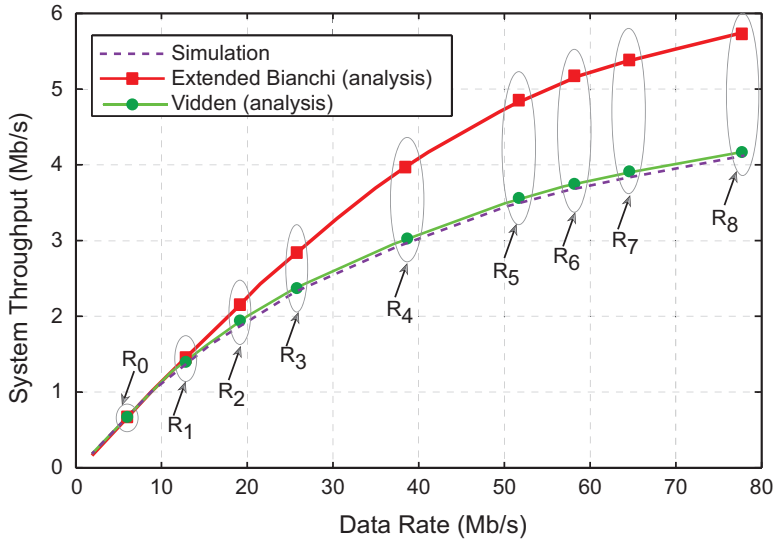

Figure 4.21: System throughput with different data rates ($n_c = 1, n_h = 1$)

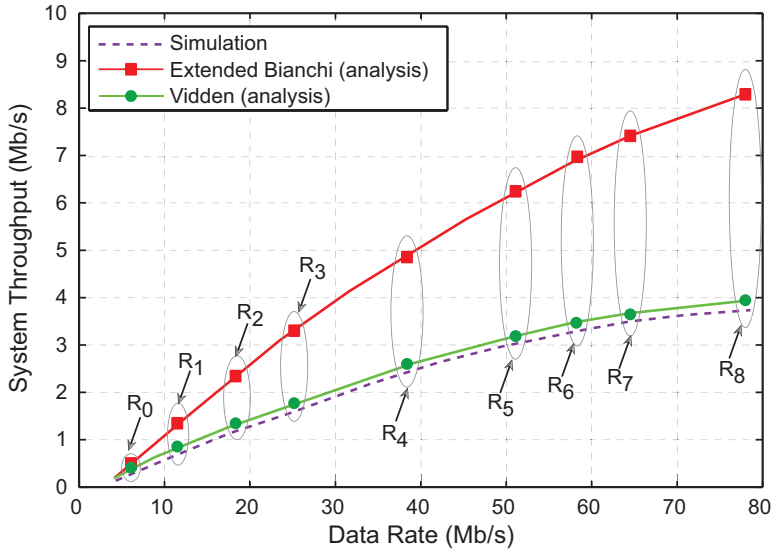

Figure 4.22: System throughput with different data rates ($n_c = 5, n_h = 5$)

4.3 Summary

This chapter presented two analytical models to investigate the performance of WD 802.11ac in terms of system throughput under its several new key features with and without hidden stations. The first theoretical model was based on the MAC and PHY layers of 802.11ac parameters in the absence of hidden stations. It was shown through simulation and theoretical analysis that the choice of a particular modulation and coding scheme, number of spatial streams, and channel size can greatly affect the total throughput of system. A MIMO multipath fading channel model was formulated to further investigate the effects of new features of 802.11ac. Although 802.11ac increases throughput many fold due to high-order modulation scheme, more bandwidth and spatial streams, the performance degraded drastically in an error-prone channel. We also investigated the performance of 802.11ac under different TGn channel models to find the performance patterns of different channel models.

In addition, a modified analytical model known as Vidden was also proposed, which comprehensively calculates the theoretical throughput of VHT 802.11ac in the presence of hidden stations by carefully considering the effects of both the contending and the hidden stations on collision probability. The Vidden model takes into account a precise calculation of the geometric backoff time, successful transmission time and the time spent in collision. The validity of analytical results are supported by simulation results. The system throughput achieved by the Vidden model closely follows the simulation results as compared to the extended Bianchi model. In future work, the Vidden model can be extended for modelling the VHT of the heterogeneous stations with unsaturated traffic conditions in the presence of hidden stations.

"Whoever is careless with the truth in small matters cannot be trusted with important matters."

Albert Einstein (1879 – 1955)

5

An Adaptive QoE-based Algorithm for Improving the System Performance

In this chapter, we focus on investigating the design parameters of the PHY layer, which could maximize the efficiency of the WD 802.11 system. For this purpose, a basic theoretical model is formulated for a WD network under a 2x2 MIMO TGn channel B model. The design level parameters, such as input symbol rate, antenna spacing, and the effects of the environment, are extensively examined in terms of path gain, spectral density, outage probability and PER. Thereafter, a novel adaptive algorithm is proposed to choose optimal parameters in accordance with the Quality of Experience (QoE) for a targeted application. In addition, a methodology is proposed to reduce PER of a VHT frame in WD 802.11ac networks by investigating loss of the individual fields of a frame. To this end, a 2x2 MIMO-OFDM transceiver is implemented under a TGn multipath fading channel D [105]. The system generates VHT Physical Layer Conformance Procedure (PLCP)- Protocol Data Unit (PPDU) frames which are passed through the TGn channel D. The performance of the system is determined by calculating the overall PER. Then the impact of each field of the VHT PPDU is analysed separately in order to estimate their percentage loss in the overall PER. The field level scrutinization of the PER provides a design level insight into the VHT PPDU performance. Based on simulation results, an efficient methodology is proposed to reduce the overall PER without changing the hardware of the current 802.11ac system. The findings of the analysis of the individual fields can also be taken into account while designing an efficient rate selection algorithms for the WD 802.11ac WLAN. The simulation results also show that the proposed method outperforms the standard method thereby achieving an optimal performance in an adaptive manner.

5.1 Introduction

The performance of WD 802.11 can be significantly affected by some key factors such as the type of application, specifications of the MAC and PHY layers, and surrounding environment. It is, therefore, important to develop a system model that takes these factors into account. In addition, we also consider the integration of the Quality of Service (QoS) algorithms from standard WiFi, as well as, cellular networks, to perform a detailed analysis of the underlying layers of the WD and the environment in which the communication takes place. In doing so, we consider a typical office environment, having stationary transmitters and receivers within a dynamic physical environment. People moving around in the office, can substantially affect the ongoing wireless communication. Thus, we concentrate on the effects of the movement of surrounding objects instead of the transmitter and receiver. As WD 802.11ac has several potential applications in a small office environment, it becomes important to explore the performance of WD 802.11ac networks under MIMO multipath fading channels.

Apart from that, it is an established fact that a packet loss in 802.11 happens either due to a collision or a weak signal strength [16]. In order to differentiate between the two losses, 802.11 uses the DCF and the number of retransmissions [12]. The DCF protocol, the transmission of a successful data frame is identified by the reception of an ACK frame. If the ACK is not received for a particular packet in a specified amount of time, the data packet is considered lost due to collision. On the other hand if the transmission of a data packet is failed after a certain number of retransmissions, then the packet loss is considered due to weak signal. The overall packet loss in 802.11 standards has been substantially analysed in the literature in the context of 802.11a/b/g/n. However, the field level investigation of a packet header in the WD 802.11ac network is yet to be explored for potential improvements. This is important due to two main reasons. Firstly the new standard i.e., 802.11ac amended the VHT PPDU and new fields were added to previous PPDU to achieve VHT. Secondly, the field level scrutinization is mandatory to get an insight into PER in the WD 802.11ac network. Thus we are motivated to estimate the field level loss of the VHT PDDU in WD 802.11ac network thereby reducing the overall PER.

To this end, this chapter makes the following contributions [105] [106].

1. We formulate a theoretical system model which is closely related to the real world network scenario (i.e., WD 802.11ac network under a 2x2 MIMO multipath fading TGn channel B) in a typical office or residence.
2. We explore the effects of different of the PHY layer parameters as well as the effects of the surrounding environment on the performance of WD 802.11ac network under a 2x2 MIMO multipath fading TGn channel B.
3. We quantify the performance loss in terms of path gain and outage probability that can be used as an adaptive model to achieve a targeted performance for QoS provisioning.
4. A novel adaptive method is proposed to choose the PHY parameters, which achieve an optimal performance in terms of QoE for a targeted application.
5. The loss percentage of individual fields is estimated in the VHT PPDU in the 802.11ac network.
6. The PER is investigated in the context of a 2x2 MIMO-OFDM transceiver which is implemented in Matlab under a TGn multipath fading channel D. Thus the analysis results apply to a specific but practical environment.

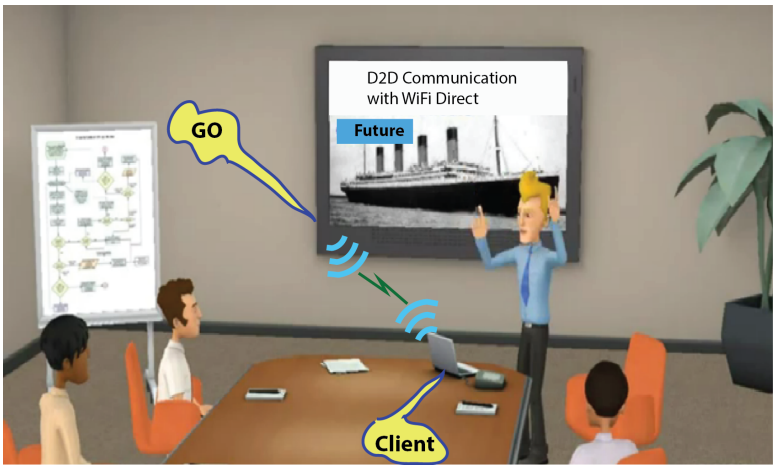

Figure 5.1: WiFi Direct network in a typical office

7. A methodology is proposed to reduce the overall PER without changing the hardware of the current WD 802.11ac system.

5.2 Example Scenario

There are a number of scenarios where WD technology is the most efficient and easiest option for D2D communication. For example: sharing data files between the devices that are in close proximity to each other, sharing services such as an office printer, streaming media in a home/office environment. One user case scenario is that of a speaker delivering a presentation during an office meeting. This is depicted in Fig. 5.1, in which the presenter shares the presentation slides from her/his laptop and displays them on a TV or LCD screen using WD technology. The image in Fig. 5.1 has been captured from an animated video in [107] and has been modified for the user case in hand. In order to develop a system model, which closely emulates the real world application in a small office environment. The proposed model consists of one GO and one client, with a laptop being the client, while the LCD screen is the GO.

5.3 System Model

We develop a system model for the PHY layer of a WD 802.11ac wireless network under a multipath flat fading MIMO channel. The system considers an OFDM-MIMO multipath fading channel to avoid frequency selective fading. The system architecture is based on the PHY layer specifications of 802.11ac. The system consists of an OFDM Transmitter (T_x) with two transmit chains, a MIMO TGn channel [99], and an OFDM Receiver (Rx) with two transmit chains. The high level blocks of the Tx, Rx and the channel as well as the subblocks of the Tx and Rx are depicted in Fig. 5.2. Different fields of the VHT PPDU are described in Appendix B. The VHT PPDU is passed through various sub-blocks of the T_x as illustrated in 5.2. The underlying technology is WD, as a result the T_x acts as a GO and the R_x works as a client.

5.3.1 Architecture

In this section, we describe the sub blocks of the T_x and R_x briefly.

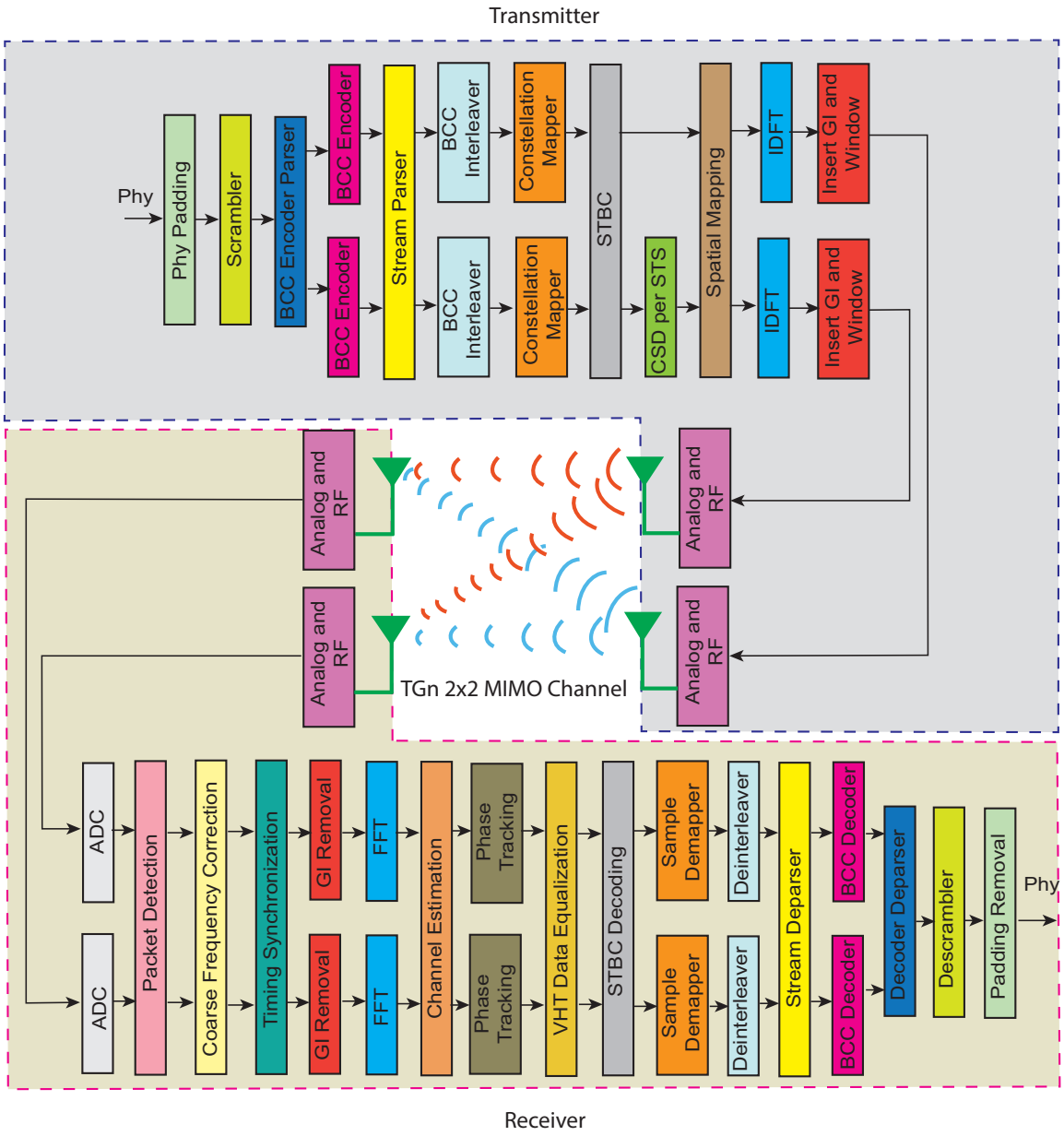

Figure 5.2: Architecture of a 2x2 MIMO-OFDM System

5.3.1.1 PHY Padding

The first part of the T_x is Padding in which extra zeroes are added to the data to match the size recommended in the IEEE standard [11].

5.3.1.2 Scrambler

The next part is the scrambler which is used to manipulate the PSDU to produce a random signal, which makes it difficult to extract the original signal. The detailed properties and structure of the scrambler can be found in [11].

5.3.1.3 BCC Encoder Parser

The Binary Convolutional Code (BCC) encoder parser demultiplexes the scrambled bits into different BCC encoders in a round robin fashion. The number of outputs depends on the number of the Forward Error

Correction (FEC) encoders.

5.3.1.4 BCC Encoder

The DATA field in the VHT PPDU is encoded using one of the FEC encoding techniques available in the 802.11ac namely: BCC or LDPC. We have used BCC to encode the DATA field.

5.3.1.5 Stream Parser

After coding and puncturing, the data bit streams at the output of the FEC encoders are processed in groups of N_{CBPS} bits, where N_{CBPS} indicates the number of the coded bits per OFDM symbol. Each of these groups is re-arranged into N_{SS} (number of spatial streams) blocks, which is the first representation of a MIMO streams. This operation is referred to as the *stream parsing* [11].

5.3.1.6 BCC Interleaver

The bits at the output of the *stream parser* are processed in groups of N_{CBPS} bits. Each of these groups is divided into N_{SS} blocks of N_{CBPS} bits, and each block shall be interleaved by an interleaver. The interleaving is performed separately for every OFDM symbol. It is carried out in three steps of permutations. The first step ensures that the adjacent codded bits are mapped into non-adjacent sub-carriers. The second permutation ensures that the adjacent bits are distributed into less and more significant bits of the constellation. Finally, the third permutation is called frequency rotation which is only applied when more than one spatial streams exist. The equations for permutation are described in [11].

5.3.1.7 Constellation Mapper

The bits from the *BCC Interleaver* are fed into the constellation mapper, which maps them to complex constellation points for BPSK, Quadrature Phase Shift Keying (QPSK),16-QAM (QAM), 64-QAM and 256-QAM [11].

5.3.1.8 Spatial Time Block Code

Spatial Time Block Code (STBC) is an optional step, which is used to transmit one spatial stream across multiple antennas for extra redundancy. The space-time block coder takes a single constellation symbol output and maps it onto multiple radio chains, transforming the spatial streams into space-time streams [108].

5.3.1.9 CSD per STC

CSD per STC stands for Cyclic Shift Delay per Space Time Code. A CSD is applied at the T_x to avoid interference among the same streams transmitted along each transmit chain. It is applied for each STC that comes from the *STBC block* [98].

5.3.1.10 Spatial Mapping

The Spatial Mapper maps the space time streams into transmit chains. We have used a direct mapping technique, such as a single space time stream is mapped into a single antenna. However, the number of spatial time streams (N_{STS}) may not be equal to the number of transmit chains (N_{Tx}), which is a common technique in beam forming [11].

5.3.1.11 Inverse Discrete Fourier Transform

An Inverse Discrete Fourier Transform (IDFT) is applied to convert the OFDM symbol from frequency domain into time domain.

5.3.1.12 Insert Guard Interval and Window

The Guard Interval (GI) is inserted at the start of each symbol, and each symbol is windowed to improve signal quality at the R_x [108].

5.3.1.13 ADC

The signal received at each antenna is first sampled and then converted into a digital signal by an Analogue to Digital Converter (ADC).

5.3.1.14 Packet Detection

The start of the VHT PPDU packet is detected with the help of OFTM training symbols in the L-STF. Afterwords, a delay and correlate algorithm is used [109].

5.3.1.15 Coarse Frequency Detection

This block returns a coarse estimate of the Carrier Frequency Offset (CFO) for the VHT PPDU passing through a TGn 2x2 MIMO channel given the received time-domain L-STF samples and channel bandwidth [104].

5.3.1.16 Timing Synchronization

The training symbols are used for Tx and Rx timing synchronization [109].

5.3.1.17 Channel Estimation

A VHT transmission has a preamble that contains VHT-LTF symbols, where the data tones of each VHT-LTF symbol are multiplied by the entries belonging to a matrix called P_{VHTLTF}, to enable the channel estimation at the Rx [11].

5.3.1.18 Phase Tracking

The multiplication of the pilot tones in the VHT-LTF symbol by the R_{VHTLTF} matrix instead of the P_{VHTLTF} matrix allows Rx to track phase and frequency offset during a MIMO channel estimation using the VHT-LTF [11].

5.3.1.19 VHT Data Equalization

The data field in the VHT PPDU is recovered using Zero Forcing (ZF) equalizer which is a linear equalization algorithm that applies an inverse of the frequency response of the channel to the received signal [110].

5.3.2 Channel Model

We chose the TGn channel model B and D for the system so that the proposed system is applicable to the office environment as shown in Fig. 5.1. Further, we consider one GO and one client. The client communicates with the GO using a WD protocol over an 802.11ac PHY layer. Both the GO and the client have two antennas for transmission and reception. Thus, the channel is a 2x2 MIMO multipath fading TGn channel. As a general rule, this channel model can be extended to any number of clients, as well as, lower or higher order MIMOs. A set of WLAN channels was presented in [99] for different environments. There are profiles proposed for channel models, labelled as TGn A to F [99]. These represent six different scenarios namely: flat fading, residential, residential/small office, typical office, large office, and large space (indoors and outdoors). In addition, each channel in 802.11ac is characterized by a particular number of taps with respect to the first path delay where the overlapping subset of these tap delays makes a cluster.

Table 5.1: Pathloss model of TGn channel B 802.11ac

Parameter	Value	Parameter	Value	Parameter	Value
K for LOS (dB)	0	Shadow fading before LOS (dB)	3	σ_{RMS} (ns)	15
K for NLOS (dB)	$-\infty$	Shadow fading after NLOS (dB)	4	σ_{Max} (ns)	80
Number of clusters	2	Number of taps	9	d_{BP} (m)	5

Table 5.2: Pathloss model of TGn channel D 802.11ac

Parameter	Value	Parameter	Value	Parameter	Value
K for LOS (dB)	3	Shadow fading before LOS (dB)	3	σ_{RMS} (ns)	50
K for NLOS (dB)	$-\infty$	Shadow fading after NLOS (dB)	4	σ_{Max} (ns)	390
Number of clusters	3	Number of taps	18	d_{BP} (m)	10

The system architecture is depicted in Fig. 5.2, in which a client is working as a T_x and a GO is a R_x. Furthermore, the client (T_x) has two transmit antennas (i.e., T_{x1} and T_{x2}), whereas the GO (R_x) has two receive antennas namely: R_{x1} and R_{x2}. Let the link between the transmit antenna i (T_{xi}) and the receive antenna j (R_{xj}) is indicated by $T_{xi} - R_{xj}$. We will use the same notations throughout this chapter.

The multipath fading 2x2 MIMO channel of a WD 802.11ac network for a TGn is derived from the transmit and receive correlation matrices [111]. The transmit and receive correlation matrices associated with each tap delay are determined from the mean AoA, mean AoD, AS at transmitter and AS at receiver. The LOS component can only be present on the 1st tap. If the distance between the T_x and the R_x is greater than d_{BP} then LOS component is not present. Note that d_{BP} is the break-point distance or distance of the fist wall (i.e., the distance of the T_x from the first reflector). The d_{BP} for channel model B and D are listed in Table 5.1 and 5.2, respectively. The path loss model considers the free space loss L_{FS} (slope of 2) up to d_{BP} and slope of 3.5 after d_{BP} [101]. For each of the models, a different breakpoint distance d_{BP} was chosen as shown in eq. (5.1).

$$L(d) = \begin{cases} L_{FS}(d) & \text{if } d <= d_{BP} \\ L_{FS}(d_{BP}) + 35log10(d/d_{BP}) & \text{if } d > d_{BP} \end{cases} \tag{5.1}$$

where d indicates the distance between the T_x and the R_x, while χ_σ indicates a zero-mean, Gaussian random variable, with standard deviation, σ (in dB), added to the path loss. It is used to model the shadow fading, or log-normal shadowing. The values were found to be in the 3-14 dB range [102]. Similarly, the zero-mean Gaussian probability distribution is given by eq. (5.2).

$$p(x) = \frac{1}{\sqrt{2\pi\sigma}} e^{[\frac{x^2}{2\sigma^2}]} \tag{5.2}$$

The 2x2 MIMO channel matrix H for each tap, at one instance of time, under a channel B delay profile can be represented as a sum of two matrices namely: fixed (constant, LOS) matrix and a Rayleigh (variable, NLOS) matrix as illustrated in eq. (5.3).

$$H = \sqrt{P}\left((\sqrt{\frac{K}{K+1}} H_F + \frac{1}{K+1} H_V\right) \tag{5.3}$$

where P is the power of each tap obtained by summing all the power of LOS and NLOS powers, K is the Ricean K-factor. The H_F and H_V in eq. (5.3) can be extended for 2x2 MIMO as follows in eq. (5.4-5.5).

$$H_F = \begin{bmatrix} e^{j\phi_{11}} & e^{j\phi_{12}} \\ e^{j\phi_{21}} & e^{j\phi_{22}} \end{bmatrix} \tag{5.4}$$

$$H_V = \begin{bmatrix} X_{11} & X_{12} \\ X_{21} & X_{22} \end{bmatrix} \tag{5.5}$$

where e^{ij} indicates the constant elements of LOS matrix H_F, whereas X_{ij} indicates the element of variable NLOS Rayleigh matrix H_V between i^{th} receiving and j^{th} transmitting antenna. It is assumed that X_{ij} is a complex Gaussian random variable with zero mean and unit variance. In order to correlate the X_{ij} elements of the matrix H_V, eq. (5.6) is used.

$$[X] = [R_{rx}]^{\frac{1}{2}}[H_{iid}][R_{tx}]^{\frac{1}{2}} \tag{5.6}$$

where R_{tx} and R_{rx} are the receive and transmit correlation matrices, respectively, and H_{iid} is a complex Gaussian random variable. All these Gaussian random variables are supposed to be identically independent with zero mean, unit variance. In addition, the R_{tx} and R_{rx} are given in eq. (5.7) and eq. (5.8), respectively.

$$[R_{tx}] = [\rho_{txij}] \tag{5.7}$$

$$[R_{rx}] = [\rho_{rxij}] \tag{5.8}$$

where ρ_{txij} indicates the complex correlation coefficients between i^{th} and j^{th} transmitting antennas, and ρ_{rxij} indicates the complex correlation coefficients between i^{th} and j^{th} receiving antennas. Alternatively, we use another approach i.e., the Kronecker product of the transmit and receive correlation matrices eq. (5.9) to calculate X.

$$[X] = ([R_{tx}] \otimes [R_{rx}])^{\frac{1}{2}}[H_{iid}] \tag{5.9}$$

It can be seen that H_{iid} is an array in this case instead of matrix. The R_{tx} and R_{rx} matrices are given in eq. (5.10) and eq. (5.11), respectively.

$$R_{tx} = \begin{bmatrix} 1 & {\rho_{tx12}}^* \\ \rho_{tx21} & 1 \end{bmatrix} \tag{5.10}$$

$$R_{rx} = \begin{bmatrix} 1 & {\rho_{rx12}}^* \\ \rho_{rx21} & 1 \end{bmatrix} \tag{5.11}$$

The values of complex correlation coefficient ρ are calculated from Power Angular Spectrum (PAS), AS, mean AoA, mean AoD and individual tap powers [99],[104]. Consequently, for the Uniform Linear Array (ULA), the complex correlation coefficient at the linear antenna array is expressed as shown in eq. (5.12)

$$\rho = R_{XX}(D) + jR_{XY}(D) \tag{5.12}$$

where $D = 2\pi d/\lambda$, R_{XX} indicates cross-correlation functions between the real parts, and R_{XY} indicates the cross-correlation between the real part and imaginary part. The expressions for R_{XX} and R_{XY} are given in eq. (5.13) and eq. (5.14), respectively.

$$R_{XX}(D) = \int_{-\pi}^{\pi} \cos(D\sin\phi)PAS(\phi)d\phi \tag{5.13}$$

$$R_{XY}(D) = \int_{-\pi}^{\pi} \sin(D\cos\phi)PAS(\phi)d\phi \tag{5.14}$$

Table 5.3: SNR values for different distances for a TGn channel B

d (m)	1	3	6	9	12	15	21	...	30	...	46
SNR (dB)	48	38.5	32.5	29	25	22	16	...	9	...	5

We calculate the correlation coefficients matrices using a uniform Gaussian PAS shape [99]. Once we have the channel matrix H, we calculate the output symbol matrix Y given the input symbol matrix, X in eq. (5.15).

$$Y = HX + W \tag{5.15}$$

The expression for a 2x2 MIMO system can be formulated as illustrated in eq. (5.16) [112].

$$\begin{bmatrix} y_1 \\ y_2 \end{bmatrix} = \begin{bmatrix} h_{11} & h_{12} \\ h_{21} & h_{22} \end{bmatrix} \begin{bmatrix} x_1 \\ x_2 \end{bmatrix} + \begin{bmatrix} w_1 \\ w_2 \end{bmatrix} \tag{5.16}$$

where y_1 and y_2 are the output symbols received at antennas R_{x1} and R_{x2} respectively. Similarly, $w1$ and $w2$ are the noise components at antennas R_{x1} and R_{x2} respectively, whereas x_1 and x_2 are the input symbols transmitted from antennas T_{x1} and T_{x2} respectively. In the same way, h_{ij} is the channel coefficient for link $T_{xi} - R_{xj}$.

We calculate the expected average SNR at the GO based on the pathloss model defined in eq. (5.1) for TGn Channel B. We assume that the client transmits with a transmit power of 5 dBm, and the receive sensitivity (or signal detection threshold) at the GO is -90 dBm. Furthermore, we ignore the presence of any other external interference. Thereafter, the SNR values for different distance values d between the GO and client are calculated as illustrated in Table 5.3.

5.3.3 Quality of Experience

The Quality of Experience (QoE) is defined as the overall acceptability of an application or service, as perceived subjectively by the end-user [113]. The QoE is a subjective measurement, which includes the complete end-to-end system effects, such as a client, a terminal, a network, and services infrastructure. In order to assess the QoE, a Mean Opinion Score (MOS) is used. The MOS test specified by International Telegraph Union-Telecommunication (ITU-T) is shown in Table 5.4. We consider five types of applications (i.e., A_5, A_4, A_3, A_2, A_1) running on our system, each with a different level of QoE requirements. While QoE is a subjective measurement that is highly dependent on a complex assortment of network, application and human factors, in this chapter as a first order approximation, we use PER in the ranges shown in Table 5.4 as a rough indicator of QoE [114]. Fixing the design parameters for the given system, so that the only parameters that can be chosen to adapt the performance of the system in accordance with the given QoE include MCS, SNR, and distance of transmitter and receiver. It permits the relationship between SNR and distance d be calculated from eq. 5.1 and the Table 5.4 as shown in eq. (5.17) .

$$d = f_{dist}(SNR) \tag{5.17}$$

We formulate the adaptive optimized function $f_{Ai}(.)$ to calculate the parameters, which achieves the optimal QoE for a targeted application A_i as shown in eq. (5.17). These parameters include minimum SNR (SNR_{min}), maximum SNR (SNR_{max}), minimum distance between GO and client (d_{min}), maximum

distance between GO and client (d_{max}), and MCS as illustrated in eq. (5.18).

$$OptimalParamters = f_{A_i}(SNR_{min}, SNR_{max}, d_{min}, d_{max}, MCS) \ \forall \ A_i \ \text{and} \ MCS_j \tag{5.18}$$

where $i = 1, 2, 3, 4, 5$ and $j = 0, 1, 2, ..., 8$ and MCS_j indicates one of the nine MCS defined for a 2x2 MIMO-OFDM WD system under a 20MHz bandwidth TGn B channel. In order to calculate the optimal values, we define a matrix $R \in R^{m \times n}$ that represents the range of SNR values for a where m and n indicate the number of applications and number of MCS, respectively. The element R_{ij} indicates SNR range for application A_i and MCS_j. We have calculated the values of R_{ij} for application A_i and MCS MCS_j from our simulation setup as illustrated in Table. 5.4. The optimized values are calculated in eq. (5.19-5.23).

A5:

$$\begin{gathered} SNR_{min} = 0, \ SNR_{max} = R_{ij} - 1, \ MCS = MCS_j \\ d_{min} = f_{dist}(SNR_{min}), \ d_{max} = f_{dist}(SNR_{max}) \end{gathered} \tag{5.19}$$

A4:

$$\begin{gathered} SNR_{min} = R_{ij}, \ SNR_{max} = R_{1j} + R_{2j} - 1, \ MCS = MCS_j \\ d_{min} = f_{dist}(SNR_{min}), \ d_{max} = f_{dist}(SNR_{max}) \end{gathered} \tag{5.20}$$

A3:

$$\begin{gathered} SNR_{min} = R_{1j} + R_{2j}, \ SNR_{max} = R_{1j} + R_{2j} + R_{3j} - 1 \\ MCS = MCS_j, \ d_{min} = f_{dist}(SNR_{min}), \ d_{max} = f_{dist}(SNR_{max}) \end{gathered} \tag{5.21}$$

A2:

$$\begin{gathered} SNR_{min} = R_{1j} + R_{2j} + R_{3j} \\ SNR_{max} = R_{1j} + R_{2j} + R_{3j} + R_{4j} - 1 \\ MCS = MCS_j, \ d_{min} = f_{dist}(SNR_{min}), \ d_{max} = f_{dist}(SNR_{max}) \end{gathered} \tag{5.22}$$

A1:

$$\begin{gathered} SNR_{min} = R_{1j} + R_{2j} + R_{3j} + R_{4j} \\ SNR_{max} = R_{1j} + R_{2j} + R_{3j} + R_{4j} + R_{5j} - 1, \ MCS = MCS_j \\ d_{min} = f_{dist}(SNR_{min}), \ d_{max} = f_{dist}(SNR_{max}) \end{gathered} \tag{5.23}$$

Table 5.4: Mean Opinion Score

MOS	Quality	Impairment	PER(%)	Application
5	Excellent	Imperceptible	0-20	A5
4	Good	Perceptible but not annoying	21-40	A4
3	Fair	Slightly annoying	41-60	A3
2	Poor	Annoying	61-80	A2
1	Bad	Very annoying	81-100	A1

5.4 Simulation Results and Discussions

5.4.1 Simulation Setup

A simulation model based on the system architecture discussed in Section 5.3 is implemented in Matlab. A VHT PPDU is constructed which is processed by the T_x. Fig. 5.2 shows the blocks through which the DATA field is passed. Some of the blocks are skipped for the sake of simplicity. The detailed diagrams for all the fields can be found in [11]. A 2x2 MIMO system is used with two independent streams (i.e., $N_{SS} = 2$) at

Table 5.5: Parameters of TGn Channel B Model

	Tap Index →	**1**	**2**	**3**	**4**	**5**	**6**	**7**	**8**	**9**
	Excess delay → (ns)	**0**	**10**	**20**	**30**	**40**	**50**	**60**	**70**	**80**
Cluster 1	**Power** (dBm)	0	-5.4	-10.8	-16.2	-21.7	-∞	-∞	-∞	-∞
	AoA (°)	4.3	4.3	4.3	4.3	4.3	-∞	-∞	-∞	-∞
	AS Tx (°)	14.4	14.4	14.4	14.4	14.4	-∞	-∞	-∞	-∞
	AoD (°)	225.1	225.1	225.1	225.1	225.1	-∞	-∞	-∞	-∞
	AS Rx(°)	14.4	14.4	14.4	14.4	14.4	-∞	-∞	-∞	-∞
Cluster 2	**Power** (dBm)	-∞	-∞	-3.2	-6.3	-9.4	-12.5	-15.6	-18.7	-21.8
	AoA (°)	-∞	-∞	118.4	118.4	118.4	118.4	118.4	118.4	118.4
	AS Tx (°)	-∞	-∞	25.2	25.2	25.2	25.2	25.2	25.2	25.2
	AoD (°)	-∞	-∞	106.5	106.5	106.5	106.5	106.5	106.5	106.5
	AS Rx (°)	-∞	-∞	25.4	25.4	25.4	25.4	25.4	25.4	25.4

each antenna. The VHT PPDU is passed through a 2x2 MIMO multipath fading TGn channel [99]. The TGn channel specifications are illustrated in TABLE 5.1, 5.2 and 5.5 where σ_{RMS}, σ_{Max} and d_{BP} indicate the Root Mean Square (RMS) delay spread, maximum delay, and breakpoint distance, respectively. The channel bandwidth is set to 20MHz/40MHz and the sampling frequency is set to 20MHz/40MHz. After the VHT PPDU passes through the multipath fading 2x2 MIMO TGn channel, an Additive White Gaussian Noise (AWGN) is added to the signal. As we consider a WD 802.11ac, thus the carrier frequency is set to 5.25GHz which is used throughout the simulation. We send a maximum of 1000 packets for each Signal to Noise (SNR) point until a 10% PER is achieved which is the requirement specified by the 802.11ac standard [11].

We describe the impact of the design parameters, such as input symbol rate, adjacent antenna spacing of transmitter and receiver, and Doppler shift on the performance of WD 802.11ac networks under a 2x2 MIMO TGn B channel. Afterwards, the proposed method is applied to the given system.

5.4.2 Effects of Input Symbol Rate

IEEE 802.11ac uses OFDM to transmit the data over the air. The OFDM divides the available wider bandwidth (i.e., 20MHz, 40MHz, 80MHz or 160MHz) into smaller slower channels, which are also called subcarriers or tones. This process is achieved through a mathematical operation known as an IFFT. All the subcarriers, which are created by the IFFT in 802.11ac are, 312.5 KHz wide each. The Number of Subcarriers (N_{SC}) is thus calculated as $N_{SC} = channel\_Bandwith/(312.15 \times 103)$ where $channel\_Bandwith$ indicates the bandwidth of the channel. The input symbol rate or baud rate for each subcarrier in the OFDM based WD 802.11ac network is defined as the number of symbols per unit time. The input symbol rate can greatly affect the impulse response in a wireless environment. To investigate the impact of a range of symbol rates, we take three different symbol rates, which are a low symbol rate (10^2), a medium symbol rate (10^3), and a higher symbol rate (10^4)). As shown in Fig. 5.3a, the fading envelope at antenna R_{x1} for path 1 of link $T_{x1} - R_{x1}$ and link $T_{x2} - R_{x1}$ is unstable and highly cross-correlated at the lower symbol rate. On the other hand, when we increase the symbol rate to medium and higher levels, as shown in Fig.

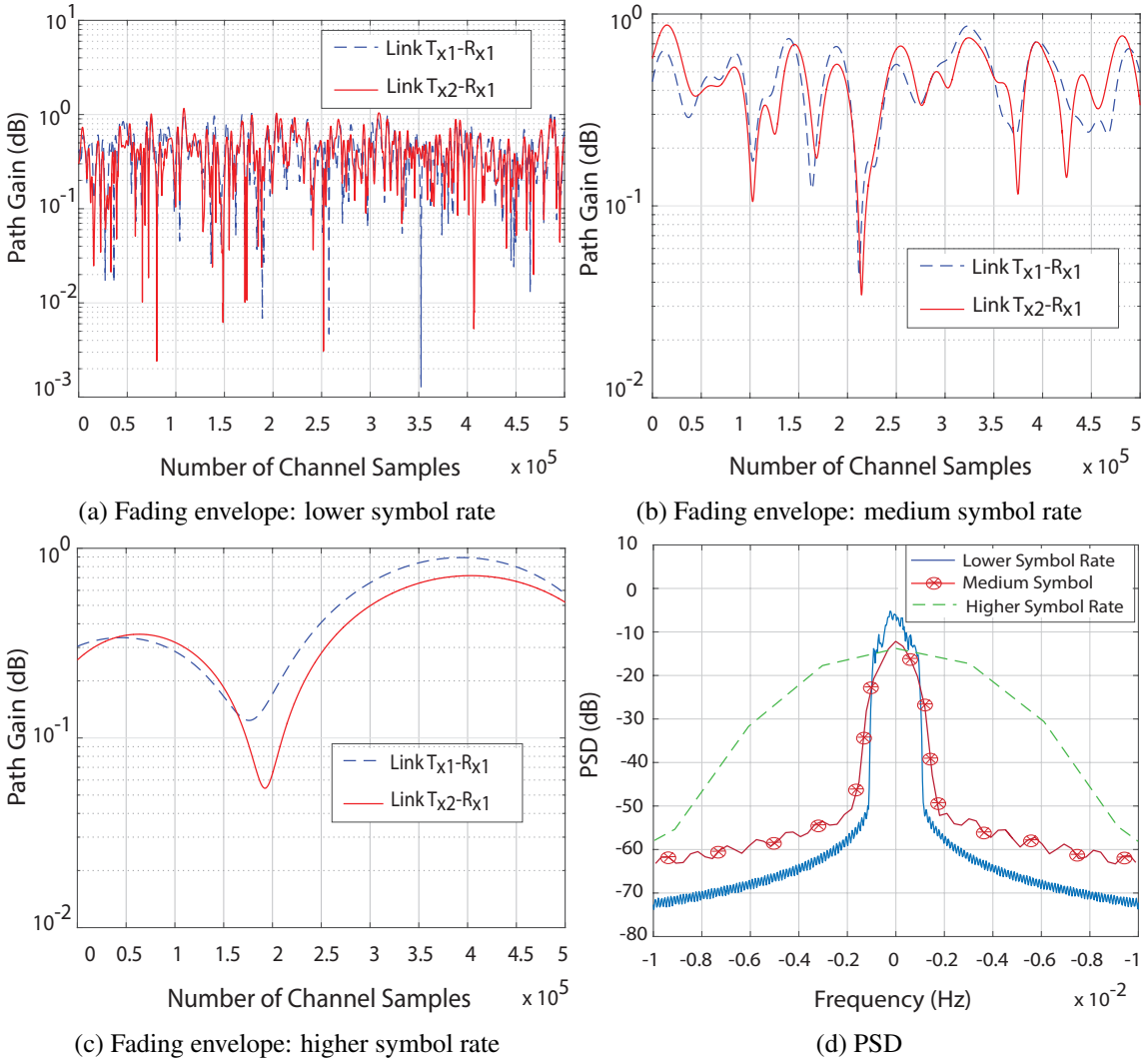

(a) Fading envelope: lower symbol rate

(b) Fading envelope: medium symbol rate

(c) Fading envelope: higher symbol rate

(d) PSD

Figure 5.3: Fading envelope and PSD of links $T_{x1} - R_{x1}$ and $T_{x2} - R_{x1}$ with different symbol rates

5.3b-5.3c, the probability of interference is reduced resulting in high performance.

Similarly, Fig. 5.3d represents the PSD for all the three levels of symbol rates along link $R_{x1} - T_{x1}$. The average PSD for the higher symbol rate is greater than that of the medium symbol rate. A similar trend can be seen for PSD of the medium symbol rate as compared to that of the lower symbol rate. Hence, increasing the input symbol rate can significantly increase the PSD.

5.4.3 Effects of Adjacent Antenna Spacing

In order to observe the impact of adjacent antenna spacing both at T_x and R_x, we simulate the model with two different sets of antenna spacing (i.e., $\lambda/2$ and 3λ). As shown in Fig. 5.4a, there is a high cross-correlation between the signals at receiver antenna R_{x1} received from transmitter antennas T_{x1} and T_{x2}, when the adjacent antenna spacing is $\lambda/2$. On the other hand, when the adjacent transmitter and receiver antenna spacing is increased to 3λ, the interference between the received signals is reduced as shown in Fig. 5.4b. Next, we repeat the simulations for different combinations of T_x and R_x antenna spacings and calculate the PER for different configurations. As shown in Fig. 5.5, the PER is 1 for all combinations of

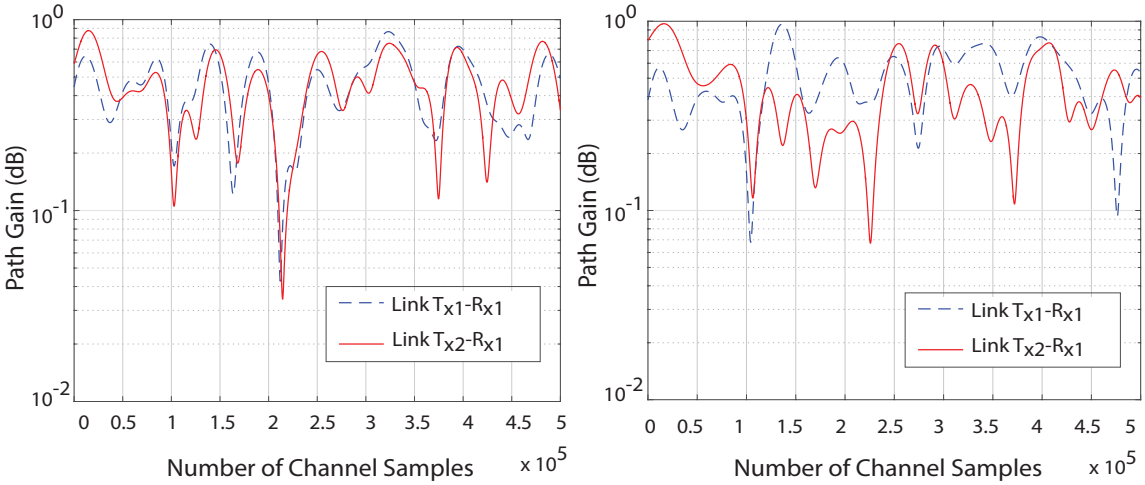

(a) $\frac{1}{2}\lambda$ (b) 3λ

Figure 5.4: Fading envelope of links $T_{x1} - R_{x1}$ and $T_{x2} - R_{x1}$ with different antenna spacing

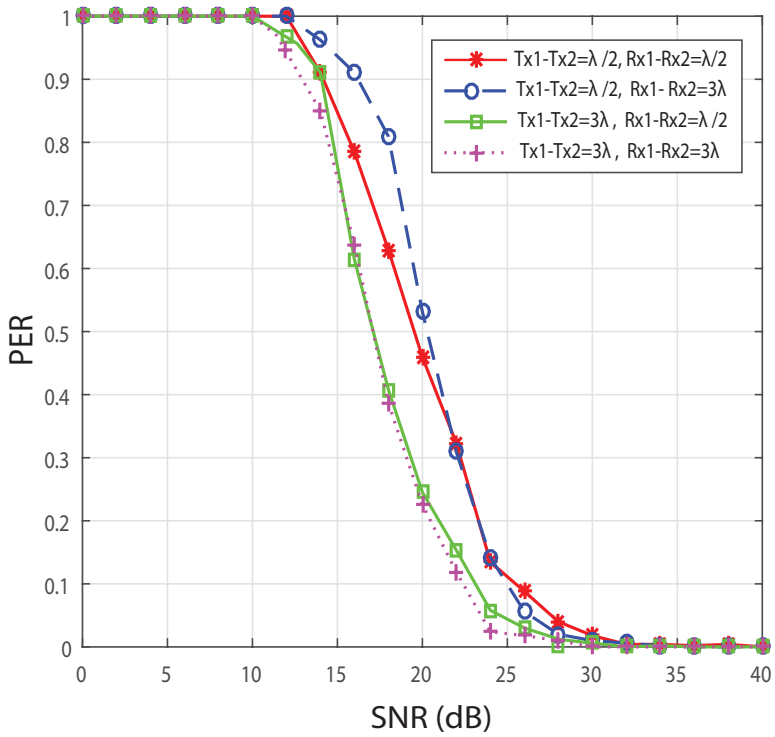

Figure 5.5: PER for different configurations of T_x and R_x antenna spacings

antenna spacings when the SNR is below 10 dB. Similarly, the PER remains 0 for all configurations after 30 dB SNR. However, when SNR is between 10-30 dB, the PER drop is different for different T_x and R_x spacings. When the spacing between both T_x antennas and R_x antennas is increased from $\lambda/2$ to 3λ, the PER is decreased by almost 10%. Alternately, the PER is decreased by almost 11% when $T_{x1} - T_{x2} = 3\lambda$ and $R_{x1} - R_{x2} = \lambda/2$ as compared to the case when $T_{x1} - T_{x2} = \lambda/2$ and $R_{x1} - R_{x2} = 3\lambda$.

5.4.4 Effects of Doppler Shift

As we consider a TGn channel B, which represents a typical small office environment, there is a low likelihood of T_x or R_x mobility relative to an outdoor environment. However, there is a high likelihood of other objects such as people moving within the environment. Therefore, we use a function known as $S(f)$ to capture the temporal Doppler component. The normalized bell Doppler spectrum can be calculated from eq. (5.24), which was derived in [99].

$$S(f) = \frac{C_b}{1 + A(\frac{f}{f_d})^2} \tag{5.24}$$

where A is a constant,which is used to define $S(f) = 0.1$, at a given frequency f_d , being the Doppler Spread as shown in eq. (5.25).

$$\big(S(f)\big) \mid_{f=f_d} = \frac{C_b}{1 + A(\frac{f}{f_d})^2} \tag{5.25}$$

Thus $A = 0.9$ and $C_b = \frac{\sqrt{A}}{\pi f_d}$ The Doppler spread f_d is defined in eq. (5.26).

$$f_d = \frac{v_0}{\lambda} \tag{5.26}$$

where v_0 is the environmental speed determined from measurements, which satisfies eq. (5.24), and λ is the wavelength defined by eq. (5.27).

$$\lambda = \frac{c}{c_f} \tag{5.27}$$

where c indicates speed of the light speed and f_c is the carrier frequency. The value for the proposed v_0 is equal to $1.2km/h$, whereas f_d is experimentally determined in indoor environments, which is found to be up to approximately 6Hz at 5.25GHz center frequency.

In order to investigate the impact of moving objects on the performance of a WD 802.11ac network under a 2x2 MIMO TGn B channel, we calculate all possible Doppler shifts using a 5GHz carrier frequency. The Doppler shift turns out to be in the range of 1Hz to 6Hz for the TGn B channel model. Fig. 5.6a-5.6b shows the fading envelope at antenna R_{x2} for path 1 of link $T_{x1} - R_{x2}$ and link $T_{x2} - R_{x2}$. As shown in Fig. 5.6a, the paths look more stable and there is less interference between the received signals in the case of 1Hz Doppler shift as compared to the same fading envelope, where the Doppler shift is 6Hz, as shown in Fig. 5.6b. Thus, the channel becomes worse when the Doppler shift changes from 1Hz to 6Hz. Consequently, this reflects the movement of objects in the real world.

We also calculate the outage probability (P_{out}) of all links between the GO and the client as shown in eq. (5.28).

$$P_{out} = \frac{\omega}{N_{total}} \tag{5.28}$$

where N_{total} indicates the total number of received channel samples, and ω indicates the cardinality of N_{th} received samples such that $N_{th} = \{x \mid x \in [1, N_{total}] \wedge x < Th\}$. The Th is the threshold power in dB; its value is fixed at -5dB for our simulation. Table 5.6 illustrates the values of P_{out} for all possible four links (i.e., $T_{x1} - R_{x1}$, $T_{x1} - R_{x2}$, $T_{x2} - R_{x1}$, and $Tx2 - R_{x2}$). The P_{out} increases as we increase the Doppler shift for all links. There is 38.53% loss when $f_d = 1$Hz, which rises to 46.67% for $f_d = 6$ Hz. Furthermore, for 1Hz increase in f_d, there is a loss of 1.56% on average. It is worth noting that the loss will decrease if the threshold Th is decreased below -5dB. Similarly, Fig. 5.7 shows the outage probability of all links with respect to Doppler shift. The P_{out} for all links increases with an increase in f_d. This is because the frequency shift causes problems in detecting the original symbols at the GO.

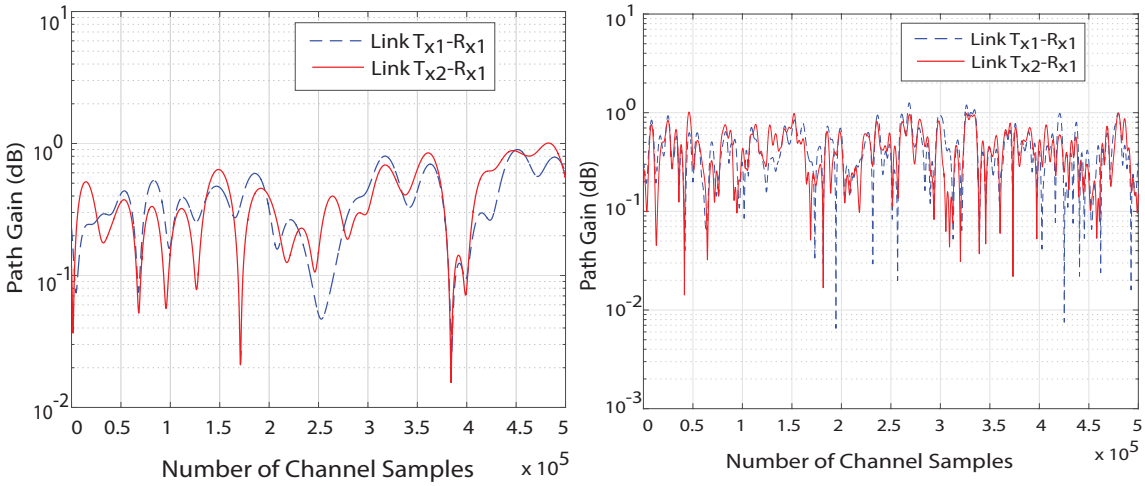

(a) Doppler shift of 1Hz

(b) Doppler shift of 6Hz

Figure 5.6: Fading envelope of links $T_{x1} - R_{x1}$ and $T_{x2} - R_{x1}$ with different Doppler shifts

Table 5.6: Outage Probability of all 4-Links w.r.t Doppler Shift

f_d	Outage Probability with $Th = -5dB$					Loss(%)
(Hz)	$T_{x1} \leftrightarrow R_{x1}$	$T_{x1} \leftrightarrow R_{x2}$	$T_{x2} \leftrightarrow R_{x1}$	$T_{x2} \leftrightarrow R_{x2}$	Average	
1	0.3758	0.4042	0.3700	0.3912	0.3853	38.53
2	0.4052	0.4337	0.3973	0.4248	0.4153	41.53%
3	0.4281	0.4539	0.4197	0.4513	0.4383	43.83%
4	0.4541	0.4643	0.4363	0.4620	0.4542	45.42%
5	0.4631	0.4681	0.4476	0.4739	0.4632	46.32%
6	0.4667	0.4676	0.4709	0.4507	0.4776	46.67%

5.4.5 Adaptive Optimized QoE

This section discusses the implementation of an QoE adaptation strategy for our system. The design parameters (i.e., input symbol rate, the antenna spacing, as well as the effects of the environment in the form of Doppler shift) can greatly change the system performance. Thus, we propose a new adaptive optimized strategy to cope with such system degradation. Given the 2x2 MIMO-OFDM WD system with a 20MHz channel bandwidth under a TGn channel B, we calculate the PER for available $MCS_0 - MCS_8$ as shown in Fig. 5.8. The PER for all MCSs decreases as we increase the SNR value, however, it is less for lower MCS as compared to higher MCS. We apply the proposed adaptive optimized method to the given system in terms two scenarios. It is assumed that in scenario-1, the GO and the client are 10m apart while in scenario-2, they are 30m apart. We calculate the MOS values for five different applications ($A_1 - A_5$) using the standard and our proposed method. The standard method refers to the regular WD 802.11 protocol [3], which chooses the MCS based on SNR values [2]. Since the implementation of the standard method may vary with different vendors, we choose average values of PER obtained from all MCS for a particular SNR value. On the other hand, the proposed method adaptively chooses the optimized MCS and distance between the GO and the client based on the type of the application, which in turns define a required QoE in terms of PER values as illustrated in Table 5.4. Consequently, we compare the performance of the standard

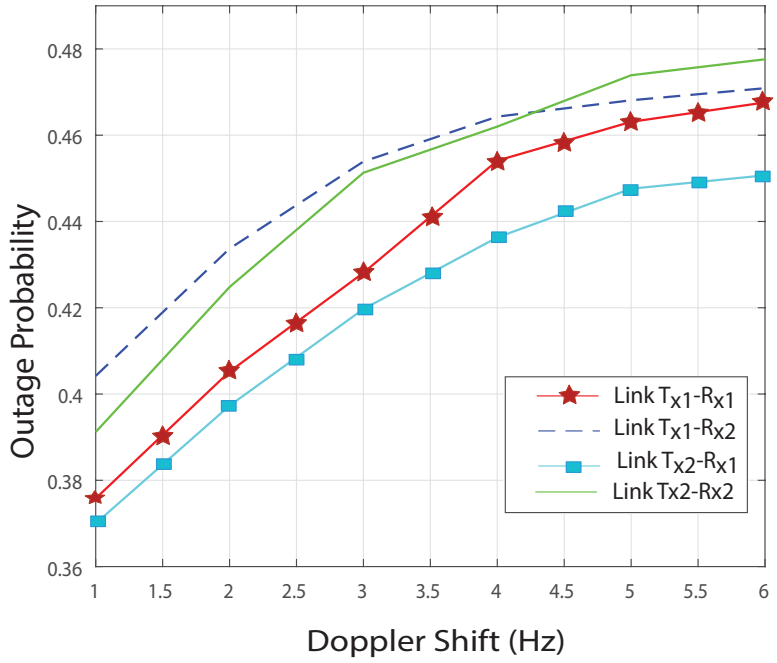

Figure 5.7: Outage probability of all links with different Doppler shifts

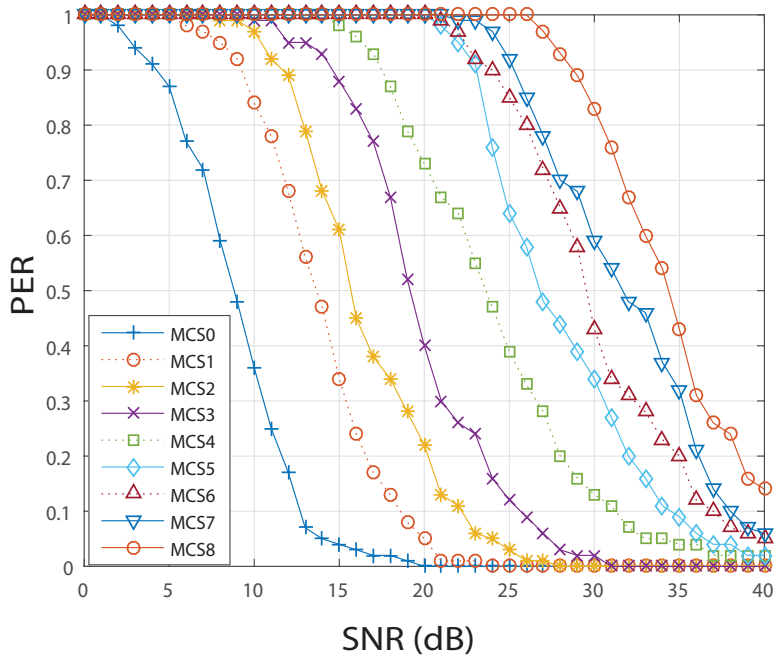

Figure 5.8: PER for different MCS in 20MHz bandwidth

and the proposed methods with an ideal case in terms of QoE values for a particular application.

5.4.5.1 Scenario-1

In this scenario, the GO and client are placed 10m apart. Thus $SNR = 28$dB for $d = 10$m as per Table 5.3. Fig. 5.9 shows the QoE for the standard and the proposed methods compared to the ideal case for five different applications ($A_5 - A_1$) with 5% error bar graphs. The QoE for the standard method remains 3.6 irrespective of the application. However, the proposed method achieves a QoE, which is within 5% of the ideal case. As shown in Fig. 5.9, the standard method results in degraded quality for A_5 and A_4 while

wasting network resources in the case of A_3, A_2, and A_1. In contrast, the proposed method optimally adapts its MCS resulting in a QoE which is quite close to the ideal case as shown by the $\pm 5\%$ error bars.

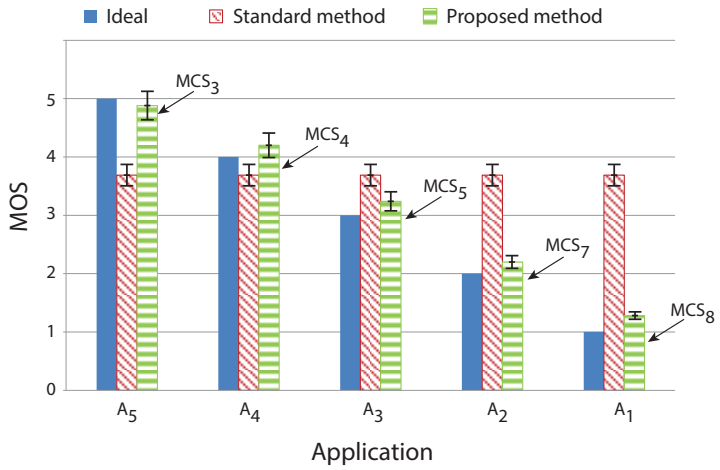

Figure 5.9: QoE of five applications for the three methods for Scenario-1

5.4.5.2 Scenario-2

In the second scenario, the $SNR = 9$dB at the GO according to Table 5.3. The performance of the given system is calculated under both methods relative to the ideal case as shown in Fig. 5.10. We observe that the standard method achieves $QoE = 1.27$ for all the applications. In this case, the standard method performs better for A_1 but its performance substantially degrades for A_2, A_3, A_4, and A_5. On the other hand, the proposed method achieves optimum performance by adapting an optimal distance d of 21m or equivalently $SNR = 16$dB and chooses the appropriate MCSs in order to follow the ideal case as shown by ± 7 error bars in Fig. 5.10.

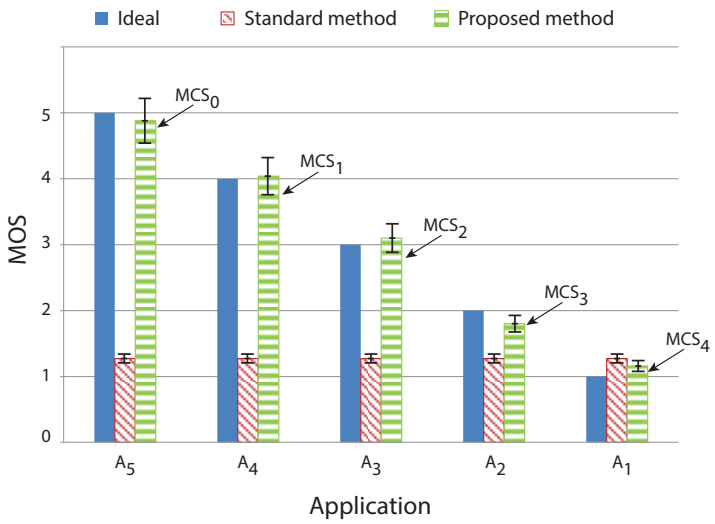

Figure 5.10: QoE of five applications for the three methods for Scenario-2

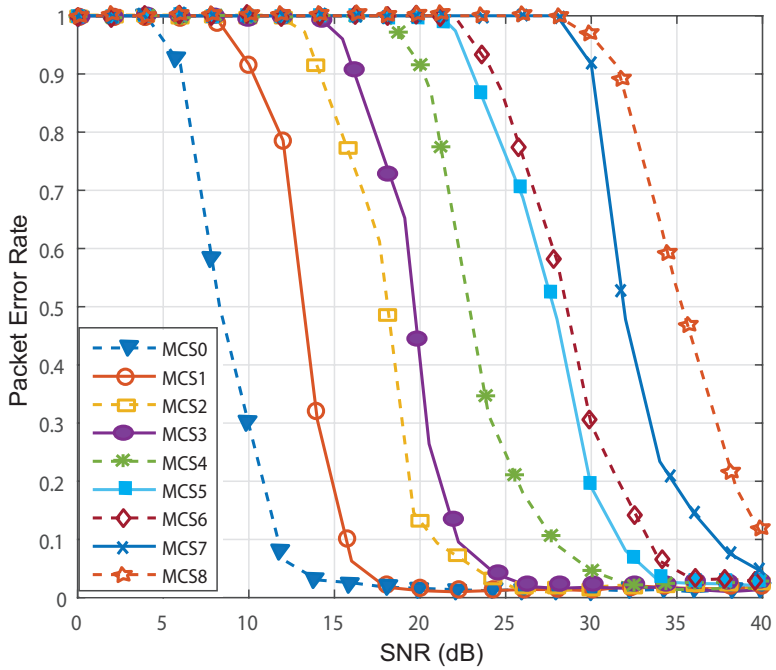

Figure 5.11: The PER for different MCSs as a function of SNR values

5.4.6 PER Analysis

In this section, the PER results are discussed, which are obtained from the system model based on a 2x2 MIMO-OFDM transceiver under a TGn Channel D model in Section 5.3.1. First of all, the statistics of the PER are calculated for different MCSs (i.e., MCS_0 to MCS_8) as a function of SNR in order to investigate the overall PER. Note that the MCS_0 in this case indicates BPSK with coding rate of 1/2, 800ns GI, and a date rate of 14 Mb/s under a 2x2 MIMO channel with 20MHz bandwidth. For more details, Section 22.5 of the standard 802.11ac [11] can be referred. As shown in Fig. 5.11, the PER can be divided into three levels namely: *initial level*, *intermediate level*, and *final level*. We observe that the PER is 100% at *initial level* for all MCSs. However, the range of SNR points, for which the PER remains 1, is different for different MCSs. Similarly, the PER reaches a minimum value between 0 and 0.1 at *final level* for all MCSs. However, the PER follows a decreasing trend from maximum to minimum for *intermediate level* for all MCSs. The negative slope of a decreasing line is different for each MCS. The range of the SNR points for which the PER falls from a maximum value to minimum (i.e., *intermediate level*) is smaller than the ranges of SNR points of *initial* and *final levels*. As shown in Fig. 5.11, in the case of MCS_0, 100% of the packets are lost when the SNR is less than 4dB, while the PER reaches 92% at SNR of 6dB and drops to almost 9% when the SNR reaches 9dB. The PER becomes 0 after the SNR reaches 15dB and stays 0 afterwords in the *final level*. A similar trend can be observed for other MCSs. The PER is increased as we move to higher modulation and coding schemes.

The first field in the VHT-PPDU is L-LTF, which helps in detecting the packet as discussed in Section 5.3.1. If this field is failed to be correctly decoded then the whole packet has to be sent again even if the rest of the packet reaches the R_x antennas without any interference. This is because the T_x does not know if there is any transmission arriving at its antennas if the detection fails. The L-LTF helps in detecting the start of a packet. In order to examine how many packets fail due to L-LTF, we run the simulations and calculate the PER, which occurs due to the failure of the L-LTF. The PER for different MCSs is shown in Fig. 5.12. It can be seen that the PER ranges from 5% to 10% for different MCS at lower SNR (< 25dB). The average PER does not change much even if we choose a higher MCS. Thus the MCS_0 is the best possible option

Table 5.7: Packet Error Rate due to L-STF field in VHT PPDU

SNR (dB) $\rightarrow$		**0**	**2**	**4**	**6**	**>6**
PER	MCS_0	90.91	72.73	27.27	0.00	0.00
	MCS_1	90.91	81.82	9.09	0.00	0.00
	MCS_2	90.91	81.82	9.09	0.00	0.00
	MCS_3	100.00	63.64	45.45	18.18	0.00
	MCS_4	100.00	90.91	36.36	0.00	0.00
	MCS_5	100.00	54.55	63.64	0.00	0.00
	MCS_6	100.00	90.91	18.18	9.09	0.00
	MCS_7	72.73	63.64	18.18	9.09	0.00
	MCS_8	100.00	81.82	27.27	9.09	0.00

as it can be decoded by all the previous standards of 802.11, which do not support a VHT PPDU. The PER drops below 5% at higher SNR ($>$ 25dB). It is also interesting to note that the MCS has no significant change on the loss of the L-LTF.

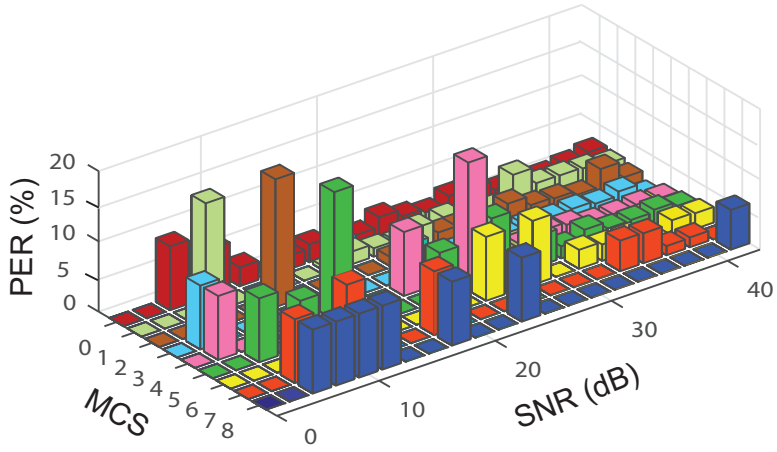

Figure 5.12: The PER due to L-LTF field in VHT PPDU

Similarly, PER due to the L-STF for different MCSs is illustrated in TABLE 5.12. We observe that a major percentage of the PER is due to the loss of the L-LTF at lower SNR. For example, 72.73% packets are lost due to L-LTF at 2dB SNR for MCS_0. The PER is 0 when the SNR reaches 6dB for lower MCSs, however there still exists some loss (9% PER) for higher MCSs at the same SNR value. The PER due to L-LTF becomes 0 after the SNR value increases to 7dB and so on. Thus the L-LTF should be taken great care of at SNR less than 6dB.

In Fig. 5.13-5.14, we consider the BER analysis of yet two more important fields of the VHT-PPDU i.e., VHT-SIG-A and L-SIG, for two different channel bandwidths i.e., 20MHz and 40MHz for a 2x2 MIMO-OFDM system under a TGn channel D model. In Fig. 5.13, the BER of the VHT-SIG-A is around 0.06 and 0.002 at 1dB SNR for 20MHz and 40MHz, respectively. The BER decreases for both the channel bandwidths as the SNR value is decreased until the BER reaches almost 0 for both the bandwidths. However, it can be seen that the BER for the 40MHz bandwidth channel is almost 97% better than that of the 20MHz

bandwidth channel.

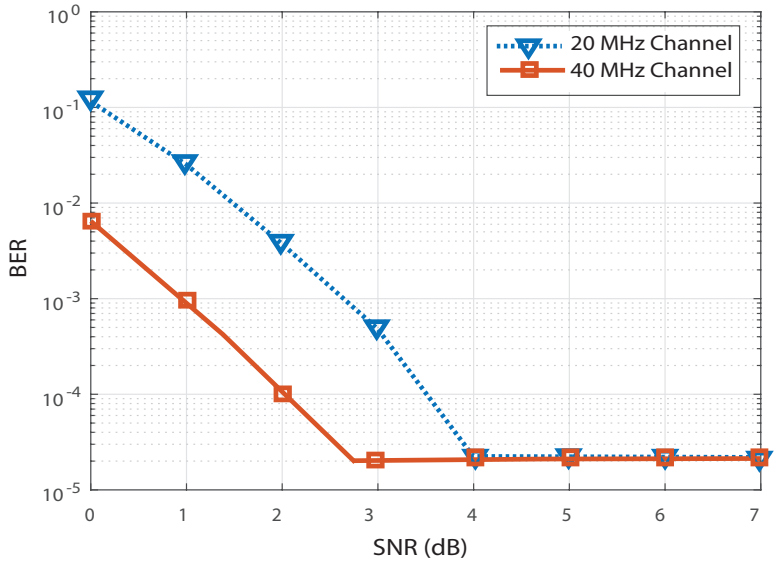

Figure 5.13: BER of VHT-SIG-A field in VHT PPDU

In the same way, the BER of L-SIG is shown in Fig. 5.14 as a function of SNR for a 20MHz and 40MHz bandwidth channels. The BER is 0.0513 for a 20MHz channel and 0.0012 for a 40MHz bandwidth channel at SNR 1dB. The BER falls down as the SNR is increased for both the channel bandwidths. However, the the BER is around 97% less for 40MHz bandwidth channel as compared to 20MHz bandwidth channel. Thus the performance of the system can be improved if 40MHz channel is used with a 2x2 MIMO-OFDM system under TGn channel D model. The simulation results are repeated for all the fields of the VHT

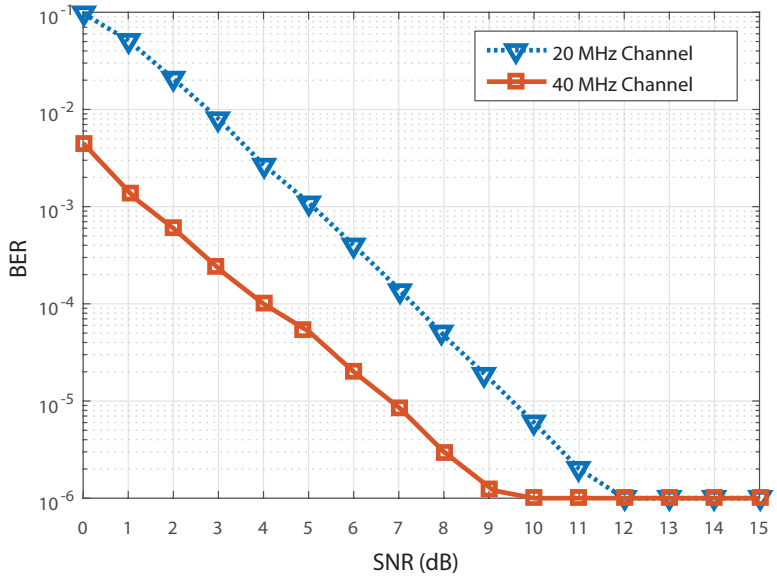

Figure 5.14: BER of LSIG field in VHT PPDU

PPDU including VHT-LTF and VHT-SIG-B. However, all the results are not included in this chapter for the sake of simplicity and comprehension. The important trends that we have observed throughout the experimentations are the same for all the fields. In a nutshell, the change of an MCS does not improve the

successful reception of the packet header. However, the use of wider channels for sending the packet header can tremendously decrease the PER and thereby improve the overall performance of the system.

5.5 Summary

This chapter investigated the design choices of a WD 802.11ac network under a MIMO multipath fading TGn channel and thereafter proposed a novel adaptive algorithm, which achieves optimal QoE for a particular application. To this end, a theoretical model was formulated for a 2x2 MIMO-OFDM under a TGn B channel. The design parameters, such as input symbol rate and antenna spacing, as well as, the effects of the moving objects in the surrounding environment are examined for the given system. It was observed that the power of the received signal can be improved by almost 10dB if the input symbol rate is increased from low symbol rate (10^2) to a higher input symbol rate (10^4). Similarly, the system performance can be enhanced up to 10% in terms of PER if the spacing between two antennas at both the transmitter and receiver is increased from $\lambda/2$ to 3λ. In addition, the investigations revealed that the loss due to the moving objects in the surrounding environment could substantially degrade the performance of the system, which may reach up to 43.71% on average for a given threshold of the receiving power. Based on simulation results, a novel method is proposed, which adapts the MCS, SNR, and the distance between the transmitter and the receiver in accordance with the required QoE for a targeted application. We also investigated the field level loss of a VHT PPDU packet in a 2x2 MIMO-OFDM transceiver under a TGn D model for a WD 802.11ac network. For this purpose, a complete system model was developed and implemented whereby the PER for a complete VHT PPDU as well as the percent PER for individual fields were analysed. Similarly, the BER analysis of different individual fields was examined for different channel bandwidths. It was shown that the system performance can be improved if the individual fields of the VHT PPDU are taken care of separately. The simulation results show that the use of different modulation and coding schemes can affect the overall PER. However, they could not substantially decrease the loss of the individual fields. The BER for individual fields can be decreased tremendously if a wider channel is used for transmissions.It was shown through the simulation results that the proposed method performs much better than the standard method in choosing the PHY parameters.

"The true sign of intelligence is not knowledge but imagination."

Albert Einstein (1879 – 1955)

6

Efficient Transmission Channel and Rate Selection

This chapter investigates the problem of selecting the most favourable channel and rate for a multicast communication system in the context of a WD 802.11 network. To this end, M^3-Cast protocol is proposed, which refers to a novel *M*ulti-rate *M*ulti-channel *M*ulticast scheme. M^3-Cast not only chooses the most favourable communication channel and transmission rate but also takes into account the implementation details of the underlying WD technology, thereby optimizing the overall system performance. M^3-Cast is formulated analytically and evaluated by a complete system level simulation. The detailed results and analysis consider a number of performance metrics such as BER, multicast capacity, and system throughput under different MIMO configurations, channel bandwidths, and various network radii. Consequently, the simulation and analytical results show that M^3-Cast protocol outperforms the standard multicast protocol of WD by almost two-fold in terms of system throughput.

The key contributions of this chapter are summarized as follows:

- The problem of multi-rate and multi-channel multicast communication is formulated in the context of a WD network.
- M^3-Cast protocol is proposed to select the most favourable channel for a multicast communication in a multi-channel environment. The M^3-Cast takes into account the SNR of all the operating channels on all clients present in a multicast group thereby choosing the most favourable channel for multicast communication.
- The M^3-Cast protocol chooses the most favourable transmission rate to increase reliability in a multi-rate group for multicast communication.
- The chapter presents a complete system level simulations i.e., MAC and PHY layers in the context of WD for M^3-Cast protocol.
- The M^3-Cast protocol is extensively analysed in terms of multicast throughput, capacity, BER for a variety of network condition such as different MIMO configurations, various bandwidths, and

different network radii wherein the results are compared with the standard multicast in WD network.

6.1 Background

New standards in WLAN provide multiple communications channels and a number of transmission rates to cope with the requirements and challenges of emerging applications in wireless communication. Although they achieve substantial benefits in terms of high throughput, it creates a performance anomaly problem wherein the selection of a particular communication channel and transmission rate can significantly affect the performance of a wireless communication system. Multicast in WD can be used in many applciations, such as Vehicle to Vehicle (V2V), Vehicle-to-anything (V2X) communications [115], and many other applications which are discussed in Chapter 1. In the context of these applications, there are many problems and issues including but not limited to reliability and efficiency. In order to address the above problems and bring a possible solution, we propose M^3-Cast protocol, which increases the overall system performance of a WD network. To the best of our knowledge, M^3-Cast is the first work on a multi-rate and multi-channel WD multicast communication. Furthermore, we have loosely coined a term 802.11ac WD throughout this chapter for the purpose of simplicity and clarity. The 802.11ac WD refers to a WD technology used with the specifications of the MAC and PHY layers of 802.11ac [11].

6.1.1 Group Formation in WD

In a WD 802.11 network, the devices that intend to communicate with each other first form a group and then exchange data with each other. In group formation, the WD protocol determines which device will act as a Group Owner (GO) and which device(s) shall join the group as client(s). In the context of WiFi alliance, a group is called a P2P group and a GO as a P2P GO. The details about the complete process of group formation can be found in [3]. Similarly, the article [116] describes the different methods of group formation as well as the L2 service discovery procedures, and the power saving mechanisms are also discussed. A client in a P2P group can be a P2P client or a legacy client. A P2P client supports both the standard WiFi and WD specifications, whereas a legacy client supports only the standard WiFi.

A P2P group may be a persistent P2P group (in which the GO keeps the P2P specifications of the group for future use) or a temporary P2P group (in which the specifications are not saved). Similarly, a group formation phase may be carried out either automatically or manually. In case of automatic group formation, the devices first discover each other and then initiate the process of GO negotiation which is defined in [3] in detail. On the other hand, in manual group formation, a user usually creates a group on a P2P device. In doing so the device announces itself as a GO and then invites other devices to join the group as clients. The latter kind of group formation is more popular in modern smart phones, tablets, and laptops such as WD in android [117] and Airplay or Airdrop in iOS [118]. The formation of a group may be further broken down into three phases namely: *device discovery*, *GO negotiation*, and *provisioning*. In the *device discovery* phase, the devices discover each other either by active or passive scanning. Similarly, the *GO negotiation* phase involves exchange of a GO negotiation request, GO negotiation response, and a GO confirmation message between two P2P devices. Lastly, the GO and clients exchange credentials of WiFi Protected Setup (WPS) protocol in the *provisioning* phase [3].

6.1.2 Frame Structure in WD

In GO negotiation phase, the devices share a Information Element (P2P IE). These IEs are little chunks of data with a numerical label which are used by management frames in order to communicate information

Table 6.1: Format of P2P an Information Element

Field	Size	Value	Description
IE ID	1	0xDD	IEEE 802.11 vendor specific usage
Length	1	variable	Length of P2P IE
P2P attribute	variable		Attributes of P2P IE

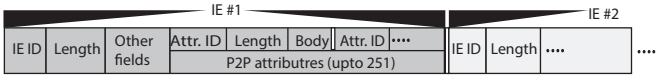

Figure 6.1: Complete WD Management Frame

to other systems as defined in [**?**]. The format of a typical P2P IE used in a WD is shown in TABLE 6.1. Furthermore, a P2P IE consists of P2P attributes to incorporate specific characteristics. A P2P attribute has a common general format that consists of a one-octet P2P attribute-ID field, a two-octet length field and a variable-length attribute-specific information field. There are certain attribute-IDs which are fixed for specific information in a P2P attribute. For example: attribute-ID 3 is used to transfer a P2P device ID; similarly attribute-ID 11 is fixed to transfer channel lists; while attribute- ID 13 is used to send the device information of a P2P device. Similarly, attribute-IDs 19 - 220 are reserved for future use [3]. Now, a complete WD frame consists of several P2P IEs which are further made of P2P attributes as shown in Fig. 6.1.

6.1.3 Channel and Rate Selection in Standard Multicast WD

In a WD group, the operating channel for a communication is chosen in one of two ways: (i) randomly if the group is not formed, (ii) by the GO in the case of an already formed group. In the former case, the channel is chosen in the device discovery phase in which a P2P device sends a probe request on all the social channels (i.e., available operating channels). There are three social channels i.e., 1, 6, and 11 in the case of a 2.4 GHz band. If another P2P device is interested in communication, it starts listening for a probe request on all the social channels. When a probe request is received on a certain channel, the device that receives the probe request sends a probe response to the transmitting station on that channel. This channel is then used for further communication between these devices. While in the second case, the GO is responsible for choosing a channel for a communication. The GO needs to choose a channel which is available at all other clients. If a new client wishes to join the group, it has to operate in the same channel that the GO has set for communication.

Similarly, the selection of a transmission rate for a multicast communication in a WD network is based on the multicast protocols for a standard WiFi. Thus, the multicast frames are sent at the basic transmission rate which is 6 Mb/s [3]. However, as we have discussed in Chapter 2, the protocols in the literature for example: LBP, LBP-RF, SARM, and PARF can be used to choose a multicast transmission rate.

6.1.4 Motivation

The traditional channel selection procedure in a WD multicast communication is random and focuses only on the fact that the channel selection results in a channel which is common between the GO and all other

clients present in a multicast group. The key benefit of this method is its simplicity, however, this simplicity comes with a cost of adverse effects on system performance. In this chapter, we investigate the problem of performance degradation that may result from choosing one channel over the other in a multi-channel environment. The performance becomes more poor as the number of operating channels increases. The new IEEE standard 802.11ac operates in a 5GHz band in which there are upto 19 non-overlapping channels in the case of a 20MHz wide band channel. Thus the problem of choosing an optimal channel for a multicast communication becomes more critical.

Similarly, we are also interested in choosing an optimal transmission rate for a multi-rate environment. We also observe that the literature explores these kinds of problems from a specific perspective. It will be significantly important and useful if the problem of a multi-rate and multi-channel multicast communication is examined in the context of WD 802.11ac. In the following sections, first we present the proposed M^3-Cast protocol to solve this problem, and then explore M^3-Cast in depth from a system level perspective.

6.2 M^3-Cast Protocol

The proposed M^3-Cast protocol works in three phases namely: *Preferences Exchange*, *Preferences Outcome*, and *Data Transfer*. In *Preferences Exchange*, the clients exchange the communication channels and transmission rates that are available for multicast communication. Similarly, in *Preferences Outcome*, the GO chooses the most favourable channel and transmission rate for multicast communication. Lastly, the multicast data is sent in the *Data Transfer* phase. The detailed steps of these phases are described in Section 6.2.1 followed by a discussions on M^3-Cast in Section 6.2.2.

6.2.1 Operation of M^3-Cast

6.2.1.1 Phase 1: Preferences Exchange in M^3-Cast

i. Each client that is interested in the multicast communication scans all the operating channels and maintains a list of the channels (*avblCh*) that are sensed free. The channels can be scanned actively as defined in [2] or using any efficient method (for example [119] that proposes a network allocation vector (NAV)-based opportunistic pre-scanning process).

ii. The GO assigns a unique ID starting from 1 and incremented by 1 to each client. The GO sends these IDs to each client at the start of the multicast communication.

iii. The GO sends a probe request to all clients in the multicast group. The probe request consists of a request for the list of the available channels (*avblCh*) at each client. The probe request also carries a general timer that defines the starting time of the probe response ($t_{startRes}$) which is sent back by each client. Each client is supposed to decode the starting time for its probe response based on its ID. A client *i* calculates the $t_{startRes}$ from the timing as follows:

$$t_{startRes}(i) = i \times T_{SIFS} + (i-1) \times T_{response} \tag{6.1}$$

where $\forall 1 \leq i \leq nClient$ while $T_{response}$ indicates the duration of the time to send the probe response from a client to the GO. We assume that $T_{response}$ is the same for all the clients. This is a reasonable assumption because first, all clients are in the same multicast group and hence they are likely to be in the close proximity of the GO. Second, the propagation delay is negligibly small due to the higher data rates and small distance. Similarly, T_{SIFS} indicates the Short Inter-Frame Space

timer while $nClient$ represents the total number of clients in the multicast group. An example of the timer for 3 clients is shown in Fig. 6.2.

iv. Each client responds to the probe request by sending a probe response to the GO using its own $t_{startRes}$. The probe response carries a list of the available channels ($avblCh$).

v The GO selects a list of common channels ($comCh$) from the probe responses. The $comCh$ is calculated in algorithm 1. If the number of common channels is one, this channel is selected for the multicast communication, otherwise phase 2 of the protocol is used to choose the most favourable channel.

6.2.1.2 Phase 2: Preferences Outcome in M^3-Cast

i. The GO sends a multicast Null Data Packet (NDP) on each channel from $commCh$ pool. At the end of the NDP packet transmissions on each $commCh$, the GO informs the clients that the NDP transmission is now over.

ii. Each client calculates the SNR for each channel from the NDP frames and maintains this information in $snrMatrix$.

iii. Each client calculates the time for sending back the $snrChan$ to the GO. The time is calculated from the timer in eq. (6.1). The $snrMatrix$ is then sent to the GO.

iv. The GO chooses the most favourable channel ($favCh$) from the snrCh received from each client for each channel. The $favCh$ is calculated as follows:

   a. An SNR matrix ($snrM$) is formed from the SNR values received for all the common channels ($comCh$) from each client. The columns of the $snrM$ contain the clients while the rows contain the channels.

   b. For each channel (row of $snrM$), a relative cost is calculated. To do so, a minimum of the snr in each row is calculated. Then the absolute difference of the minimum form each entry in the row is calculated and finally the absolute differences are summed to get the relative cost for each channel. The cost of each channel is collected into a cost vector ($costV$).

   c. The channel with the minimum in $costV$ is chosen as the most favourable channel ($favCh$).

v. The GO chooses the most favourable rate ($favRate$) as follows:

   a. The GO calculates the transmission rate matrix ($Rate$) that contains the transmission rate for each client for $favCh$ from TABLE. 6.2.

   b. The minimum transmission rate in the $Rate$ is chosen as the most favourable transmission rate ($favRate$).

The details of the *Preferences Exchange* are given in Algorithm 3 and the detailed steps of *Preferences Outcome* are listed in Algorithm 4.

6.2.1.3 Phase 3: Data Transfer in M^3-Cast

In this phase, the GO sends multicast data to all its clients on $favCh$ communication channel with $favRate$ transmission rate.

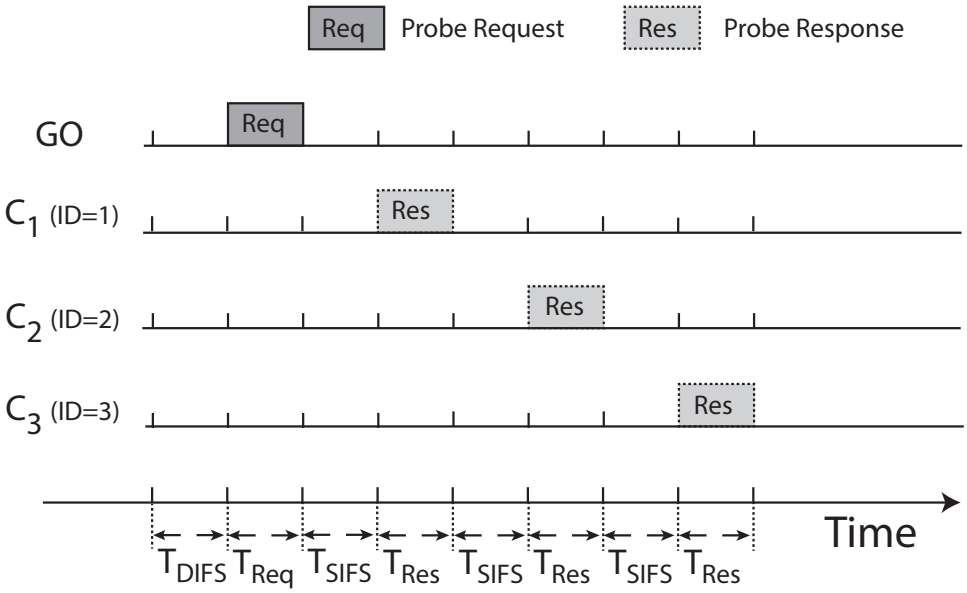

Figure 6.2: Time of probe response for three clients

Algorithm 3 Preferences Exchange M^3-Cast

Input: $nClient, nCh_i, maxCh, avblCh$
▷ where nCh_i is the number of available channels at
▷ client i while $maxCh = \max_{1 \leq i \leq nClient} (nCh_i)$
▷ where $avblCh \in \mathbb{N}^{nClient \times maxCh}$
▷ The algorithm pads $maxCh - nCh_i$ zeros to nCh_i
▷ if $nCh_i < maxCh$
Output: $comCh$ ▷ where $comCh \in \mathbb{N}^{1 \times nComCh}$

1: $nComCh \leftarrow 0$
2: **for** $i = 1$: to $maxCh$ **do**
3: $state \leftarrow 1$
4: **for** $j = 2$ to $nClient$ **do**
5: $size = length\,(avblCh\,[j]\,[maxCh])$
6: **for** $k = 1$ to $size$ **do**
7: **if** $avblCh[1][i] == avblCh[j][k]$ **then**
8: $state \leftarrow state + 1$
9: **end if**
10: **end for**
11: **end for**
12: **if** $state == nClient$ **then**
13: $nComCh \leftarrow nComCh + 1$
14: $comCh[nComCh] \leftarrow avblCh[1][i]$
15: **end if**
16: **end for**
17: **return** $comCh$

Table 6.2: Minimum Receiver Sensitivity

MCS	Modulation	Rate (R)	Min Sens. 20MHz PPDU (dBm)	Min Sens. 40MHz PPDU (dBm)	Min Sens. 80MHz PPDU (dBm)	Min Sens. 160MHz PPDU (dBm)
0	BPSK	1/2	-82	-79	-76	-73
1	QPSK	1/2	-79	-76	-73	-70
2	QPSK	3/4	-77	-74	-71	-68
3	16-QAM	1/2	-74	-71	-68	-65
4	16-QAM	3/4	-70	-67	-64	-61
5	64-QAM	2/3	-66	-63	-60	-57
6	64-QAM	3/4	-65	-62	-59	-55
7	64-QAM	5/6	-64	-61	-58	-55
8	256-QAM	3/4	-59	-56	-53	-50
9	256-QAM	5/6	-57	-54	-51	-48

Table 6.3: Format of the proposed P2P attribute

Field	Size	Value	Description
Attribution ID	1	0x13	Identifying the P2P attribute
Length	2	variable	Length of P2P attribute
Client ID	variable		Unique ID assigned to a client

6.2.2 Discussions on M^3-Cast Protocol

Let us discuss the different aspects of the proposed M^3-Cast protocol.

6.2.2.1 Unique IDs Assignment

The first challenge is to assign unique IDs to all clients in the multicast group. As described in Section II-B, the P2P devices use P2P attributes in Information Element to exchange the required information with each other. The attribute ID 3 is fixed for exchanging the 6 byte MAC addresses with each other. However, in addition to MAC addresses, we exploit the P2P attribute of IE for sending unique IDs to client by the GO. We use the reserved ID 19 (0x13) for this purpose and define a new P2P attribute as shown in TABLE 6.3. The IDs are assigned by the GO once the group is formed.

6.2.2.2 A New Client Joins/Leaves

We describe the required procedure if a new client joins or leaves the multicast group. In the case where a new client joins the multicast group, the GO assigns it the next possible ID. For example, if there are three clients with IDs 1,2,3 in the group and a new client joins the group, it is assigned an ID=4. On the other

Algorithm 4 Preferences Outcome M^3-Cast

Input: $nClient, nComCh, comCh[], snrM[][]$
▷ where $comCh \in \mathbb{N}^{nComCh \times 1}$
▷ and $snrM \in \mathbb{N}^{nComCh \times nClient}$
Output: $favCh$, $favRate$

$costM \leftarrow 0$ ▷ $costM \in \mathbb{N}^{nComCh \times nClient}$
$costV \leftarrow 0$ ▷ $costV \in \mathbb{N}^{nComCh \times 1}$
for $i = 1$ to $nClient$ **do**
    $max \leftarrow$ Maximum of $snrM[1{:}nComCh][i]$
    for $j = 1$ to $nComCh$ **do**
        $costM = abs(max - snrM[j][i])$
        ▷ $abs(.)$ returns the absolute value
    end for
end for
for $i = 1$ to $nComCh$ **do**
    $sum \leftarrow 0$
    for $j = 1$ to $nClient$ **do**
        $sum = snrM[i][j] + sum$
    end for
    $costV[i] = sum$
end for
$costMin \leftarrow$ Minimum of $costV[]$
$index \leftarrow i$ where $costV[i] = costMin$
$favCh \leftarrow comCh[index]$
$Rate[] \leftarrow$ transmission rate of $nClient$ for $favCh$ ▷ $Rate \in \mathbb{N}^{1 \times nClient}$
$favRate \leftarrow$ Minimum of $Rate[]$
return $favCh$ $favRate$

hand, if a client leaves the multicast group, the GO assigns the ID of the leaving client to the client with the highest ID. For example, there are four clients i.e., c1, c2, c3, and c4 with IDs 1,2,3,4 respectively. Suppose c2 leaves the group. Then the GO assigns c4 with ID=2 instead of reshuffling the IDs of all clients in the group. If two clients leave the group, then the clients with highest and 2nd highest IDs are assigned the IDs of the leaving clients. If a client with the highest ID leave the group, then there is no need for changing the IDs of the existing members.

6.3 Analytical Model

In this section, an analytical model is formulated to evaluate the theoretical performance of M^3-Cast protocol in terms of multicast throughput, capacity and BER.

6.3.1 System Model

Let there be a GO and N_{client} clients in a multicast group. Let $N_{H,i}$ and N_H indicate the total number of available channels at client i and the total number of common channels at GO, respectively. Let $H_{com} \in \mathbb{N}^{N_H \times 1}$ show the common channels at GO while $Cl \in \mathbb{N}^{1 \times N_{clients}}$ indicate the N_{client} clients in the

multicast group as shown in eq. (6.2).

$$H_{com} = \begin{bmatrix} 1 \\ 2 \\ \vdots \\ N_H \end{bmatrix}, Cl = [1 \quad 2 \quad \dots \quad N_{client}] \tag{6.2}$$

Let $\Omega \in \mathbb{R}^{N_H \times N_{client}}$ represent the SNR values of all common channels for each client. Without the loss of generality, let $R \in \mathbb{R}^{N_H \times N_{client}}$ show the transmission rate for N_H common channels for N_{client} clients. Let ω_{ij} indicate an element of Ω that represents the SNR of channel i for client j. The elements of the Ω are illustrated in eq. (6.3).

$$\Omega = \begin{bmatrix} \omega_{11} & \omega_{12} & \dots & \omega_{1N_{client}} \\ \omega_{21} & \omega_{22} & \dots & \omega_{2N_{client}} \\ \vdots & \vdots & \ddots & \vdots \\ \omega_{N_H 1} & \omega_{N_H 2} & \dots & \omega_{N_H N_{client}} \end{bmatrix} \tag{6.3}$$

The probability distribution of the Ω is discussed in Section 6.3.6. Let r_{ij} indicate an element of R that represent the transmission rate of client j for channel i as shown in eq. (6.4).

$$R = \begin{bmatrix} r_{11} & r_{12} & \dots & r_{1N_{client}} \\ r_{21} & r_{22} & \dots & r_{2N_{client}} \\ \vdots & \vdots & \ddots & \vdots \\ r_{N_H 1} & r_{N_H 2} & \dots & r_{N_H N_{client}} \end{bmatrix} \tag{6.4}$$

where the transmission rate r_{ij} is determined based on SNR value ω_{ij} as discussed later on and illustrated in TABLE 6.2.

Let $\Delta \in \mathbb{R}^{N_H \times N_{client}}$ illustrate the relative cost matrix corresponding to each channel for every client as shown in eq. (6.5).

$$\Delta = \begin{bmatrix} \delta_{11} & \delta_{12} & \dots & \delta_{1N_{client}} \\ \delta_{21} & \delta_{22} & \dots & \delta_{2N_{client}} \\ \vdots & \vdots & \ddots & \vdots \\ \delta_{N_H 1} & \delta_{N_H 2} & \dots & \delta_{N_H N_{client}} \end{bmatrix} \tag{6.5}$$

where the element δ_{ij} is calculated in eq. (6.6).

$$\delta_{ij} = abs\big(\max_{1 \le k \le N_H} (\omega_{kj}) - \omega_{ij}\big) \tag{6.6}$$

where the function $abs(.)$ calculates the absolute value. Let $\Psi \in \mathbb{R}^{N_H \times 1}$ represent the relative cost of each channel. The element ψ_i of the vector ψ indicates the cost of channel i as shown in eq. (6.7).

$$\Psi = \begin{bmatrix} \psi_1 \\ \psi_2 \\ \vdots \\ \psi_{N_H} \end{bmatrix} \tag{6.7}$$

where element ψ_i for a channel i is calculated in eq. (6.8).

$$\psi_i = \sum_{j=1}^{N_{client}} \delta_{ij} \tag{6.8}$$

6.3.2 Most Favourable Communication Channel Selection for M^3-Cast

At this point, we have a relative cost for each common channel at GO. Let f be an injective function that maps the cost vector Ψ to the common channels vector H_{com} as shown in eq. (6.9).

$$f : \Psi \rightarrow H_{com} \tag{6.9}$$

Then the most favourable channel (θ) can be calculated in eq. (6.10).

$$\theta = f\big(\min_{1 \leq i \leq N_H}(\psi_i)\big) \tag{6.10}$$

Thus the SNR values for the optimal channel $\theta \in \mathbb{N}^{N_H \times 1}$ are given by the vector Ω_θ where $\Omega_\theta \subset \Omega$ for N_C clients as shown in eq. (6.11).

$$\Omega_\theta = [\omega_{\theta 1} \quad \omega_{\theta 2} \quad \dots \quad \omega_{\theta N_{client}}] \tag{6.11}$$

The element $\omega_{\theta i}$ indicates the SNR value of the optimal channel for client i.

6.3.3 Most Favourable Transmission Rate Selection for M^3-Cast

Let R_θ where $R_\theta \subset R$ indicate the transmission rates of N_{client} clients for the most favourable channel θ as shown in eq. (6.12).

$$R_\theta = [r_{\theta 1} \quad r_{\theta 2} \quad \dots \quad r_{\theta N_{client}}] \tag{6.12}$$

The GO chooses the minimum transmission rate as the most favourable transmission rate $r_{optimal}$ in order to make the transmission reliable for the client with the worst channel condition as shown in eq. (6.13).

$$r_{fav} = \min_{1 \leq i \leq N_H}\big(r_{\theta i}\big) \tag{6.13}$$

The GO informs the clients about the most favourable channel and rate in a multicast message. The clients listen to the multicast transmission on the most favourable channel.

6.3.4 Bit Error Rate Calculation

Let BER_i indicate the BER of a client i, then an expression can be derived for BER_i based on $\omega_{\theta i}$. There are two main methods to calculate BER from a given SNR. One method is based on standard formula [112] that takes into account the SNR value, and data rate which in return can be calculated from given modulation and coding schemes. The second method uses empirical curves for a specific vendor to calculate BER from a given SNR value [120].

In order to calculate BER_i using the first method, let γ_i and B_i denote the E_b/N_o i.e., the energy per bit and bandwidth of the given channel, respectively for a client i. Then γ_i is calculated as shown in eq. (6.14).

$$\gamma_i = \frac{B \times 10^{\omega_{\theta i}/10}}{r_{fav}} \tag{6.14}$$

BER_i can be derived as a function of γ_i and MCS which indicates the modulation and coding scheme used by GO as shown in eq. (6.15).

$$BER_i = f(\gamma_i, MCS) \tag{6.15}$$

A complete list of formula for BER for different MCS can be found in [112]. Conversely, BER for different

SNR can be calculated from empirical curves as discussed in [120].

Let $P_{e,i}$ denote the probability of channel error for a client i.

$$P_{e,i} = 1 - (1 - BER_i)^L \tag{6.16}$$

where L is the packet length in bits.

6.3.5 Multicast Throughput of M^3-Cast

The throughput S_i is the number of successful bits transmitted in a unit time to client i from the GO. In order to estimate the total multicast throughput S at GO, the individual throughput from GO to each client is calculated. For this purpose, the throughput from GO to a client i in the multicast group is formulated. Thus the multicast throughput S is calculated in eq. (6.17).

$$S = \frac{1}{N_C} \sum_{n=1}^{N_C} S_n \tag{6.17}$$

We calculate the throughput S_i as the number of total bits successfully transmitted in a single frame per the total time T for a single frame including the overhead as shown in eq. (6.18).

$$S_i = \frac{1 - P_{e,i}}{T} \tag{6.18}$$

$$T = T_{DIFS} + T_{DATA} \tag{6.19}$$

where T_{DIFS} and T_{DATA} indicate the DCF Inter-Frame Spacing time, and the transmission time of the multicast data frame, respectively. The T_{DIFS} is illustrated in TABLE. 6.4 whereas T_{DATA} is calculate in Appendix A

6.3.6 Calculation of SNR Values

In this subsection, the probability distribution of the SNR values in Ω is discussed. Let the element ω_{ij} of the matrix Ω be represented by a random variable X. An element ω_{ij} of the Ω for a channel i of a client j can be modelled by a log normal distribution. Then X can be defined in eq. (6.20).

$$X = E + W \tag{6.20}$$

where E and W indicate the RSS (Received Signal Strength) and the noise floor, respectively. E and W in eq. 6.20 are expressed in logarithmic scales i.e., (dBm). The noise floor W depends on many factors in the environment. However, its value can be be approximately measured using eq. (6.21) while E is calculated in eq. (6.22).

$$W = 10 \times log_{10}(k \times T \times F_s) + NF \tag{6.21}$$

where T indicates the ambient temperature in $Kelvin(K)$, k is the Boltman's constant ($k = 1.3806 \times 10^{-23} J/K$), F_s indicates the sampling frequency in Hz which is equal to the channel's bandwidth, while NF indicates the noise factor of the system's hardware.

$$E = P_t - PL(d) \tag{6.22}$$

where P_t indicates the power of the transmitter in dBm. Its value depends on the standard and vendor's implementation. Similarly, the $PL(d)$ indicates the Path Loss in dBm at a distance d (m) between transmitter and receiver. $PL(d)$ is calculated in eq. (6.23).

$$PL(d) = \begin{cases} PL_{FS}(d) + \chi_\sigma & \text{i} \\ PL_{FS}(d_{BP}) + 3.5 \times 10log_{10}(\frac{d}{d_{BP}}) + \chi_\sigma & \text{ii} \end{cases} \tag{6.23}$$

where eq. (6.23-i) holds if $d \leq d_{BP}$ and eq. (6.23-ii) holds if $d > d_{BP}$. Similarly, d_{BP} in eq. (6.23) indicates the breakpoint distance in (m) while $PL_{FS}(.)$ refers to the free space path loss in dB. Similarly, χ_σ shows a Guassian random variable with zero mean, i.e., $\mu = 0$ and with standard deviation of σ i.e., $\chi_\sigma \sim ln\mathcal{N}(\mu, \sigma^2)$. It is used to model the log normal shadowing in the path loss. The $PL_{FS}(.)$ is calculated in eq. 6.24 while the Probability Distribution Function (PDF) of the Guassian random variable $\chi_\sigma$with zero mean ($\mu = 0$) and the standard deviation σ of the χ_σ is given in eq. (6.25).

$$PL_{FS}(d) = -10 \times log_{10}\left(\frac{G_t G_r \lambda^2}{(4\pi d)^2}\right) \tag{6.24}$$

where G_t and G_r indicate the transmitter and receiver antenna gains, respectively, d is the distance between transmitter and receiver in meters, and λ indicates the wavelength of the transmitted signal in meters.

$$P(\chi_\sigma) = \frac{1}{\sqrt{2\pi}\sigma} \times \exp^{\left(-\frac{\chi^2}{2\sigma^2}\right)} \tag{6.25}$$

6.3.7 Multicast Channel Capacity of M^3-Cast

We may subsequently derive the channel capacity (C_{ij}) of a channel i for a client j using the information of SNR values (ω_{ij}) and a channel matrix H_{ij} where H_{ij} represents the narrowband time-invariant wireless channel i for a client j. Let N_R and N_T represents the number of transmitter and receiver antennas, respectively then $H_{ij} \in \mathbb{C}^{N_R \times N_T}$. We assume that each transmitter sends an independent steams of input symbols $x \in \mathbb{C}^{N_T \times 1}$ with power E_x such that the total transmitted power is $P_t = N_T \times E_x$. Then, the received symbols $y \in \mathbb{C}^{N_R \times 1}$ for a channel i and client j can be written in a matrix form as shown in eq. (6.26).

$$\mathbf{y} = \mathbf{H}_{ij}\mathbf{x} + \mathbf{n}_{ij} \tag{6.26}$$

where n_{ij} represents the noise vector of channel i at client j. We assume that the noise is iid i.e., independent and identically distributed with zero mean and variance of σ^2. Thus the auto-correlation matrix is $R_{nn} = \sigma^2 I$ where I is an $N_R \times N_T$ identity matrix.

The Shannon capacity Cij for this stationary channel i for client j can be written as [121].

$$C_{ij} = log_2\left[det\left(I + \frac{E_x}{\sigma^2} H_{ij} H_{ij}^\dagger\right)\right] \tag{6.27}$$

where $H_{ij}^\dagger$ indicates the Hermitian or the complex conjugate transpose of the channel matrix H_{ij}. Note that the eq. (6.26) gives the capacity of the channel in bits per sec (bps)/Hz.

In order to calculate the ergodic capacity $\overline{C_{ij}}$ of the channel C_{ij}, S realization of the channel matrix H_{ij} are considered. Thus $\overline{C_{ij}}$ becomes the expected value of the stationary capacity [121]. Eq. (6.28) is used to calculate the $\overline{C_{ij}}$.

$$\overline{C_{ij}} = E_S[C_{ij}] = E_S\left[log_2\left\{det\left(I + \frac{E_x}{\sigma^2} H_{ij} H_{ij}^\dagger\right)\right\}\right] \tag{6.28}$$

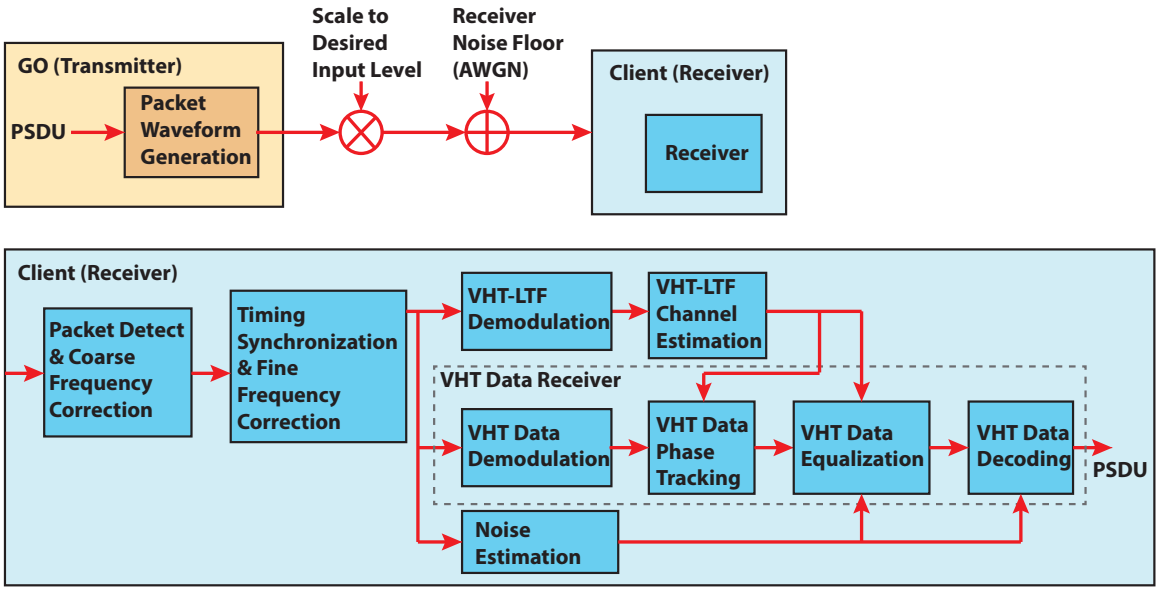

Figure 6.3: Simulation System Model

6.4 Results and Discussions

6.4.1 Simulation Setup

The simulation setup is defined in this section. In order to evaluate the performance of the M^3-Cast protocol, a detailed system is implemented in matlab as shown in Fig. 6.3. The model is based on the architecture of 802.11ac physical layer [11] and TGn channel 802.11 [122]. TABLE. 6.2 illustrates the minimum sensitivity level for different modulations and coding schemes (MCS) and different channel bandwidths.

Table 6.4: MAC and PHY Parameters

Parameter	Value	Parameter	Value	Parameter	Value
Slot time (σ)	9 μs	CW_{min}	16	T_{DIFS}	34 μs
L_{macH}	34 bits	CW_{max}	1024	T_{SIFS}	16 μs
$T_{VHT-STF}$	4 μs	T_{SYMS}	3.6 μs	T_{STF}	8 μs
$T_{VHT-SIG-A}$	8 μs	T_{L-SIG}	4 μs	T_{LTF}	8 μs
$T_{VHT-SIG-B}$	4 μs	T_{SYML}	4 μs	N_{tail}	6 bits
$T_{VHT-LTF}$	4 μs	$N_{service}$	16 bits	ρ	1 μs

6.4.2 Network Architecture

A general network scenario has been created to evaluate the performance of M^3-Cast protocol. There is one GO and k clients in a multicast group in a 2-D coordinate system of 50x50 m^2 area. As shown in Fig. 6.4, the GO is situated in the centre of this area, i.e. at coordinates (25,25), and the clients are randomly deployed around GO in a circle where the radius varies from 1m to 25m based on the chosen MCS. This is because we consider isotropic transmit antenna(s) with unity gains at GO. Thus a circular region of radius 1-25m around GO is considered as the transmission region of GO. The motive behind choosing a minimum

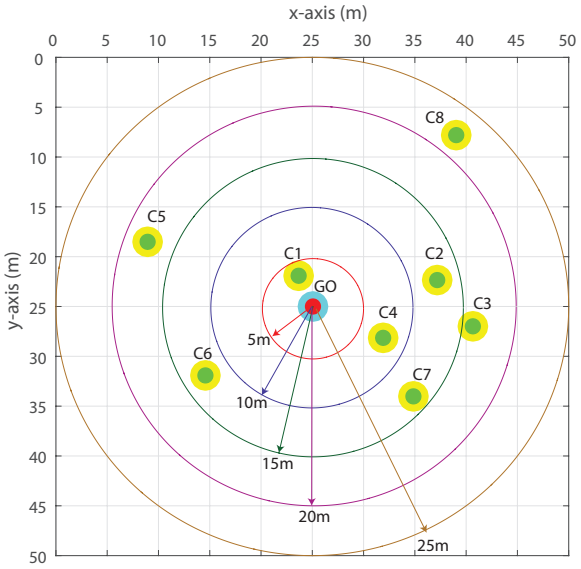

Figure 6.4: Network Architecture

of 1m distance is to avoid any near field communication losses, while a maximum of 25m is to avoid the total loss of signals.

6.4.3 Impact of SNR on Channel

First of all we investigate the impact of selecting a channel with different SNR on the performance of the system in terms of BER. For this purpose, we consider four common channels namely: Ch1, Ch2, Ch3, and Ch4 available for a multicast communication between the GO and five clients. The GO can choose any channel and start transmission to its clients. To this end, the GO chooses a 20MHz channel bandwidth with MCS=2 i.e., QPSK modulation and a coding rate of 3/4. Thus the minimum sensitivity level at the clients is -77 dBm as illustrated in TABLE. 6.2. Due to the random nature of the wireless medium, it is reasonably possible that each channel may add different noise and interference to the transmitted signal when it reaches any specific client. For the sake of argument, let us examine the SNR at each channel at a certain client. The relationship between SNR and distance d can be found in Appendix B. We further proceed by carefully choosing d, such that the transmitted signal is received -9 dBm, -10 dBm, -11 dBm, and -12 dBm below the minimum sensitivity level (-77 dBm) at channels Ch1, Ch2, Ch3, and Ch4, respectively. The receive noise floor is set to -95dBm in this case. The packet length is 1500 bytes while SISO is used. Thus using eq. (6.20), the final SNR values of each channel is shown in TABLE. 6.5. The purpose of this experiment is to assess the loss in terms of BER when the SNR of a channel changes by 1 dB. The BER of each channel is shown in the Fig. 6.5.

We observe that the change of SNR over 1 dB can have greater impact on the distribution of BER. As shown in Fig. 6.5, almost 95% of BER for Ch1 is below 0.01, while almost 30% of BER for Ch2 is between 0.1 and 0.01. Similarly, around 85% BER lies between 0.1 and 0.01 interval for Ch3. Lastly approximately 85% of BER is above 0.1 for Ch4. Thus as the SNR value decreases over 1 dB, the BER increases by almost 10%.

Next, we examine the BER of the above four channels using M^3-Cast protocol and the standard method. With standard protocol, the GO can select any of the four channels with equal probability, while with the M^3-Cast protocol, the GO selects the best possible channel. As shown in Fig. 6.6, almost 98% of BER is below 0.01 in the case of M^3-Cast protocol. On the other hand, around 60% of BER is above 0.01 and 5%

Table 6.5: The RSS and SNR values of the four channels at the receiver

Channel	RSS (dBm)	SNR (dB)
Ch1	-86	9
Ch2	-87	8
Ch3	-88	7
Ch4	-89	6

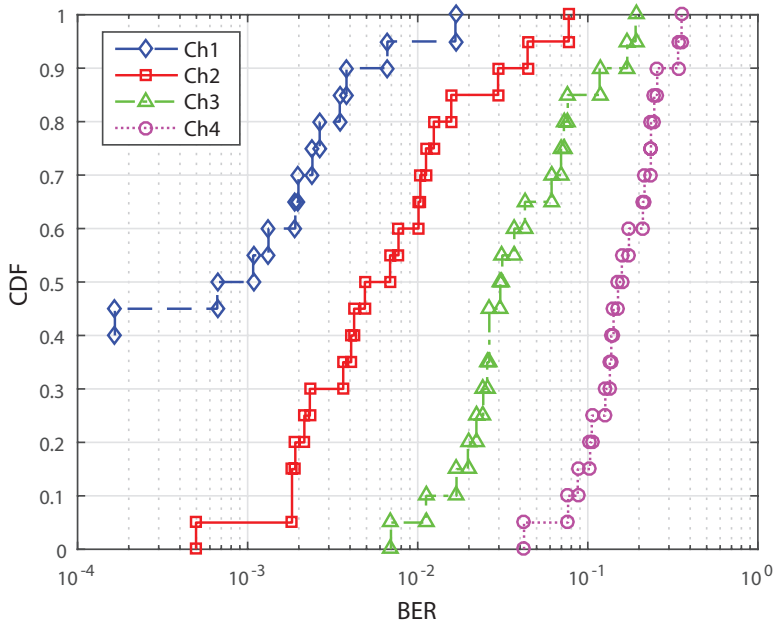

Figure 6.5: BER of four different channels

of BER is even greater than 0.1 in the case of the standard protocol.

6.4.4 Impact of MIMO Configurations

In order to asses the effects of Single Input Single Output (SISO) and different MIMO configurations on M^3-Cast protocol, we calculate the multicast BER for four different channels with different SNR values as illustrated in Table 6.5. The results under a SISO and different MIMO configurations (i.e., 2x2, 4x4, and 8x8) are shown in Fig. 6.7a-6.7d in terms of Cumulative Distribution Function (CDF) vs. BER . We notice that the BER increases as we increase the number of transmitter and receiver antennas for all MIMO configurations for all four channels. However, the multicast BER for the channel chosen by M^3-Cast is less than that of the standard protocol. As shown in Fig. 6.7a, almost 84%, 95%, and 100% of BER is above 0.1 for SISO, 2x2 and 4x4 MIMO configurations in the case of Ch4 using standard protocol. Similarly, 20% of BER is above 0.5 for 8x8 MIMO when Ch4 is chosen by standard protocol. On the other hand, 50% BER for SISO and 100% of BER in the case of 2x2, 4x4, and 8x8 MIMO configuration is under 0.001 when the proposed method is used. Hence, M^3-Cast protocol tremendously reduces the multicast BER as compared to the standard method for SISI and all MIMO configurations in WD.

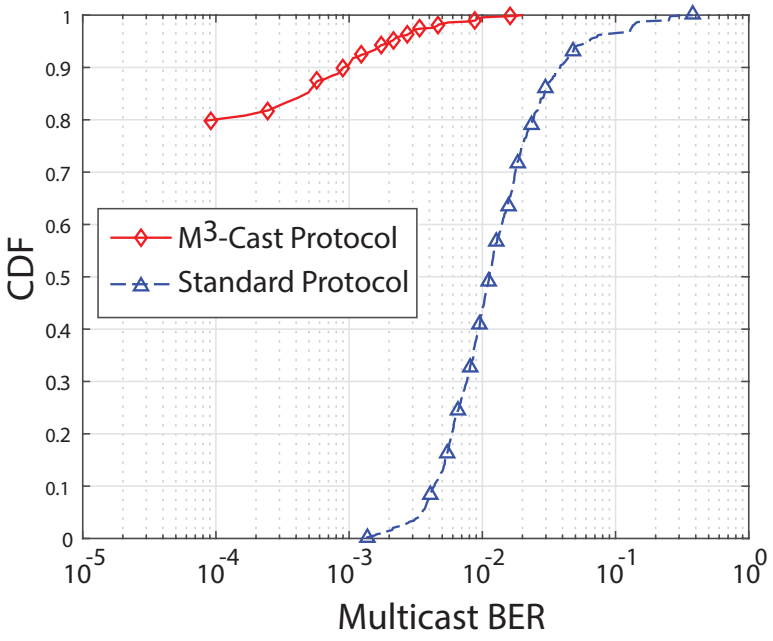

Figure 6.6: BER of the proposed method and standard method

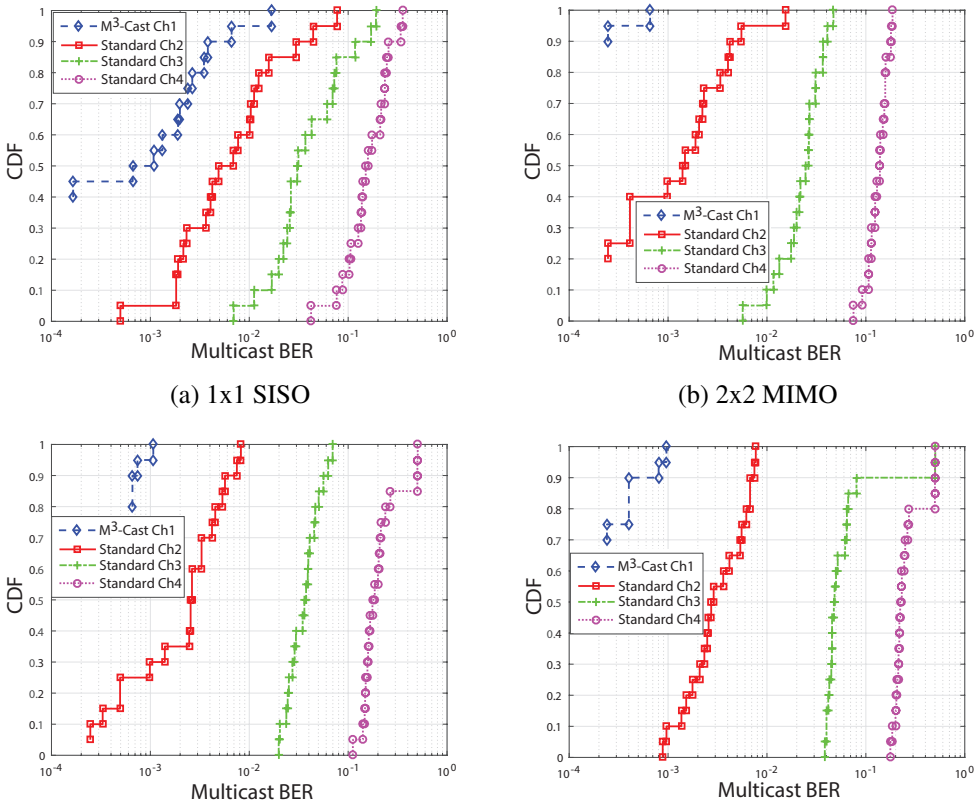

(a) 1x1 SISO

(b) 2x2 MIMO

(c) 4x4 MIMO

(d) 8x8 MIMO

Figure 6.7: CDF of Multicast BER for SISI and different MIMO configurations

6.4.5 Impact of Channel Bandwidth

[!h] Next we examine the impact of different channel bandwidths on the performance of a multicast communication in terms of BER for our four representative channels. As shown in Fig. 6.8a-6.8d, the overall BER increases as we increase the channel bandwidth. However, the BER of the proposed method is substantially smaller as compared to the standard method. For example, 90%, 95%, 100%, and 100% BER are greater than 0.01 for 20MHz, 40MHz, 80MHz, and 160MHz bandwidths respectively, when a standard protocol is used. On the contrary, 50%, 80%, 80%, and 100% BER is less than 0.001 with M^3-Cast protocol. Thus the M^3-Cast protocol surpasses the standard method for different channel bandwidths.

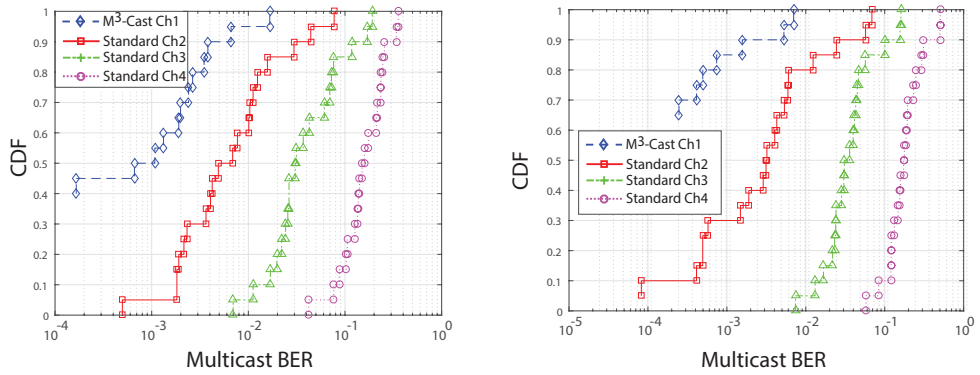

(a) 20 MHz channel

(b) 40 MHz channel

(c) 80 MHz channel

(d) 160 MHz channel

Figure 6.8: CDF of multicast BER for different channel bandwidths

6.4.6 Multicast Channel Capacity

In this section, we examine the numerical multicast channel capacity of M^3-Cast protocol and the standard protocol as derived in Section. IV. The multicast channel capacity can vary for different network parameters. Thus in order to reflect the validity of the proposed method for different network parameters, we calculate the channel capacity for different network radii i.e., 5m, 10m, 15m, 20m, and 25m. As shown in Fig. 6.4, we consider one GO and choose seven multicast clients. The clients are randomly distributed around the GO for a given network radius. Fig. 6.9-6.13 show the multicast capacity of four channels for different network radii. We observe the multicast capacity decreases as we increase the radius of the network. This is because increasing the network size results in increasing the probability of lower SNR due to greater distance. However, M^3-Cast protocol increases the multicast capacity as compared to the standard method

for all network sizes.

We also calculate the average multicast capacity for different network sizes both for M^3-Cast and standard algorithm as shown in Fig.6.14. It can be seen that in the case of 1m to 5m network radius, the average multicast capacity of M^3-Cast is 11.19bps/Hz (Ch2) while it is 10.32bps/Hz (Ch1), 9.39bps/Hz (Ch3), and 8.83bps/Hz (Ch4) for standard method. Thus the capacity gain by M^3-Cast is 17.65% for a network of radius 5m. Similarly, M^3-Cast achieves a capacity gain of 20.64%, 21.43%, 44.02%, and 28.85% for network of radii 10m, 15m, 20m, and 25m, respectively as compared to average multicast capacity of the standard method. Hence M^3-Cast outperforms the standard method in terms of multicast capacity for different network sizes.

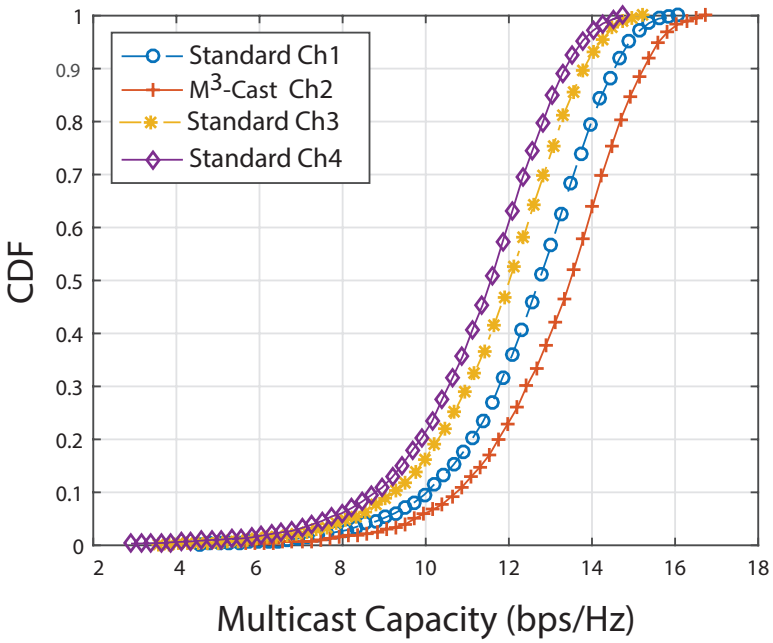

Figure 6.9: Multicast Capacity for a Network of radius 5m {7 Clients | 4 Channels}

6.4.7 Multicast Throughput

In order to assess the performance of M^3-Cast protocol from a system perspective i.e., (MAC and PHY layers), we calculate the multicast throughput from our theoretical model derived in Section. IV and simulation model shown in Fig. 6.3. For this purpose, we deploy five clients around GO with three common channels namely Ch1, Ch2, and Ch3 among all clients such that the SNR of each channel is different than others by at least 1dB. We use 20MHz bandwidth with 16-QAM under TGn channel C with parameters shown in TABLE C.1. The theoretical multicast throughput is calculated from eq. (6.17) in Section 6.3.5. TABLE 6.4 lists the parameters used in eq. (6.17) and APPENDIX A to calculate the multicast throughput.

The theoretical (theo) and simulation (sim) average multicast throughput for Ch1, Ch2, and Ch3 are illustrated in Fig. 6.15. As we increase the packet length at MAC layer, average multicast theoretical and simulation throughput increases for all the three common channels. However, each channel gives a different throughput. Next, we calculate the average multicast throughput for the standard and M^3-Cast protocol as shown in Fiq. 6.16. The simulation results in Fig.6.16 indicates that M^3-Cast improves the average multicast throughput by almost 38% i.e., from about 12.02Mb/s to 16.6Mb/s as compared to standard method when the packet length is 500 bytes. The throughput gain rises tremendously as we increase the packet size.

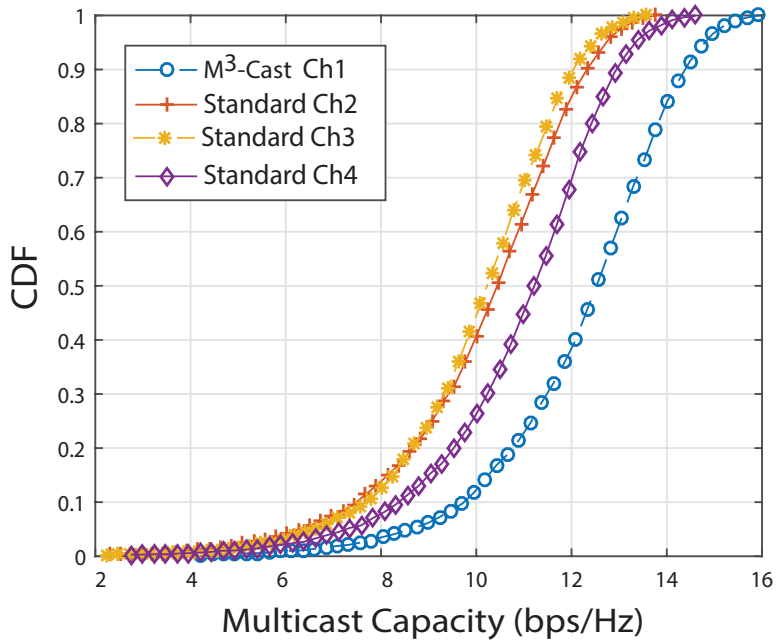

Figure 6.10: Multicast Capacity for a Network of radius 10m {7 Clients | 4 Channels}

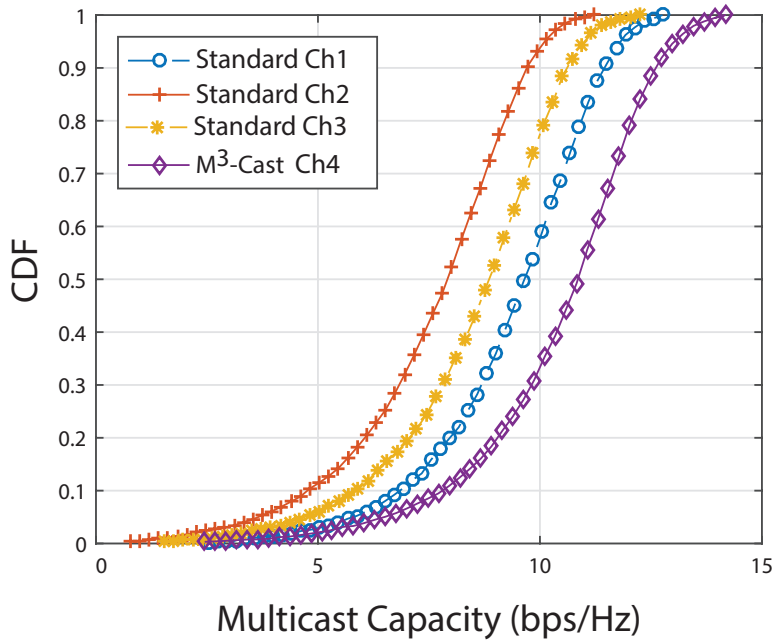

Figure 6.11: Multicast Capacity for a Network of radius 15m {7 Clients | 4 Channels}

For example, M^3-Cast achieves 23.5Mb/s throughput for a packet size of 1000 bytes whereas the standard algorithm achieves 14.2Mb/s for the same packet size. The improvement is 65% in this case. Similarly, for a packet size of 1500 bytes, M^3-Cast almost doubled the average multicast throughput. The theoretical results confirm the simulation results.

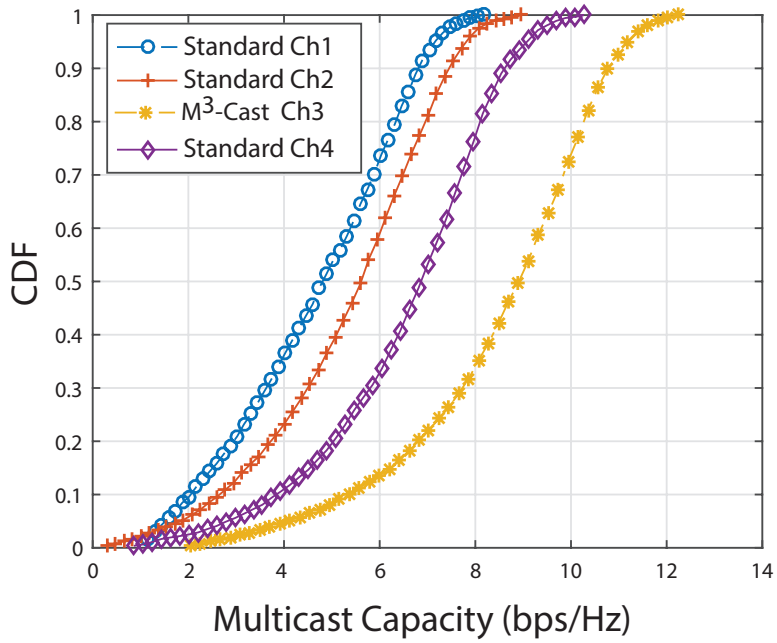

Figure 6.12: Multicast Capacity for a Network of radius 20m {7 Clients | 4 Channels}

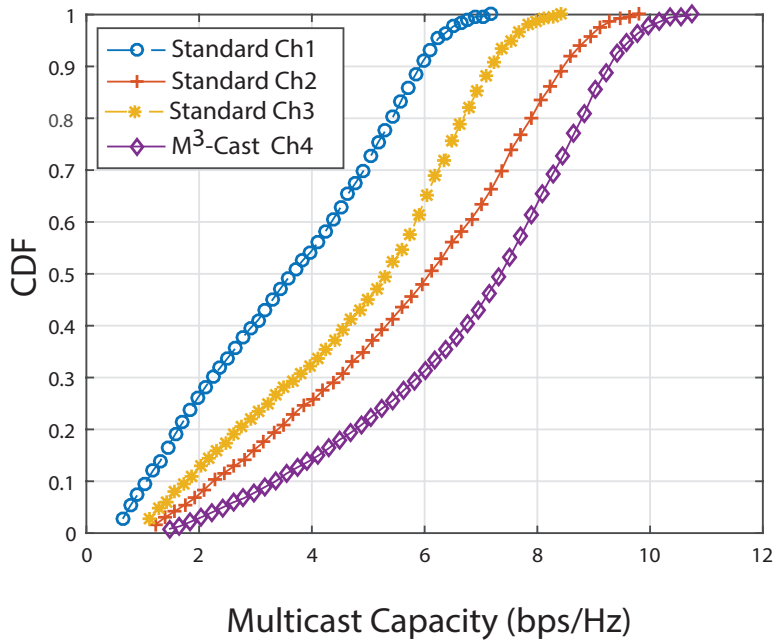

Figure 6.13: Multicast Capacity for a Network of radius 25m {7 Clients | 4 Channels}

6.5 Summary

In this chapter we presented our proposed M^3-Cast protocol. M^3-Cast is more effective than the standard multicast protocol because it chooses the most favourable communication channel and transmission rate for a multi-channel and multi-rate multicast communication in the context of a WD 802.11ac network. M^3-Cast was evaluated by a theoretical formulation as well as tested on a complete system level simulation model that implements the MAC and PHY layers of a WD 802.11ac system. The simulation and theoretical results show that the M^3-Cast protocol surpasses the standard method by almost two times in terms of multicast

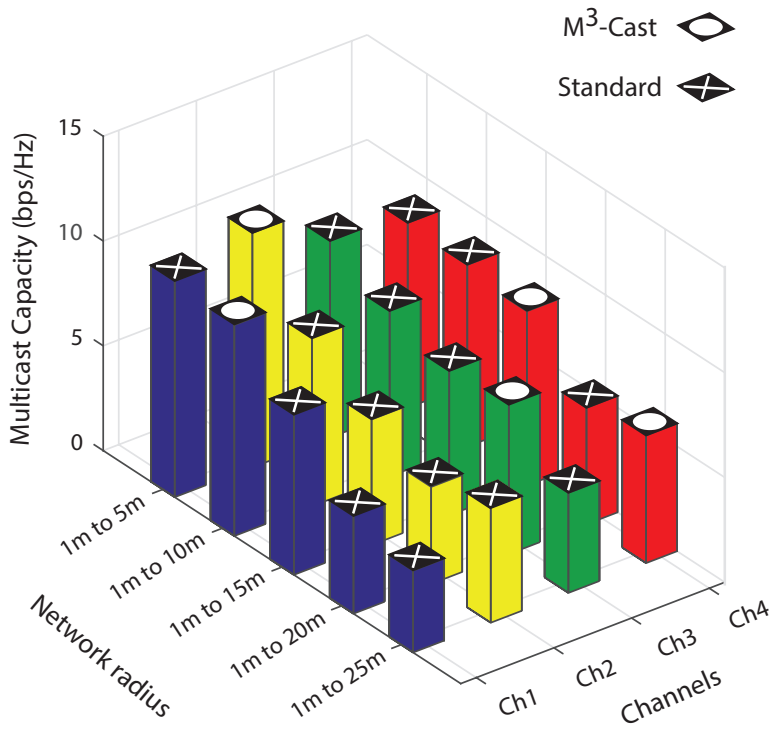

Figure 6.14: Average multicast capacity for network of radius 5m, 10m,15m, 20m, 25m {7 Clients | 4 Channels}

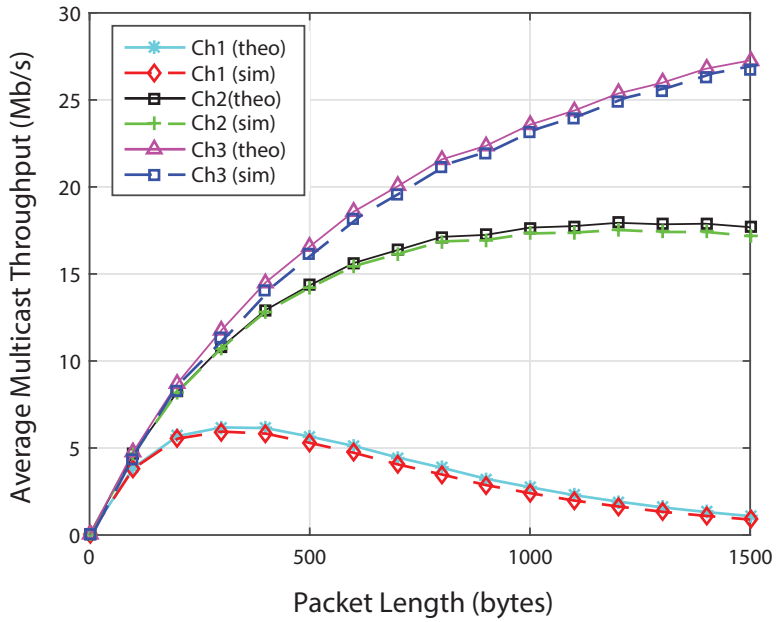

Figure 6.15: Average multicast throughput for different channels

throughput, capacity, and BER under different MIMO configurations, various channel bandwidths, and different network sizes.

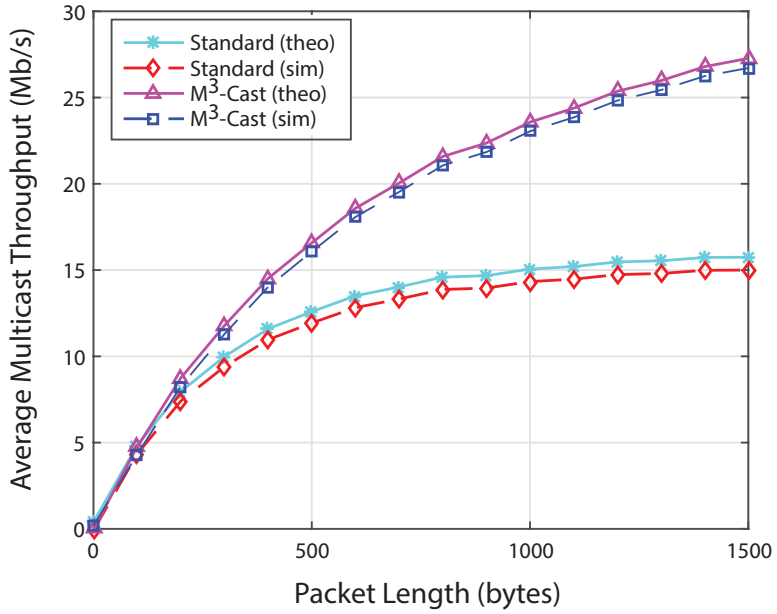

Figure 6.16: Average multicast throughput of the proposed and standard methods

"I hated every minute of training, but I said, 'Don't quit. Suffer now and live the rest of your life as a champion'."

Muhammad Ali (1942 – 2016)

7

Conclusion and Future Work

This chapter concludes the thesis by summarising the research contributions, limitations and suggests a few recommendations for further research. The objective of this research was to develop a multicast protocol, which achieves reliability and efficiency at the MAC and PHY layers for WD 802.11 networks. Therefore the significance of the MAC and PHY layers techniques, which can reduce collision and interference and improve throughput, was investigated in detail. The problems of reliability and efficiency were explored for standard WiFi. It was found from the investigation that although the current literature focuses on improving the multicast communication for standard WiFi, these protocols do not improve the reliability and efficiency of a multicast communication in WD networks. Moreover, when WD network is implemented with a new standard of 802.11 protocol family, for example 802.11ac, the problem of reliable and efficient multicast communication needs to be addressed using the new features of the MAC and PHY layers under TGn channel models. The extant literature review in Chapter 2 determined the major categories of the existing multicast protocols for standard WiFi and WD, thereby identified many potential areas of application for multicast in WD networks. As a result, it was important to carry out more research in this field to address the issues in the current literature. Consequently, collision reduction methods were proposed in Chapter 3, which was followed by a detailed throughput analysis under the new MAC and PHY features of 802.11ac, such as different MIMO configurations, new MCSs, and wider channel bandwidths in Chapter 4. An adaptive QoE-based protocol was then proposed in Chapter 5 and a novel multicast protocol was proposed for the most favourable transmission channel and rate in WD 802.11 networks in Chapter 6.

The problem of reliability was investigated for multicast communication in WD networks and subsequently a novel algorithm known as ELBM was proposed. The ELBM achieved improved reliability in terms of PDR and throughput as compared to standard multicast protocol. It reduced collision and interference from AP and other stations due to an improved access method, an optimal CTS-R selection and an enhanced RTS/CTS mechanism. In addition, Early Packet Loss Detection (EPLD) was proposed, which is an analytical model to investigate the performance of early detection of packet collision in WD networks. EPLD model considered the DCF backoff counter, successful transmission time, and the time spent in col-

lision at the MAC layer. The analytical results of the EPLD protocol showed almost 12-15% enhanced throughput than the standard algorithm under different configurations

In order to evaluate the performance of VHT, a theoretical model was presented by taking into account the key features of the MAC and PHY layers of 802.11ac under six TGn channel models. It was shown through simulation and theoretical analysis that the choice of a particular modulation and coding scheme, number of spatial streams, and the channel bandwidth can greatly affect the total throughput of the system. A MIMO multipath fading channel model was formulated to further investigate the effects of the new features of 802.11ac. Although 802.11ac increases throughput many-fold due to high-order modulation schemes, wider bandwidths and more spatial streams, the performance can also be degraded drastically in an error-prone channel. Moreover, an analytical model known as Vidden was also proposed, which comprehensively calculated the theoretical throughput of VHT 802.11ac in the presence of hidden stations. Vidden precisely calculated the geometric backoff time, successful transmission time and the time spent in collision. The results of the analytical model were validated by simulation results for different number of stations and various packet sizes.

Similarly, a novel adaptive algorithm was proposed to achieves an optimal QoE for a particular application keeping in mind the design choices of WD 802.11ac networks under a MIMO multipath fading TGn channel. To this end, a theoretical model was formulated for a 2x2 MIMO-OFDM using a TGn B channel. The design parameters, such as the input symbol rate and the antenna spacing and, the effects of the moving objects in the surrounding environment, were examined for the given system. The proposed protocol adapted the MCS, SNR, and the distance between the transmitter and the receiver in accordance with the required QoE for a targeted application. Moreover, the field level loss of a VHT PPDU packet was also investigated using a 2x2 MIMO-OFDM transceiver for a TGn D model in WD 802.11ac network. For this purpose, a complete system model was developed and implemented whereby the PER of a complete VHT PPDU and individual fields were analysed. It was shown that the system performance can be improved if the individual fields of the VHT PPDU are managed separately. The simulation results showed that the choice of a particular MCS can affect the overall PER. However, this could not substantially decrease the loss of the individual fields. The BER for individual fields decreases significantly if a wider channel is used for transmissions. It was shown through simulation results that the performance of the proposed method was enhanced in choosing the PHY parameters as compared to standard method.

Finally, a novel multicast protocol known as *M*ulti-rate *M*ulti-channel *M*ulticast (M^3-Cast) protocol was proposed to choose the most favourable communication channel and transmission rate for WD 802.11ac networks. M^3-Cast was evaluated by a theoretical formulation as well as tested on a complete system level simulation model, which was implemented using the MAC and PHY layers of a WD 802.11ac system. The simulation and theoretical results showed that the M^3-Cast protocol surpassed the standard method by almost two times in terms of multicast throughput, capacity, and BER under different MIMO configurations, various channel bandwidths, and different network sizes.

In summary, this thesis has made the following contributions to improve the reliability and efficiency of multicast communication in WD 802.11 networks:

- Enhanced Leader Based Multicast Protocol, Khan et al. [87].
- Analytical model of early packet loss detection in WD 802.11 networks, Khan et al. [91]
- Very High Throughput analysis of MAC and PHY layers of WD 802.11ac networks under TGn channel models, Khan et al. [123], Khan et al. [100].
- **Vidden**: an analytical model for **V**ery High Throughput of 802.11ac **i**n the presence of hi**dden**

stations (under review)

- QoE based adaptive protocol for an efficient WD 802.11 under a TGn MIMO multipath fading channel, Khan et al. [105]
- Field level loss analysis of a packet in a MIMO-OFDM System for a WiFi Direct 802.11ac WLAN, Khan et al. [106]
- M^3-Cast: *M*ulti-rate *M*ulti-channel *M*ulticast protocol to choose the most favourable communication channel and transmission rate for multicast communication in WD networks (under review)

The major focus of the research was to improve the reliability and efficiency of multicast communication in WD 802.11 networks. As a result, the main scope of the research was limited to proposing methodologies which are based on specification of the MAC and PHY layers of WD in order to achieve the research objectives. However, in future the scope of the research can be extended to include the other contemporary D2D technologies such as Bluetooth and D2D communication in mobile communication in general, and LTE and 5G in particular [124][125].

In addition, the following important points can be considered for future work.

- The proposed ELBM protocol can be extended to include another set of unicast stations, which are hidden nodes to CTS-R by adding new strategies to reduce collision and interference between a GO and CTS-R. This will enable the ELBM protocol to be used for more complex and practical use scenarios.
- A hybrid analytical model can be developed, which takes into account the early packet loss detection due to collision and weak signal in WD 802.11 networks.
- The proposed methodologies, such as ELBM, Vidden, M^3-Cast can be enhanced under the MAC and PHY layers specifications of 802.11ad to enable the operation and capability of VHT in frequencies around 60 GHz [126].
- The proposed QoE based adaptive protocol can be modified and extended for more complex traffic scenarios, such as multimedia and real time applications .
- The proposed model of individual field level loss of a VHT-PPDU can be extended to develop techniques, which can predict the early packet loss in WD networks.
- The proposed Vidden model can be extended to model the VHT of the heterogeneous stations with unsaturated traffic conditions in the presence of hidden stations.
- The proposed M^3-Cast protocol can be extended to develop another channel selection criteria, which not only takes into account the RSSI and the number of available channels at the PHY layer but also collision at the MAC layer.

A

Transmission Time

In this section, we calculate the transmission time of a data frame T_{DATA} and the transmission time of an ACK frame T_{ACK}. T_{DATA} and T_{ACK} are calculated in eq. (A.1-A.13).

$$T_{DATA} = T_{LEG-PREAMBLE} + T_{L-SIG} + T_{VHT-SIG-A} + T_{VHT-PREAMBLE} + T_{VHT-SIG-B} + T_D \quad \text{(A.1)}$$

$$T_{ACK} = T_{LEG-PREAMBLE} + T_{L-SIG} + T_{VHT-SIG-A} + T_{VHT-PREAMBLE} + T_{VHT-SIG-B} + T_A \quad \text{(A.2)}$$

$$T_{LEG-PREAMBLE} = T_{L-STF} + T_{L-LTF} \quad \text{(A.3)}$$

$$T_{VHT-PREAMBLE} = T_{VHT-STF} + N_{VHTLTF} \times T_{VHT-LTF} \quad \text{(A.4)}$$

where T_{L-STF}, T_{L-LTF}, T_{L-SIG}, $T_{VHT-SIG-A}$, $T_{VHT-STF}$, $T_{VHT-LTF}$, and $T_{VHT-SIG-B}$, indicate the different fields of a VHT-PPDU frame as illustrated in TABLE A.1. N_{VHTLTF} indicate the number of long training symbols determined from the number of space-time streams [112]. The values T_{STF} and T_{LTF} are calculated in eq. (A.5) and eq. (A.6), respectively.

$$T_{STF} = 10\left(\frac{T_{FFT}}{4}\right) \quad \text{(A.5)}$$

where $T_{FFT} = 1/\triangle F$ while $\triangle F$ indicates the subcarrier frequency spacing in kHz. For a 20MHz channel bandwidth under OFDM, the $\triangle F = 312.5$ kHz. Thus $T_{FFT} = 3.12$ μs and $T_{SHORT} = 8$ μs. It can also be calculated for a 40MHz channel bandwidth and other channel bandwidths [11].

$$T_{LTF} = 2.T_{FFT} + T_{GI2} \quad \text{(A.6)}$$

By using T_{GI2} and T_{FFT} in eq. (A.6), the $T_{LTF} = 8$ μs. Similarly T_D and T_A are calculated in eq. (A.7) and eq. (A.8), respectively.

$$T_D = \begin{cases} N_{SYM-DATA} \times T_{SYM} & \text{for long GI} \\ T_{SYML}\lceil \frac{T_{SYMS} \times N_{SYM-DATA}}{T_{SYML}} \rceil & \text{for short GI} \end{cases} \quad \text{(A.7)}$$

$$T_A = \begin{cases} N_{SYM-ACK} \times T_{SYM} & \text{for long GI} \\ T_{SYML}\lceil \frac{T_{SYMS} \times N_{SYM-ACK}}{T_{SYML}} \rceil & \text{for short GI} \end{cases} \quad \text{(A.8)}$$

Table A.1: Parameters of VHT PPDU

Parameter	Details
T_{L-STF}	Transmission time of Legacy Short Training Field
T_{L-LTF}	Transmission time of Legacy Long Training Field
T_{L-SIG}	Transmission time of Legacy Signal field
$T_{VHT-SIG-A}$	Transmission time of Very High Throughput-Signal A field
$T_{VHT-STF}$	Transmission time of Very High Throughput Short Training Field
$T_{VHT-LTF}$	Transmission time of Very High Throughput Long Training Field
$T_{VHT-SIG-B}$	Transmission time of Very High Throughput-Signal B field

where GI, T_{SYM}, T_{SYMS} and T_{SYML} indicate Guard Interval, symbol interval, short GI symbol interval, and long GI symbol interval, respectively. Their values are listed in TABLE 6.4.

$$T_{SYM} = \begin{cases} T_{SYML} & \text{for long GI} \\ T_{SYMS} & \text{for short GI} \end{cases} \tag{A.9}$$

$$N_{SYM-DATA} = m_{STBC} \times \lceil \frac{M}{m_{STBC} \times N_{DBPSL}} \rceil \tag{A.10}$$

where $\lceil x \rceil$ = smallest integer $\geq x$ and N_{DBMS} indicates the number of data bits per symbol.

$$M = 8 \times APEP_{LENGTH} + N_{Service} + N_{tail} \times N_{ES} \tag{A.11}$$

$$m_{STBC} = \begin{cases} 2 & \text{if STBC is used} \\ 1 & \text{otherwise} \end{cases} \tag{A.12}$$

where $APEP_{LENGTH}$ indicates the final value of A-MPDU i.e., payload size and N_{ES} represents the number of Binary Convolution Code (BCC) encoders. The value of N_{ES} depends on the MCS and channel bandwidth and their details can be found in [11]. Space-Time Block Coding (STBC) is an encoding technique that greatly improves the reliability of communication in 802.11ac.

Similarly, $N_{SYM-ACK}$ is calculated in eq. (A.13)

$$N_{SYM-ACK} = m_{STBC} \times \lceil \frac{N_{SERVICE} + N_{tail} * N_{ES}}{26 \times m_{STBC}} \rceil \tag{A.13}$$

B

VHT PPDU

In this section we describe the basics of a PHY frame in a MIMO-OFDM WD 802.11ac system. When a packet is received by a PHY layer from a MAC layer, it is called a PHY-Layer Protocol Service Data Unit (PSDU). The PHY layer consists of two sub layers namely: Physical Layer Conformance Procedure (PLCP) and Physical Medium Dependent Sublayer (PMD). A VHT preamble i.e., PLCP header and trailer is added to the PSDU which is then called a PCLP Protocol Data Unit (PPDU). Thus the PPDU is a complete PLCP frame, including PLCP headers, MAC headers, MAC data field, and MAC/PLCP trailers. The PPDU is called a VHT PPDU because it achieves high data rate. The field structure for the VHT PPDUs consist of a preamble and data portions. The VHT PPDU also contains legacy preamble fields (i.e., L-STF, L-LTF, and L-SIG) which are common with HT and non-HT format preambles. However, VHT format preamble fields include additional format-specific training and signalling fields. Each format defines a data field for the transmission of a user payload data. The VHT PPDU is shown in TABLE B.1. We describe each of the

Table B.1: VHT PPDU Frame Structure

L-STF	L-LTF	L-SIG	VHT-SIG-A1	VHT-SIG-A2	VHT-STF	VHT-LTF1	...
...	VHT-LTF2	...	VHT-LTFN	VHT-SIG-B	SF	VHT-Data	Tail

fields as follows [11] and [127].

L-STF

The Legacy Short Training Field (L-STF) is a common field among VHT, HT, and Non-HT preambles. It consists of 10 short preambles of duration 0.8 μs each. This preamble is constructed by 12 OFDM subcarriers out of 52 subcarriers to detect the start of a 802.11 packet. The 12 individual subcarriers are modulated with Binary Phase Shift Keying (BPSK) to ensure a low peak to average power ratio. The L-STF can be decoded by any receiver who is compatible with the OFDM technology. It is also used for synchronizing timers and selecting an antenna. Eq. (B.1) indicates how to calculate the duration of the L-STF, i.e., T_{STF} [11].

$$T_{STF} = 10\left(\frac{T_{FFT}}{4}\right) \tag{B.1}$$

where T_{FFT} indicates the length of a Fast Fourier Transform (FFT) and is given by eq. (B.2).

$$T_{FFT} = \frac{1}{\triangle F} \tag{B.2}$$

where $\triangle F$ indicates the subcarrier frequency spacing in kHz. For a 20MHz channel bandwidth under OFDM, the $\triangle F = 312.5$ kHz. Thus $T_{FFT} = 3.12$ μs and $T_{SHORT} = 8$ μs. It can also be calculated for a 40MHz channel bandwidth and other channel bandwidths [11].

L-LTF

The Legacy Training Field (L-LTF) is also part of the VHT, HT, and Non-HT preambles. It is used to estimate the underlying channel, frequency offset and time synchronization. The duration of the L-LTF, i.e., T_{LTF} is computed in eq. (B.3 [11]).

$$T_{LTF} = 2.T_{FFT} + T_{GI2} \tag{B.3}$$

where T_{GI2} indicates a double guard interval which is 1.6 μs. By using T_{GI2} and T_{FFT} in eq. (B.3), the $T_{LTF} = 8$ μs.

L-SIG

The Legacy Signal Field (L-SIG) is used to calculate data rate, length, and parity information. It consists of 24 bits. The L-SIG is a component of the VHT, HT, and non-HT PPDUs. It is transmitted using BPSK modulation with a rate of 1/2 Binary Convolutional Coding (BCC) [127].

VHT-SIG-A

The VHT Signal A (VHT-SIG-A) field consists of two symbols: VHT-SIG-A1 and VHT-SIG-A2. The VHT-SIG-A carries information required to interpret VHT PPDUs. Only an 802.11ac system can decode the VHT-SIG-A fields. These fields are modulated and coded using either of 0 to 9 MCS. For a detailed structure of the VHT-SIG-A, [11] can be refereed.

VHT-STF

The VHT STF serves the same purpose as the L-STF. Just as the first training fields help a receiver tune in the signal, the VHT-STF assists the receiver in detecting a repeating pattern and setting receiver gain [127].

VHT-LTF

The VHT-LTF is used to estimate a MIMO channel and track pilot subcarriers. The VHT-LTF includes one VHT long training symbol for each spatial stream indicated by the selected MCS. Each symbol is 4 μs long . The number of OFDM symbols in the VHT-LTF (N_{VHTLTF}) is derived from the total number of space-time streams i.e., $N_{STS,total}$ which is computed in eq. (B.4) [11]).

$$N_{STS,total} = \sum_{u=0}^{N_{user}-1} N_{STS}(u) \tag{B.4}$$

where N_{user} indicates the total number of users and $N_{STS}(u)$ is the number of space-time streams per user u. It may consist of 1, 2, 4, 6, or 8 symbols; the number of required symbols is rounded up to the next highest value, so a link with five streams would require six symbols [127].

VHT-SIG-B

The Very High Throughput Signal B (VHT-SIG-B) carries information about the data rate, the length of A-MPDU per user and the MIMO for multi-user case. It is transmitted with MCS0 and consists of a single OFDM symbol located between the VHT-LTF and the data portion of the VHT format PPDU. The size of the VHT-SIG-B depends on the channel bandwidth and the number of users (SU, MU) [128].

Service Field (SF)

The SF is part of the VHT-Data portion. It consists of 16 bits out of which 7 bits are used for scrambler initialization to avoid long runs of identical bits; 1 bit is reserved for future use while 8 bits are used for Cyclic Redundancy Check (CRC) to detect errors in VHT-SIG-B [11].

VHT-Data

The VHT-Data field contains a variable size PSDU from the higher layers. The PSDU may contain one or more MAC Protocol Data Unit (MPDU) or several MPDUs in an aggregate MPDU (A-MPDU). The size of the PSDU may vary from 1 to 1048575 bytes [11]. If no Data field is present in the physical layer payload, it is called a Null Data Packet (NDP), which is used by the VHT PHY for setting up beamforming, measurement, and tuning [128].

Tail

It is a 6-bit field which is used to terminate a convolutional code. Tail bits are not needed when a Low-Density Parity-Check (LDPC) is used [128].

C

TGn Channel Models

The equations derived for SNR values in the eq. (6.20-6.24) show that calculation of SNR values depends on different path loss parameters. In order to model the channel for 802.11 in different environments, a set of six profiles namely TGn channel models A-F as illustrated in TABLE C.1 is proposed in [129]. Each profile represents a different environment with specific Root Mean Square (RMS) delay spread (σ_{RMS}), standard deviation (σ) and Line-Of-Sight (LOS)/Non-Line-Of-Sight (NLOS) conditions, as illustrated in TABEL C.2. More details on channel profiles for 802.11 can be found in [129].

Table C.1: TGn Channel Profile Models

Channel Model	**Details**
A	A typical office environment with NLOS conditions and $\sigma_{RMS} = 0ns$ (Optional)
B	A typical large open space and office environments, NLOS conditions with $\sigma_{RMS} = 15ns$
C	A large open space (indoor and outdoor) NLOS conditions with $\sigma_{RMS} = 30ns$
D	A large open space (indoor and outdoor) LOS conditions with $\sigma_{RMS} = 50ns$
E	A large open space (indoor and outdoor) LOS conditions with $\sigma_{RMS} = 100ns$
F	A large open space (indoor and outdoor) LOS conditions with $\sigma_{RMS} = 150ns$

Thus based on a specific channel model as illustrated in TABLE C.2, the path loss, RSS, and SNR can be calculated. For example for TGn channel D, the path loss, RSS values, and SNR are calculated in Fig. . We assume unit antenna gains at transmitter and receiver, thus $G_t = G_r = 1$. Similarly, the values of

Table C.2: Path Loss Parameters for TGn Channel Models 802.11

Channel Model	d_{BP} (m)	Slope before d_{BP}	Slope after d_{BP}	Shadow Fading Std. dev(dB) before d_{BP} (LOS)	Shadow Fading Std. dev(dB) after d_{BP} (NLOS)
A	5	2	3.5	3	4
B	5	2	3.5	3	4
C	5	2	3.5	3	5
D	10	2	3.5	3	5
E	20	2	3.5	3	6
F	30	2	3.5	3	6

λ is determined from the carrier frequency of 802.11ac which is $f_c = 5.23GHz$, therefore C/λ where C is the speed of electromagnetic waves i.e., $C = 3 \times 10^8$m/s. The values of d_{BP} and σ for channel D are taken from TABLE C.2. Note that the slope and σ are different before and after d_{BP}. The $PL(d)$ in dBm for a T-R separation of d (in m) is calculated from eq. (6.23). We assume that the transmitter power is +5dBm and the noise at the receiver is equal to the noise floor value of -90dBm. Consequently using the values of $PL(d)$ and $P_t = 5$dBm in eq. (6.22), the RSS value E is determined. Lastly, substituting E and $W = -90$dBm in eq. (6.20), the SNR value X is calculated at the receiver (client).

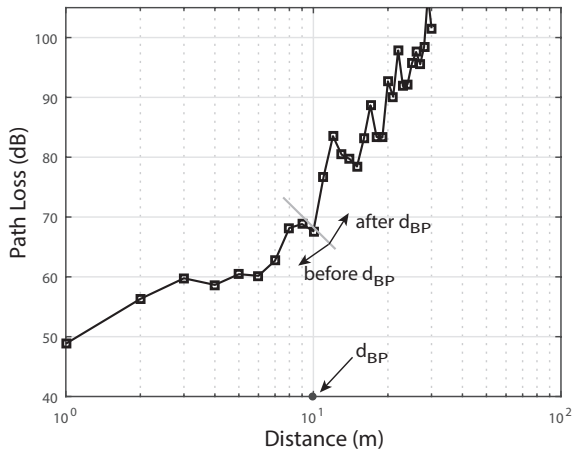

(a) Path Loss

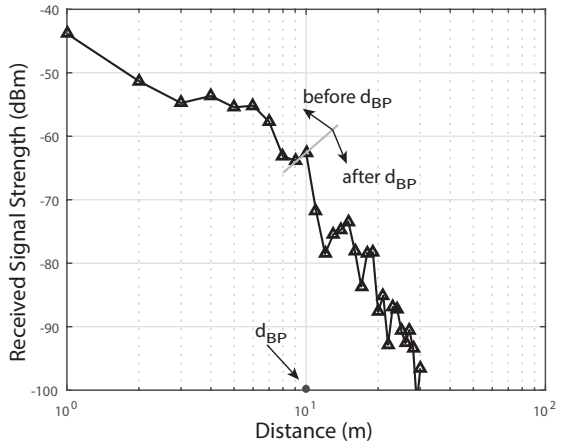

(b) RSS

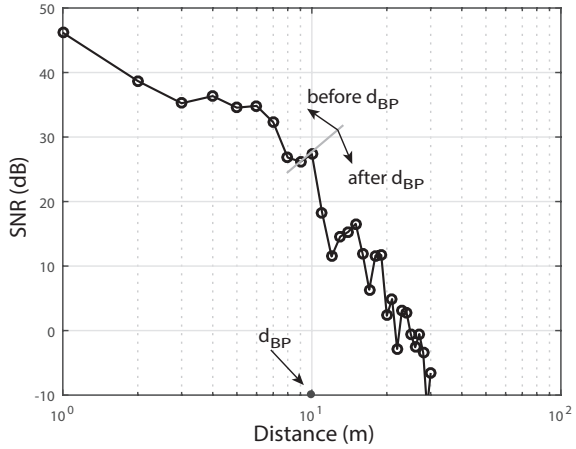

(c) SNR

Figure C.1: Loss in the received signal as a function of distance

REFERENCES

[1] A. Asadi, Q. Wang, and V. Mancuso, "A Survey on Device-to-Device Communication in Cellular Networks," *IEEE Communications Surveys Tutorials*, vol. 16, no. 4, pp. 1801–1819, Fourthquarter 2014.

[2] "IEEE Standard for Information technology–Telecommunications and information exchange between systems local and metropolitan area networks–Specific requirements Part 11: Wireless LAN Medium Access Control (MAC) and Physical Layer (PHY) Specifications," *IEEE Std 802.11-2012 (Revision of IEEE Std 802.11-2007)*, pp. 1–5229, March 2012.

[3] W. Alliance, "Wi-fi peer-to-peer (p2p) specification v1.1," *Wi-Fi Alliance Specification*, vol. 1, pp. 1–159, 2010.

[4] "WiFi Alliance, Annual Report," pp. 1–20, Dec 2013.

[5] W. Alliance. (2016) Wifi device shipments to surpass 15 billion by end of 2016. [Online]. Available: http://www.wi-fi.org/news-events/newsroom/wi-fi-device-shipments-to-surpass-15-billion-by-end-of-2016

[6] S. Andreev, O. Galinina, A. Pyattaev, K. Johnsson, and Y. Koucheryavy, "Analyzing Assisted Offloading of Cellular User Sessions onto D2D Links in Unlicensed Bands," *IEEE Journal on Selected Areas in Communications*, vol. 33, no. 1, pp. 67–80, Jan 2015.

[7] J. Lee, Y. Yi, S. Chong, and Y. Jin, "Economics of wifi offloading: Trading delay for cellular capacity," in *2013 Proceedings IEEE INFOCOM*, April 2013, pp. 3309–3314.

[8] A. Pyattaev, K. Johnsson, S. Andreev, and Y. Koucheryavy, "3gpp lte traffic offloading onto wifi direct," in *2013 IEEE Wireless Communications and Networking Conference Workshops (WCNCW)*, April 2013, pp. 135–140.

[9] W. Alliance, "Wi-fi peer-to-peer (p2p) technical specification, version 1.7," *Wi-Fi Alliance Technical Committee P2P Task Group*, vol. 7, pp. 1–201, 2016.

[10] M. A. Khan, W. Cherif, F. Filali, and R. Hamila, "Wi-fi direct research-current status and future perspectives," *Journal of Network and Computer Applications*, 2017.

[11] "IEEE Approved Draft Standard for IT - Telecommunications and Information Exchange between Systems - LAN/MAN - Specific Requirements - Part 11: Wireless LAN Medium Access Control and Physical Layer Specifications - amd 4: Enhancements for Very High Throughput for operation in bands below 6ghz," *IEEE P802.11ac/D7.0, September 2013*, pp. 1–456, Dec 2013.

[12] "Ieee standard for wireless lan medium access control (mac) and physical layer (phy) specifications," *IEEE Std 802.11-1997*, pp. 1–445, Nov 1997.

[13] S. Deering, "Host Extensions for IP Multicasting," Internet Requests for Comments, RFC Editor, RFC 1112, August 1989. [Online]. Available: https://tools.ietf.org/html/rfc1112

[14] C. Thorpe and L. Murphy, "A survey of adaptive carrier sensing mechanisms for ieee 802.11 wireless networks," *IEEE Communications Surveys Tutorials*, vol. 16, no. 3, pp. 1266–1293, Third 2014.

[15] M. Abusubaih, "Approach for discriminating losses in 802.11 wireless lans," *IET Communications*, vol. 6, no. 10, pp. 1262–1269, July 2012.

[16] S. Rayanchu, A. Mishra, D. Agrawal, S. Saha, and S. Banerjee, "Diagnosing wireless packet losses in 802.11: Separating collision from weak signal," in *INFOCOM 2008. The IEEE 27th Conference on Computer Communications*, 2008, pp. 735–743.

[17] Q. Pang, S. C. Liew, and V. C. M. Leung, "Design of an effective loss-distinguishable mac protocol for 802.11 wlan," *IEEE Communications Letters*, vol. 9, no. 9, pp. 781–783, Sep 2005.

[18] M. Heusse, F. Rousseau, G. Berger-Sabbatel, and A. Duda, "Performance anomaly of 802.11 b," in *INFOCOM 2003. Twenty-Second Annual Joint Conference of the IEEE Computer and Communications. IEEE Societies*, vol. 2. IEEE, 2003, pp. 836–843.

[19] "Ieee standard for information technology– local and metropolitan area networks– specific requirements– part 11: Wireless lan medium access control (mac) and physical layer (phy) specifications amendment 8: Ieee 802.11 wireless network management," Tech. Rep., Feb 2011.

[20] "Iso/iec/ieee international standard for information technology–telecommunications and information exchange between systems local and metropolitan area networks–specific requirements part 11: Wireless lan medium access control (mac) and physical layer (phy) specifications amendment 2: Mac enhancements for robust audio video streaming (adoption ofieee std 802.11aa-2012)," *ISO/IEC/IEEE 8802-11:2012/Amd.2:2014(E)*, pp. 1–168, March 2014.

[21] "Ieee standard for information technology– local and metropolitan area networks– specific requirements– part 11: Wireless lan medium access control (mac)and physical layer (phy) specifications amendment 5: Enhancements for higher throughput," Tech. Rep., Oct 2009.

[22] Y. Park, C. Jo, S. Yun, and H. Kim, "Multi-room iptv delivery through pseudo-broadcast over ieee 802.11 links," in *2010 IEEE 71st Vehicular Technology Conference*, May 2010, pp. 1–5.

[23] "Ieee standard for information technology– local and metropolitan area networks– specific requirements– part 11: Wireless lan medium access control (mac)and physical layer (phy) specifications amendment 1: Radio resource measurement of wireless lans," Tech. Rep., June 2008.

[24] P. Ge and P. K. McKinley, "Comparisons of error control techniques for wireless video multicasting," in *Conference Proceedings of the IEEE International Performance, Computing, and Communications Conference (Cat. No.02CH37326)*, 2002, pp. 93–102.

[25] P. Pace, G. Iannitelli, and G. Aloi, "Eavesdropping wireless video packets to improve standard multicast transmission in wi-fi networks," in *IEEE 5th International Symposium on Wireless Pervasive Computing 2010*, May 2010, pp. 471–476.

[26] P. Pace and G. Aloi, "Wevcast: Practical implementation and testing of effective multicast services for wi-fi networks," in *2012 IEEE Wireless Communications and Networking Conference (WCNC)*, April 2012, pp. 3233–3238.

[27] J. Tourrilhes, "Robust broadcast: improving the reliability of broadcast transmissions on csma/ca," in *Ninth IEEE International Symposium on Personal, Indoor and Mobile Radio Communications (Cat. No.98TH8361)*, vol. 3, Sep 1998, pp. 1111–1115 vol.3.

[28] "Optimizing Enterprise Video Over Wireless LAN," Tech. Rep.

[29] L. C. I. M. M. W. R. P. S. M. N. K. G. V. A. M. L. Q. B. Hart, H.L. and A. Ashley, "Group addressed normative text," Tech. Rep., March 2008.

[30] A. Ashley and N. Kakani, "Splitting gcr from dms," Tech. Rep., Jan 2011.

[31] R. Chandra, S. Karanth, T. Moscibroda, V. Navda, J. Padhye, R. Ramjee, and L. Ravindranath, "Dircast: A practical and efficient wi-fi multicast system," in *2009 17th IEEE International Conference on Network Protocols*, Oct 2009, pp. 161–170.

[32] J. Kuri and S. K. Kasera, "Reliable multicast in multi-access wireless lans," in *INFOCOM '99. Eighteenth Annual Joint Conference of the IEEE Computer and Communications Societies. Proceedings. IEEE*, vol. 2, Mar 1999, pp. 760–767 vol.2.

[33] S. K. S. Gupta, V. Shankar, and S. Lalwani, "Reliable multicast mac protocol for wireless lans," in *Communications, 2003. ICC '03. IEEE International Conference on*, vol. 1, May 2003, pp. 93–97 vol.1.

[34] H.-W. Ferng and P.-C. Yeh, "Study on window-based reliable multicast protocols for wireless lans," in *2004 IEEE 15th International Symposium on Personal, Indoor and Mobile Radio Communications (IEEE Cat. No.04TH8754)*, vol. 1, Sept 2004, pp. 120–124 Vol.1.

[35] Y. Daldoul, D. E. Meddour, and T. Ahmed, "A reliable plcp-based multicast protocol for ieee 802.11 wlan," in *Global Information Infrastructure Symposium - GIIS 2011*, Aug 2011, pp. 1–6.

[36] D. Dujovne and T. Turletti, "Multicast in 802.11 wlans: An experimental study," in *Proceedings of the 9th ACM International Symposium on Modeling Analysis and Simulation of Wireless and Mobile Systems*, ser. MSWiM 06. New York, NY, USA: ACM, 2006, pp. 130–138. [Online]. Available: http://doi.acm.org/10.1145/1164717.1164741

[37] T. Turletti and Y. Seok, "Practical rate-adaptive multicast schemes for multimedia over ieee 802.11 wlans," INRIA, Research Report RR-5993, 2006. [Online]. Available: https://hal.inria.fr/inria-00104699

[38] N. Letor, W. Torfs, and C. Blondia, "Multimedia multicast performance analysis for 802.11n network cards," in *2012 IFIP Wireless Days*, Nov 2012, pp. 1–3.

[39] M.-t. Sun, L. Huang, S. Wang, A. Arora, and T.-H. Lai, "Reliable mac layer multicast in ieee 802.11 wireless networks," *Wireless Communications and Mobile Computing*, vol. 3, no. 4, pp. 439–453, 2003.

[40] Z. Li and T. Herfet, "Blbp: A beacon-driven leader based protocol for mac layer multicast error control in wireless lans," in *2008 4th International Conference on Wireless Communications, Networking and Mobile Computing*, Oct 2008, pp. 1–4.

[41] X. Wang, L. Wang, Y. Wang, and D. Gu, "Reliable multicast mechanism in wlan with extended implicit mac acknowledgment," in *VTC Spring 2008 - IEEE Vehicular Technology Conference*, May 2008, pp. 2695–2699.

[42] Z. Li and T. Herfet, "Hlbp: A hybrid leader based protocol for mac layer multicast error control in wireless lans," in *IEEE GLOBECOM 2008 - 2008 IEEE Global Telecommunications Conference*, Nov 2008, pp. 1–6.

[43] ——, "Mac layer multicast error control for iptv in wireless lans," *IEEE Transactions on Broadcasting*, vol. 55, no. 2, pp. 353–362, June 2009.

[44] J. Villalon, P. Cuenca, L. Orozco-Barbosa, Y. Seok, and T. Turletti, "Arsm: a cross-layer auto rate selection multicast mechanism for multi-rate wireless lans," *IET Communications*, vol. 1, no. 5, pp. 893–902, Oct 2007.

[45] S. Choi, N. Choi, Y. Seok, T. Kwon, and Y. Choi, "Leader-based rate adaptive multicasting for wireless lans," in *IEEE GLOBECOM 2007 - IEEE Global Telecommunications Conference*, Nov 2007, pp. 3656–3660.

[46] N. Choi, Y. Seok, T. Kwon, and Y. Choi, "Multicasting multimedia streams in ieee 802.11 networks: A focus on reliability and rate adaptation," *Wirel. Netw.*, vol. 17, no. 1, pp. 119–131, Jan. 2011. [Online]. Available: http://dx.doi.org/10.1007/s11276-010-0268-9

[47] ——, "Leader-based multicast service in ieee 802.11v networks," in *2010 7th IEEE Consumer Communications and Networking Conference*, Jan 2010, pp. 1–5.

[48] A. Kamerman and L. Monteban, "Wavelan-ii: A high-performance wireless lan for the unlicensed band," *Bell Labs Technical Journal*, vol. 2, no. 3, pp. 118–133, Summer 1997.

[49] W. C. Fenner, "Internet group management protocol, version 2," 1997.

[50] G. Holland, N. Vaidya, and P. Bahl, "A rate-adaptive mac protocol for multi-hop wireless networks," in *Proceedings of the 7th annual international conference on Mobile computing and networking*. ACM, 2001, pp. 236–251.

[51] M. Lacage, M. H. Manshaei, and T. Turletti, "Ieee 802.11 rate adaptation: a practical approach," in *Proceedings of the 7th ACM international symposium on Modeling, analysis and simulation of wireless and mobile systems*. ACM, 2004, pp. 126–134.

[52] H.-J. Chiou, Y.-R. Lee, and C.-W. Lin, "Error-resilient transcoding using adaptive intra refresh for video streaming," in *2004 IEEE International Symposium on Circuits and Systems (IEEE Cat. No.04CH37512)*, vol. 3, May 2004, pp. III–777–80 Vol.3.

[53] C. M. Chen, C. W. Lin, and Y. C. Chen, "Adaptive error-resilience transcoding and fairness grouping for video multicast over wireless networks," in *2007 IEEE International Conference on Communications*, June 2007, pp. 1661–1666.

[54] C.-M. Chen, C.-W. Lin, and Y.-C. Chen, "Adaptive error-resilience transcoding using prioritized intra-refresh for video multicast over wireless networks," *Signal Processing: Image Communication*, vol. 22, no. 3, pp. 277–297, 2007.

[55] Z. Liu, H. Liu, and Y. Wang, "Cross layer adaptation for h.264 video multicasting over wireless lan," in *2006 IEEE International Conference on Multimedia and Expo*, July 2006, pp. 1121–1124.

[56] A. Basalamah, H. Sugimoto, and T. Sato, "Rate adaptive reliable multicast mac protocol for wlans," in *2006 IEEE 63rd Vehicular Technology Conference*, vol. 3, May 2006, pp. 1216–1220.

[57] J. Villalon, P. Cuenca, L. Orozco-Barbosa, Y. Seok, and T. Turletti, "Cross-layer architecture for adaptive video multicast streaming over multirate wireless lans," *IEEE Journal on Selected Areas in Communications*, vol. 25, no. 4, pp. 699–711, May 2007.

[58] Y. Park, Y. Seok, N. Choi, Y. Choi, and J. M. Bonnin, "Rate-adaptive multimedia multicasting over ieee 802.11 wireless lans," in *CCNC 2006. 2006 3rd IEEE Consumer Communications and Networking Conference, 2006.*, vol. 1, Jan 2006, pp. 178–182.

[59] L. Rizzo, "Effective erasure codes for reliable computer communication protocols," *SIGCOMM Comput. Commun. Rev.*, vol. 27, no. 2, pp. 24–36, Apr. 1997. [Online]. Available: http://doi.acm.org/10.1145/263876.263881

[60] O. Alay, C. Li, A. Rai, T. Korakis, Y. Wang, and S. Panwary, "Dynamic rate and fec adaptation for video multicast in multi-rate wireless networks," in *2009 5th International Conference on Testbeds and Research Infrastructures for the Development of Networks Communities and Workshops*, April 2009, pp. 1–8.

[61] A. J. McAuley, "Reliable broadband communication using a burst erasure correcting code," *SIGCOMM Comput. Commun. Rev.*, vol. 20, no. 4, pp. 297–306, Aug. 1990. [Online]. Available: http://doi.acm.org/10.1145/99517.99566

[62] P. A. Chou, A. E. Mohr, A. Wang, and S. Mehrotra, "Error control for receiver-driven layered multicast of audio and video," *IEEE Transactions on Multimedia*, vol. 3, no. 1, pp. 108–122, Mar 2001.

[63] W.-T. Tan and A. Zakhor, "Video multicast using layered fec and scalable compression," *IEEE Transactions on Circuits and Systems for Video Technology*, vol. 11, no. 3, pp. 373–386, Mar 2001.

[64] M. Wu, S. Makharia, H. Liu, D. Li, and S. Mathur, "Iptv multicast over wireless lan using merged hybrid arq with staggered adaptive fec," *IEEE Transactions on Broadcasting*, vol. 55, no. 2, pp. 363–374, June 2009.

[65] D. Xu, B. Li, and K. Nahrstedt, "Qos-directed error control of video multicast in wireless networks," in *Proceedings Eight International Conference on Computer Communications and Networks (Cat. No.99EX370)*, 1999, pp. 257–262.

[66] A. Majumda, D. G. Sachs, I. V. Kozintsev, K. Ramchandran, and M. M. Yeung, "Multicast and unicast real-time video streaming over wireless lans," *IEEE Transactions on Circuits and Systems for Video Technology*, vol. 12, no. 6, pp. 524–534, Jun 2002.

[67] I. Kozintsev, "Improving last-hop multicast streaming video over 802.11," in *Proceedings of BROADNETS*, San Jose, California, USA 38, Oct 2004.

[68] S. Makharia, D. Raychaudhuri, M. Wu, H. Liu, and D. Li, "Experimental study on wireless multicast scalability using merged hybrid arq with staggered adaptive fec," in *2008 International Symposium on a World of Wireless, Mobile and Multimedia Networks*, June 2008, pp. 1–12.

[69] Z. Liu, Z. Wu, P. Liu, H. Liu, and Y. Wang, "Layer bargaining: multicast layered video over wireless networks," *IEEE Journal on Selected Areas in Communications*, vol. 28, no. 3, pp. 445–455, April 2010.

[70] A. Basalamah and T. Sato, "Adaptive fec reliable multicast mac protocol for wlan," in *2007 IEEE 66th Vehicular Technology Conference*, Sept 2007, pp. 244–248.

[71] M. van der Schaar, S. Krishnamachari, S. Choi, and X. Xu, "Adaptive cross-layer protection strategies for robust scalable video transmission over 802.11 wlans," *IEEE Journal on Selected Areas in Communications*, vol. 21, no. 10, pp. 1752–1763, Dec 2003.

[72] P. K. McKinley and A. P. Mani, "An experimental study of adaptive forward error correction for wireless collaborative computing," in *Proceedings 2001 Symposium on Applications and the Internet*, 2001, pp. 157–166.

[73] C. Tang and P. K. McKinley, "Queueing losses and adaptive reliable multicast in wireless lans," in *Joint International Conference on Wireless LANs and Home Networks (ICWLHN 2002) and Networking (ICN 2002)*, Aug 2002, pp. 395–406.

[74] T. Guoping, T. Herfet *et al.*, "A novel adaptive hybrid error correction scheme for wireless dvb services," *Int'l J. of Communications, Network and System Sciences*, vol. 1, no. 02, p. 187, 2008.

[75] M. Heusse, F. Rousseau, G. Berger-Sabbatel, and A. Duda, "Performance anomaly of 802.11b," in *IEEE INFOCOM 2003. Twenty-second Annual Joint Conference of the IEEE Computer and Communications Societies (IEEE Cat. No.03CH37428)*, vol. 2, March 2003, pp. 836–843 vol.2.

[76] J. Xiong and R. R. Choudhury, "Peercast: Improving link layer multicast through cooperative relaying," in *2011 Proceedings IEEE INFOCOM*, April 2011, pp. 2939–2947.

[77] A. Russo and R. L. Cigno, "Pullcast: Peer-assisted video multicasting for wireless mesh networks," in *2013 10th Annual Conference on Wireless On-demand Network Systems and Services (WONS)*, March 2013, pp. 60–67.

[78] R. Ahlswede, N. Cai, S.-Y. Li, and R. W. Yeung, "Network information flow," *IEEE Transactions on information theory*, vol. 46, no. 4, pp. 1204–1216, 2000.

[79] C. Gkantsidis and P. R. Rodriguez, "Network coding for large scale content distribution," in *INFOCOM 2005. 24th Annual Joint Conference of the IEEE Computer and Communications Societies. Proceedings IEEE*, vol. 4. IEEE, 2005, pp. 2235–2245.

[80] A. G. Dimakis, P. B. Godfrey, Y. Wu, M. J. Wainwright, and K. Ramchandran, "Network coding for distributed storage systems," *IEEE Transactions on Information Theory*, vol. 56, no. 9, pp. 4539–4551, Sept 2010.

[81] Z. Li, B. Li, and L. C. Lau, "On achieving maximum multicast throughput in undirected networks," *IEEE Transactions on Information Theory*, vol. 52, no. 6, pp. 2467–2485, June 2006.

[82] S. Katti, H. Rahul, W. Hu, D. Katabi, M. Médard, and J. Crowcroft, "Xors in the air: Practical wireless network coding," in *ACM SIGCOMM computer communication review*, vol. 36, no. 4. ACM, 2006, pp. 243–254.

[83] O. Alay, P. Liu, Y. Wang, E. Erkip, and S. S. Panwar, "Cooperative layered video multicast using randomized distributed space time codes," *IEEE Transactions on Multimedia*, vol. 13, no. 5, pp. 1127–1140, Oct 2011.

[84] O. Alay, P. Liu, Y. Wang, E. Erkip, and S. Panwar, "Error resilient video multicast using randomized distributed space time codes," in *2010 IEEE International Conference on Acoustics, Speech and Signal Processing*, March 2010, pp. 5554–5557.

[85] O. Alay, R. Ding, E. Erkip, Y. Wang, and A. Scaglione, "Layered randomized cooperation for multicast," in *2008 42nd Asilomar Conference on Signals, Systems and Computers*, Oct 2008, pp. 1484–1488.

[86] J. M. Vella and S. Zammit, "A survey of multicasting over wireless access networks," *IEEE Communications Surveys Tutorials*, vol. 15, no. 2, pp. 718–753, Second 2013.

[87] G. Z. Khan, R. Gonzalez, E.-C. Park, and X.-W. Wu, "A reliable multicast mac protocol for wifi direct 802.11 networks," in *European Conference on Networks and Communications (EuCNC), 2015*, 2015, pp. 224–228.

[88] P. Bahl and V. N. Padmanabhan, "Radar: An in-building rf-based user location and tracking system," in *INFOCOM 2000. Nineteenth Annual Joint Conference of the IEEE Computer and Communications Societies. Proceedings. IEEE*, vol. 2. Ieee, 2000, pp. 775–784.

[89] S. Saha, K. Chaudhuri, D. Sanghi, and P. Bhagwat, "Location determination of a mobile device using ieee 802.11 b access point signals," in *Wireless Communications and Networking, 2003. WCNC 2003. 2003 IEEE*, vol. 3. IEEE, 2003, pp. 1987–1992.

[90] Y.-T. Chan, W.-Y. Tsui, H.-C. So, and P.-c. Ching, "Time-of-arrival based localization under nlos conditions," *IEEE Transactions on Vehicular Technology*, vol. 55, no. 1, pp. 17–24, 2006.

[91] G. Z. Khan, E.-C. Park, and R. Gonzalez, "Performance Analysis of Early Packet Loss Detection in WiFi Direct 802.11 Networks," in *The 13th IEEE International Conference on Wireless and Mobile Computing, Networking and Communications*, Oct 2017.

[92] S. Sen, R. R. Choudhury, and S. Nelakuditi, "Csma/cn: carrier sense multiple access with collision notification," *IEEE/ACM Transactions on Networking (ToN)*, vol. 20, no. 2, pp. 544–556, 2012.

[93] K. Jamieson and H. Balakrishnan, "Ppr: Partial packet recovery for wireless networks," in *ACM SIGCOMM Computer Communication Review*, vol. 37, no. 4. ACM, 2007, pp. 409–420.

[94] T. Nilsson, G. Wikstrand, and J. Eriksson, "Early multicast collision detection in CSMA/CA networks," in *4th International Workshop on Mobile and Wireless Communications Network, 2002.*, 2002, pp. 294–298.

[95] G. Bianchi, "Performance analysis of the IEEE 802.11 distributed coordination function," *IEEE Journal on selected areas in communications*, vol. 18, no. 3, pp. 535–547, 2000.

[96] A. Heck and A. Heck, *Introduction to MAPLE*. Springer-Verlag New York, 1993, vol. 1993.

[97] O. Ekici and A. Yongacoglu, "Ieee 802.11 a throughput performance with hidden nodes," *IEEE Communications Letters*, vol. 12, no. 6, 2008.

[98] A. Networks, "802.11ac In-Depth," Tech. Rep., 2014. [Online]. Available: http://www.arubanetworks.com/assets/wp/WP_80211acInDepth.pdf

[99] V. Erceg, "Ieee p802. 11 wireless lans tgn channel models," *IEEE 802.11-03/940r4*, 2004.

[100] G. Z. Khan, R. Gonzalez, E. C. Park, and X. W. Wu, "Analysis of very high throughput (vht) at mac and phy layers under mimo channel in 802.11ac wlan," vol. 37, no. 4, pp. 877–888, 2017.

[101] V. Rhodes, "Path loss proposal for the ieee 802.11 htsg channel model ad hoc group," *April*, vol. 22, 2003.

[102] J. B. Andersen, T. S. Rappaport, and S. Yoshida, "Propagation measurements and models for wireless communications channels," *IEEE Communications Magazine*, vol. 33, no. 1, pp. 42–49, 1995.

[103] L. Schumacher, K. I. Pedersen, and P. E. Mogensen, "From antenna spacings to theoretical capacities-guidelines for simulating mimo systems," in *Personal, Indoor and Mobile Radio Communications, 2002. The 13th IEEE International Symposium on*, vol. 2. IEEE, 2002, pp. 587–592.

[104] E. Perahia and R. Stacey, *Next generation wireless LANs: 802.11 n and 802.11 ac*. Cambridge university press, 2013.

[105] G. Z. Khan, R. Gonzalez, and E. C. Park, "On the design of a wifi direct 802.11ac wlan under a tgn mimo multipath fading channel," *KSII Transactions on Internet and Information Systems*, vol. 11, no. 3, pp. 1373–1392.

[106] G. Z. Khan, R. Gonzalez, X. W. Wu, and E. C. Park, "On the field level loss of a vht ppdu in a mimo-ofdm system for a wifi direct 802.11ac wlan," in *2016 International Conference on Frontiers of Information Technology (FIT)*, Dec 2016, pp. 164–169.

[107] ZombieSymmetry. [Online]. Available: https://www.youtube.com/user/ZombieSymmetry/videos

[108] M. S. Gast, *802.11 ac: A survival guide*. " O'Reilly Media, Inc.", 2013.

[109] T. M. Schmidl and D. C. Cox, "Robust frequency and timing synchronization for ofdm," *IEEE transactions on communications*, vol. 45, no. 12, pp. 1613–1621, 1997.

[110] V. Garg, *Wireless communications & networking*. Morgan Kaufmann, 2010.

[111] L. Schumacher, K. I. Pedersen, and P. E. Mogensen, "From antenna spacings to theoretical capacities-guidelines for simulating mimo systems," in *Personal, Indoor and Mobile Radio Communications, 2002. The 13th IEEE International Symposium on*, vol. 2. IEEE, 2002, pp. 587–592.

[112] Y. S. Cho, J. Kim, W. Y. Yang, and C. G. Kang, *MIMO-OFDM wireless communications with MATLAB*. John Wiley & Sons, 2010.

[113] I. SG12, "Definition of quality of experience," *TD 109rev2 (PLEN/12), Geneva, Switzerland*, pp. 16–25, 2007.

[114] I.-H. Mkwawa, E. Jammeh, and L. Sun, "Mapping of received signal strength indicator to qoe in voip applications over wlan," in *Quality of Multimedia Experience (QoMEX), 2012 Fourth International Workshop on*. IEEE, 2012, pp. 156–157.

[115] K. Abboud, H. A. Omar, and W. Zhuang, "Interworking of dsrc and cellular network technologies for v2x communications: A survey," *IEEE Transactions on Vehicular Technology*, vol. 65, no. 12, pp. 9457–9470, 2016.

[116] D. Camps-Mur, A. Garcia-Saavedra, and P. Serrano, "Device-to-device communications with wi-fi direct: overview and experimentation," *IEEE Wireless Communications*, vol. 20, no. 3, pp. 96–104, June 2013.

[117] Android. Android 7.0 nougat. [Online]. Available: https://developer.android.com/about/versions/nougat/android-7.0.html

[118] Apple. ios 10. [Online]. Available: https://developer.apple.com/ios/

[119] S. Kim, B.-S. Kim, and Y. Fang, "Network allocation vector (nav)-based opportunistic prescanning process for wlans," *Electronics letters*, vol. 46, no. 24, pp. 1630–1632, 2010.

[120] D. Halperin, W. Hu, A. Sheth, and D. Wetherall, "Predictable 802.11 packet delivery from wireless channel measurements," in *ACM SIGCOMM Computer Communication Review*, vol. 40, no. 4. ACM, 2010, pp. 159–170.

[121] P. Kyritsi, R. A. Valenzuela, and D. C. Cox, "Channel and capacity estimation errors," *IEEE Communications Letters*, vol. 6, no. 12, pp. 517–519, Dec 2002.

[122] "TGn Channel Models, IEEE Std. 802.11 03/940r," Tech. Rep., May 2004. [Online]. Available: https://mentor.ieee.org/802.11/dcn/03/11-03-0940-04-000n-tgn-channel-models.doc

[123] G. Z. Khan, R. Gonzalez, and E. C. Park, "A performance analysis of mac and phy layers in ieee 802.11ac wireless network," in *18th International Conference on Advanced Communication Technology (ICACT)*, Jan 2016, pp. 20–25.

[124] R. Rajadurai, K. S. Gopalan, M. Patil, and S. Chitturi, "Enhanced interworking of lte and wi-fi direct for public safety," *IEEE Communications Magazine*, vol. 54, no. 4, pp. 40–46, April 2016.

[125] H. Zhang, Y. Liao, and L. Song, "D2d-u: Device-to-device communications in unlicensed bands for 5g system," *IEEE Transactions on Wireless Communications*, vol. 16, no. 6, pp. 3507–3519, June 2017.

[126] "Iso/iec/ieee international standard for information technology–telecommunications and information exchange between systems–local and metropolitan area networks–specific requirements-part 11: Wireless lan medium access control (mac) and physical layer (phy) specifications amendment 3: Enhancements for very high throughput in the 60 ghz band (adoption of ieee std 802.11ad-2012)," *ISO/IEC/IEEE 8802-11:2012/Amd.3:2014(E)*, pp. 1–634, March 2014.

[127] M. S. Gast, *802.11 ac: A Survival Guide: Wi-Fi at Gigabit and Beyond*. O'Reilly Media, Inc., 2013.

[128] "Mathwork, howpublished = http://www.mathwork.com, note = Accessed: 2017-07-02."

[129] G. Bianchi, "Ieee p802.11 wireless lans, tgn channel models," Tech. Rep., 2004.